Dissertation zur Erlangung des Doktorgrades
der Fakultät für Chemie und Pharmazie
der Ludwig-Maximilians-Universität München

Consequences of HtrA1 deficiency on TGF-β signaling

Eva Scharrer
aus
Weißenburg i. Bay., Deutschland
2014

Erklärung

Diese Dissertation wurde im Sinne von § 7 der Promotionsordnung vom 28. November 2011 von Herrn PD Dr. Christof Haffner betreut und von Herrn Prof. Dr. Christian Wahl-Schott von der Fakultät für Chemie und Pharmazie vertreten.

Eidesstattliche Versicherung

Diese Dissertation wurde eigenständig und ohne unerlaubte Hilfe erarbeitet.

München, den

_____

(Eva Scharrer)

Dissertation eingereicht am 14.11.2014

1. Gutachter: Prof. Dr. Christian Wahl-Schott

2. Gutachter: PD Dr. Christof Haffner

Mündliche Prüfung am 12.01.2015

Summary

Cerebral small vessel disease (SVD), a main cause of ischemic stroke leading to cognitive decline and vascular dementia, is recognized as a considerable health care problem in aging societies. However, mechanisms underlying this disease are poorly understood and no specific and preventive treatment options are available. Several monogenic forms of SVD have been identified which share a number of clinical and pathological features with the sporadic disease. They are thus considered as valuable model diseases to understand SVD pathomechanisms. One of these inherited forms is the rare disease CARASIL (**C**erebral **A**utosomal **R**ecessive **A**rteriopathy with **S**ubcortical **I**nfarcts and **L**eukoencephalopathy), which is caused by loss-of-function mutations in the gene encoding the serine protease high temperature requirement protein A1 (HtrA1). HtrA1 has been proposed to inhibit transforming growth factor beta (TGF-β) signaling by degrading pathway components. Evidence indicating increased TGF-β activity in CARASIL brain vessels led to the hypothesis that TGF-β plays a critical role in CARASIL development. The goal of this thesis was to provide further experimental evidence for this hypothesis using an HtrA1-deficient mouse model and patient fibroblasts. Newly created HtrA1$^{-/-}$ mice were found to be viable and fertile and displayed a normal life expectancy. Even though HtrA1-deficient mice did not show CARASIL-typical extraneurological manifestations such as spondylosis and alopecia, evidence for white matter changes and a reduction of vessel marker proteins were detected indicating the presence of pathological alterations similar to those observed in CARASIL patients. Investigation of TGF-β signaling in mouse brain tissue and embryonic fibroblasts (MEF) provided evidence for a decreased TGF-β activity upon HtrA1 deficiency. This finding was substantiated by results from human skin fibroblasts of two CARASIL patients suggesting a facilitative role of HtrA1 in TGF-β signaling. This observation contrasted with previous studies showing the opposite effect, but was in agreement with the identification of latent TGF-β-binding protein (LTBP-1), a well-described regulator of TGF-β bioactivity, as a novel HtrA1 substrate. LTBP-1 processing possibly results in a release of mature TGF-β from the extracellular matrix (ECM). Using HtrA1-deficient and wild-type MEF cells this study helped to further establish LTBP-1 as an HtrA1 target under endogenous conditions with a putative role in CARASIL pathogenesis. The results obtained from these analyses have deepened our knowledge about the role of HtrA1 in TGF-β signaling and suggest TGF-β pathway as a target for therapeutical intervention in CARASIL.

Zusammenfassung

Die zerebrale Mikroangiopathie, eine Hauptursache ischämischer Schlaganfälle und somit kognitiver Störungen und vaskulärer Demenz, wird als ernsthaftes Problem des Gesundheitswesens alternder Gesellschaften angesehen. Bisher sind die der Krankheit zugrundeliegenden Mechanismen noch wenig verstanden und weder spezifische noch vorbeugende Behandlungsmaßnahmen bekannt. Mehrere monogene Formen der zerebralen Mikroangiopathie sind identifiziert worden, die eine Reihe von klinischen und pathologischen Symptomen mit der sporadischen Form gemeinsam haben. Sie werden deshalb als wertvolle Modellerkrankungen zur Aufklärung der zugrundeliegenden Pathomechanismen angesehen. Eine dieser vererbbaren Formen ist die seltene Erkrankung CARASIL (**C**erebral **A**utosomal **R**ecessive **A**rteriopathy with **S**ubcortical **I**nfarcts and **L**eukoencephalopathy), die durch Funktionsverlust-Mutationen im Gen der Serinprotease HtrA1 (high temperature requirement protein A1) verursacht wird. Mehrere Studien deuten darauf hin, dass HtrA1 den Transforming Growth Factor beta (TGF-β)-Signalweg inhibiert, indem es Signalwegmoleküle abbaut. Aufgrund einer erhöhten TGF-β-Aktivität in Gehirngefäßen von CARASIL-Patienten wurde die Hypothese aufgestellt, dass TGF-β eine entscheidende Rolle im Krankheitsverlauf von CARASIL spielen könnte. Das Ziel der vorliegenden Arbeit war es, weitere experimentelle Beweise für diese Theorie zu finden. Hierfür wurden sowohl HtrA1-defiziente Mäuse als auch Fibroblasten aus Patienten verwendet. Wir konnten nachweisen, dass unsere neu generierten $HtrA1^{-/-}$ Mäuse sowohl lebensfähig und fertil sind als auch eine normale Lebenserwartung haben. Auch wenn HtrA1-defiziente Mäuse keine CARASIL-typischen extraneurologischen Merkmale wie Spondylose oder Alopezie zeigten, haben wir dennoch Anzeichen für Veränderungen in der weißen Hirnsubstanz und für eine Reduktion von Gefäßmarkerproteinen detektieren können, was auf ähnliche pathologische Veränderungen wie in CARASIL-Patienten hindeutete. Untersuchungen des TGF-β-Signalweges in Mausgehirngewebe und embryonalen Fibroblasten (MEF) haben eine verminderte TGF-β Aktivität bei HtrA1-Defizienz ergeben. Dieser Befund wurde durch Ergebnisse aus humanen Hautfibroblasten zweier CARASIL-Patienten bestätigt und lässt vermuten, dass HtrA1 die TGF-β-Signalwirkung verstärkt. Diese Beobachtung kontrastiert zwar mit früheren Studien, die den gegenteiligen Effekt zeigten, steht jedoch in Einklang mit der Identifizierung von LTBP-1 (latent TGF-β binding protein 1), einem gut beschriebenen Regulator der TGF-β-Bioaktivität, als ein bisher unbekanntes HtrA1-Substrat. Die Spaltung von LTBP-1 führt vermutlich zu einer Freisetzung von aktivem TGF-β aus der extrazellulären Matrix. Durch die Verwendung HtrA1-defizienter- und Wildtyp-MEF Zellen konnte in der vorliegenden Arbeit eine LTBP-1-Prozessierung durch endogenes HtrA1 nachgewiesen und eine mögliche Rolle bei der CARASIL-Pathogenese weiter untermauert werden. Die Ergebnisse dieser Studie tragen zu einem tieferen Verständnis über die Rolle von HtrA1 im TGF-β-Signalweg bei und deuten auf TGF-β als potentielles Target für therapeutische Maßnahmen bei CARASIL hin.

Content

1 Introduction

Stroke is the third most common cause of death after cardiac infarction and cancer, and the major cause of acquired disability in adults worldwide (Warlow et al., 2003, Donnan et al., 2008). Besides Alzheimer´s disease, it represents the leading cause of cognitive impairment including dementia as a long term deficit (Aguero-Torres et al., 2006, Pinkston et al., 2009). Strokes can be sub-divided into two categories: hemorrhagic (~20 % of all cases) and ischemic (~80 %) (Figure 1.1) (Warlow et al., 2003). While hemorrhagic stroke results from the rupture of vessels leading to localized bleeding in the surrounding tissue, ischemic stroke is caused by either acute occlusion of a blood vessel or systemic hypoperfusion resulting in a reduced supply of brain tissue with oxygen and nutrients (Dirnagl et al., 1999). Together with large-artery atherosclerosis and cardioembolism, small vessel disease (SVD) accounts for the majority of ischemic strokes (Adams et al., 1993).

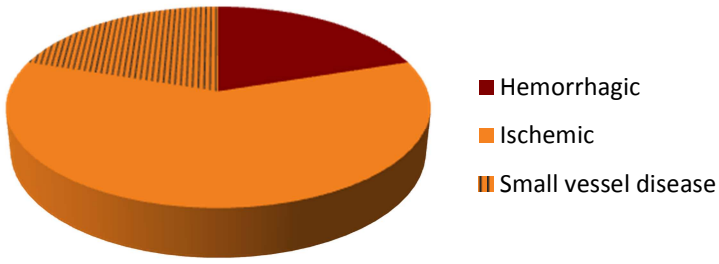

Figure 1.1: Frequency of stroke subtypes. About 20 % of all strokes are hemorrhagic and 80 % are ischemic, with small vessel disease (SVD) accounting for roughly 20 % of all strokes.

1.1 Cerebral small vessel disease

The term small vessel disease comprises all angiopathies that affect the structure or function of small cerebral vessels including small arteries, arterioles, capillaries and small veins (Pantoni, 2010, Petty et al., 2000). SVD results in small infarctions in the white and/or gray matter (Wardlaw et al., 2013), leading to the development of white matter (WM) lesions, presented as hypointense areas in computed tomography (CT) scans or hyperintense areas on T2-weighted magnetic resonance imaging (MRI) (Duering et al., 2013).

Currently the most effective treatment to improve outcomes for acute ischemic stroke is intravenous administration of recombinant tissue-type plasminogen activator (tPA) (Fugate and Rabinstein, 2014). However, the application of this thrombolysis enzyme is highly time-dependent (Ozark and Jauch, 2014) and the need for alternative therapeutical approaches for SVD is immense. The lack of specific treatment and prevention options is largely due to the fact that the molecular

mechanisms underlying SVD are poorly understood. Age and arterial hypertension, smoking, diabetes and obesity represent the main environmental risk factors for SVD (Dichgans, 2007, Pantoni, 2010), even though their impact might be overestimated (Wardlaw et al., 2014). But also genetic factors contribute to this disorder. This is reflected by several monogenic forms of SVD which share a number of clinical and pathological features with the sporadic disease and are thus considered as valuable model diseases to understand SVD pathomechanisms. The underlying gene defects have been identified for several of them (Table 1.1) including CADASIL (cerebral autosomal dominant arteriopathy with subcortical infarcts and leukoencephalopathy), the most prevalent monogenic SVD, which is caused by mutations in the *NOTCH3* gene (Joutel et al., 1996). CADASIL is characterized by progressive WM degeneration, accumulation of electron-dense granular osmiophilic material (GOM) and large proteinaceous deposits in blood vessel walls (Joutel et al., 2010, Chabriat et al., 2009).

Table 1.1: Monogenic cerebral small vessel diseases. CADASIL: cerebral autosomal dominant arteriopathy with subcortical infarcts and leukoencephalopathy; CARASIL: cerebral autosomal recessive arteriopathy with subcortical infarcts and leukoencephalopathy; *HTRA1* encodes the protein high temperature requirement A1; COL4A1: collagen, type IV, alpha 1-related cerebral small vessel disease; RVCL: retinal vasculopathy with cerebral leukodystrophy; *TREX1* encodes the protein three prime repair exonuclease 1. Adapted from Dichgans (2007), Federico et al. (2012), Yamamoto et al. (2011).

	Gene	Onset	Key features
CADASIL	*NOTCH3* (autosomal dominant)	IV-V decades	Recurrent subcortical cerebral infarctions, progressive dementia, diffuse WM changes, migraine with aura, GOM deposition.
CARASIL	*HTRA1* (autosomal recessive)	II-III decades	Recurrent small strokes, diffuse WM lesions, progressive dementia; scalp alopecia in the teen, spondylosis, kyphosis.
COL4A1	*COL4A1* (autosomal dominant)	II-IV decades	Subcortical infarcts, intracerebral haemorrhages, diffuse WM changes and dilated perivascular spaces, migraines with/without aura, dementia; kidney defects.
RVCL	*TREX1* (autosomal dominant)	IV-V decades	Diffuse WM changes and lacunar strokes, headaches; retinal vasculopathy with visual loss, liver and kidney dysfunction.

1.2 Cerebral autosomal recessive arteriopathy with subcortical infarcts and leukoencephalopathy (CARASIL)

Almost 40 years ago, a rare familial form of non-hypertensive cerebral SVD was reported in the Japanese population (Maeda et al., 1976). Affected persons shared clinical symptoms with CADASIL patients but the recessive inheritance pattern and the absence of GOMs pointed to a so far unidentified arteriopathy, which was initially called Maeda syndrome (Maeda et al., 1976) before the term CARASIL (cerebral autosomal recessive arteriopathy with subcortical infarcts and leukoencephalopathy) was coined in the mid-nineties (Bowler and Hachinski, 1994). As until 2010 only Japanese patients and two patients from China had been described, CARASIL was believed to be restricted to the Asian population (Yanagawa et al., 2002, Zheng et al., 2009). Since then, case reports from Europe and India (Bayrakli et al., 2014, Bianchi et al., 2014, Diwan et al., 2012) suggest a more widespread distribution. To date only 60-70 patients have been reported world-wide (Bianchi et al., 2014).

1.2.1 Clinical features

The age of onset of encephalopathy in CARASIL patients is between 20 and 45 years (Fukutake, 2011). Typical hallmarks are diffuse white matter abnormalities seen by T2-weighted MRI and multiple lacunar infarctions mainly in the basal ganglia or brain stem (Figure 1.2 A, B). Moreover, reduced cerebral blood flow in several areas of CARASIL brains was observed by single photon emission computed tomography (Fukutake, 2011). Patients suffer from stepwise deterioration of brain functions leading to cognitive deficits including forgetfulness, loss of sense of time, personality changes, emotional instability, and finally to dementia. Other neurological symptoms include facial palsy and gait disturbances. After occurrence of the first neurological signs, patients become bed-ridden and die within 10-30 years.

One of the first indications in the vast majority of CARASIL patients is premature alopecia (diffuse hair loss), an extraneurological symptom developing in the second decade of life (Figure 1.2 C) (Nishimoto et al., 2011, Yanagawa et al., 2002). Furthermore, in the same time period when neurological symptoms occur, about 80 % of affected persons develop lower back pain, as a result of spondylosis deformans and/or disk herniation (Figure 1.2 D). Degenerative changes and osteoarthritis in the knee joints or elbows are also observed in some patients (Fukutake, 2011, Yanagawa et al., 2002). Interestingly, an association between a polymorphism in the *HTRA1* gene and disk degeneration or spondylosis deformans was detected (Urano et al., 2010).

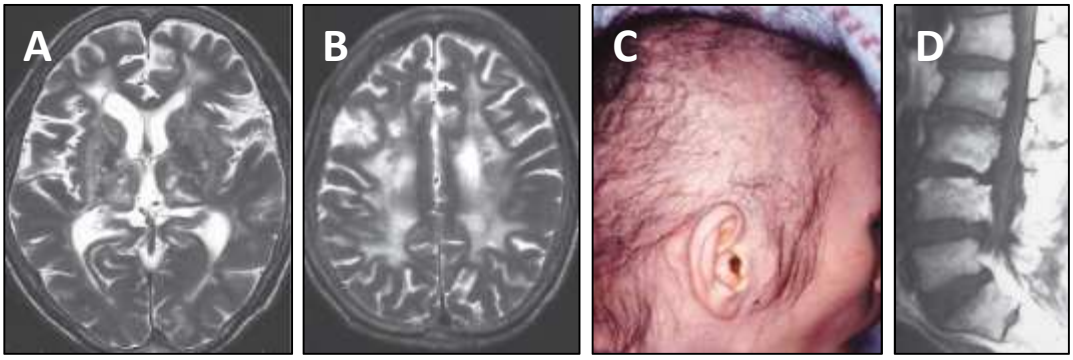

Figure 1.2: Manifestations of CARASIL. (A, B) T2-weighted MRI images of a CARASIL patient depict hyperintense lesions in the basal ganglia and white matter. (C) Alopecia of a CARASIL patient. (D) MRI image of spondylotic changes of the lumbar spine. Adapted from Hara et al. (2009).

1.2.2 Neuropathology

CARASIL-typical histopathological alterations include arteriosclerotic changes of cerebral blood vessels with fibrous intimal proliferation, splitting of the internal elastic membrane and hyalinosis of the vessel wall, resulting in luminal stenosis of small vessels in the white matter and basal ganglia and subsequently in WM abnormalities (Figure 1.3 B, D) (Arima et al., 2003, Federico et al., 2012). Moreover, leukoencephalopathy detected by diffuse myelin pallor in the cerebral WM with relative preserved subcortical U-fibers is characteristic for CARASIL (Arima et al., 2003). Marked loss of arterial smooth muscle cells (SMCs) even in arteries without sclerotic changes is a hallmark of this disease (Oide et al., 2008) (Figure 1.3 A, B). Interestingly, Oide et al. (2008) demonstrated strongly decreased collagen type I, III, VI and fibronectin immunoreactivities in thinned arterial tunica adventitia. Moreover, they found a significantly reduced type IV collagen expression in CARASIL vessels that is limited to intimal endothelial cells (Figure 1.4 C, D). In the tunica media, remaining SMCs showed pericellular type IV collagen expression (Oide et al., 2008). Thus, a loss of extracellular matrix (ECM) proteins might represent an early event in CARASIL pathogenesis and trigger the degeneration of SMCs.

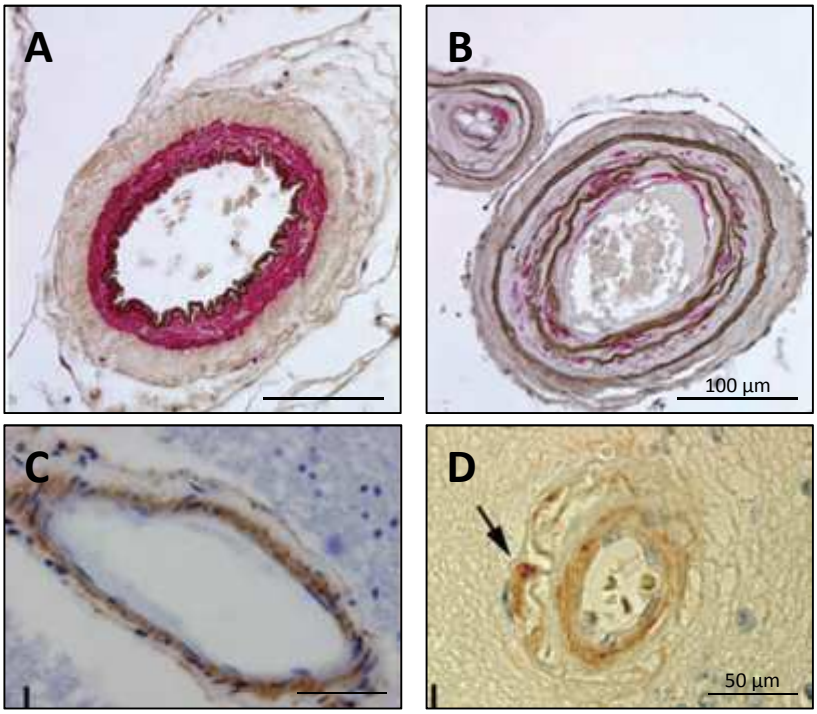

Figure 1.3: SMC and type IV collagen loss in small arteries of CARASIL patients. (A, B) Weigert and α-smooth muscle actin (SMA) staining; (C, D) type IV collagen staining; (A, C) nonarteriosclerotic control; (B, D) CARASIL. Medial SMCs are almost completely lost in narrowed lumen arteries showing splitting of the internal elastic lamina and intimal thickening (B). Decreased type IV collagen immunoreactivity in CARASIL arteries (D). Pericellular type IV collagen positive staining in ag few surviving medial SMCs is indicated by an arrow in D. Adapted from Oide et al. (2008).

1.2.3 Genetics

Consanguinity frequently seen in parents of CARASIL patients pointed to a recessive inheritance pattern (Yamamura et al., 1987). Recently, a genome-wide linkage analysis using microsatellite markers and involving eleven subjects from five consanguineous Japanese families has revealed a link to the 2.4-Mb region on chromosome 10q containing several genes including the high temperature requirement A1 (HtrA1) gene (Hara et al., 2009). As *HTRA1* is expressed in bone, skin and vasculature, the tissues mainly affected in CARASIL, it was selected as candidate gene. Mutational screening discovered homozygous mutations in all patients: two nonsense and two missense mutations, that either lead to protein products with strongly reduced protease activity (A252T, V297M, R302X) or to the loss of HtrA1 expression by nonsense mediated mRNA decay (R370X) (Hara et al., 2009). This demonstrated the identity of *HTRA1* as CARASIL causing gene. Subsequently, additional *HTRA1* mutations in five different countries including European countries were reported (Bayrakli et al., 2014, Bianchi et al., 2014, Chen et al., 2013, Mendioroz et al., 2010, Nishimoto et al., 2011, Wang et al., 2012). The mutations mainly locate in the protease domain (R274Q, P285L, G295R, A321T, L364P) and likely interfere with substrate binding or the three-dimensional structure of the catalytic pocket (Truebestein et al., 2011). This might also be true for

the previously uncharacterized mutation A173T (see chapter 3.4.3.3), even though it is located outside of the catalytic domain. Protease assays performed by our group demonstrated that this variant shows strongly reduced catalytic activity, however the underlying mechanism is yet unknown. The E42fs mutation (Bianchi et al., 2014) results in a frameshift and a premature translation termination. Distribution of all so far known CARASIL mutations within *HTRA1* is indicated in Figure 1.4.

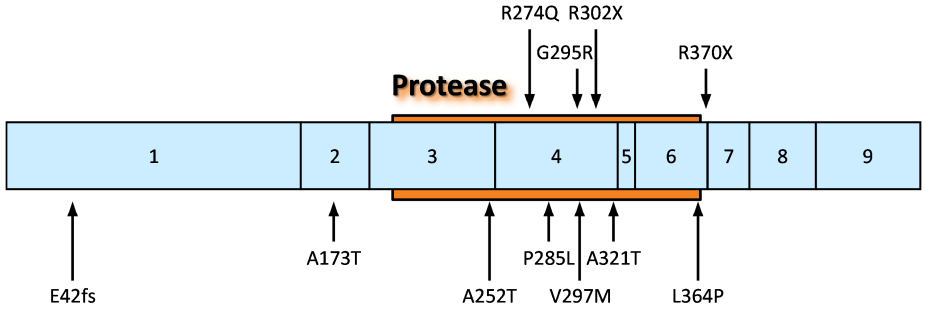

Figure 1.4: Schematic representation showing *HTRA1* exon (blue rectangles) organization and distribution of CARASIL mutations in HtrA1. Orange rectangle indicates the location of the serine protease domain.

1.3 High temperature requirement A1 (HtrA1) serine protease

The first member of the HtrA family was initially identified in *E. coli* (Lipinska et al., 1988) where it plays an important role in protein quality control. Prokaryotic HtrAs (DegP, DegS and DegQ) combine dual activities: on the one hand, these heat-shock proteins are chaperones refolding misfolded proteins at low temperatures (Spiess et al., 1999), and on the other hand, they act as proteases requiring elevated temperatures to degrade damaged proteins (Skorko-Glonek et al., 1995). HtrA proteins are members of the trypsin-like serine protease family containing a serine as a nucleophilic amino acid at the enzyme´s active site (Clausen et al., 2011).

Four mammalian HtrA proteins have been identified to date, HtrA1 (L56, PRSS11) (Hu et al., 1998, Zumbrunn and Trueb, 1996), HtrA2 (Omi) (Faccio et al., 2000, Gray et al., 2000), HtrA3 (PRSP) (Nie et al., 2003a) and HtrA4 (Clausen et al., 2002). While little biochemical and mechanistic information is available for HtrA3 and 4, the HtrA family members HtrA1 and 2 are better studied. Eukaryotic HtrAs are highly conserved among species (Figure 1.5 A). As HtrA1, 3 and 4 share the same domain architecture, as well as secretory properties and expression patterns, it is likely that they have related functions (Nie et al., 2003b, Tocharus et al., 2004). In contrast, the distinct protease HtrA2, which is known to be a mitochondrial protein with proapoptotic properties, is the only HtrA family member with a clear intracellular localization (Clausen et al., 2002, Li et al., 2002). However, the protease domain is structurally well conserved in all HtrAs. CARASIL mutations located in this

domain affect residues that are completely or largely conserved among the HtrA homologues (Figure 1.5 B).

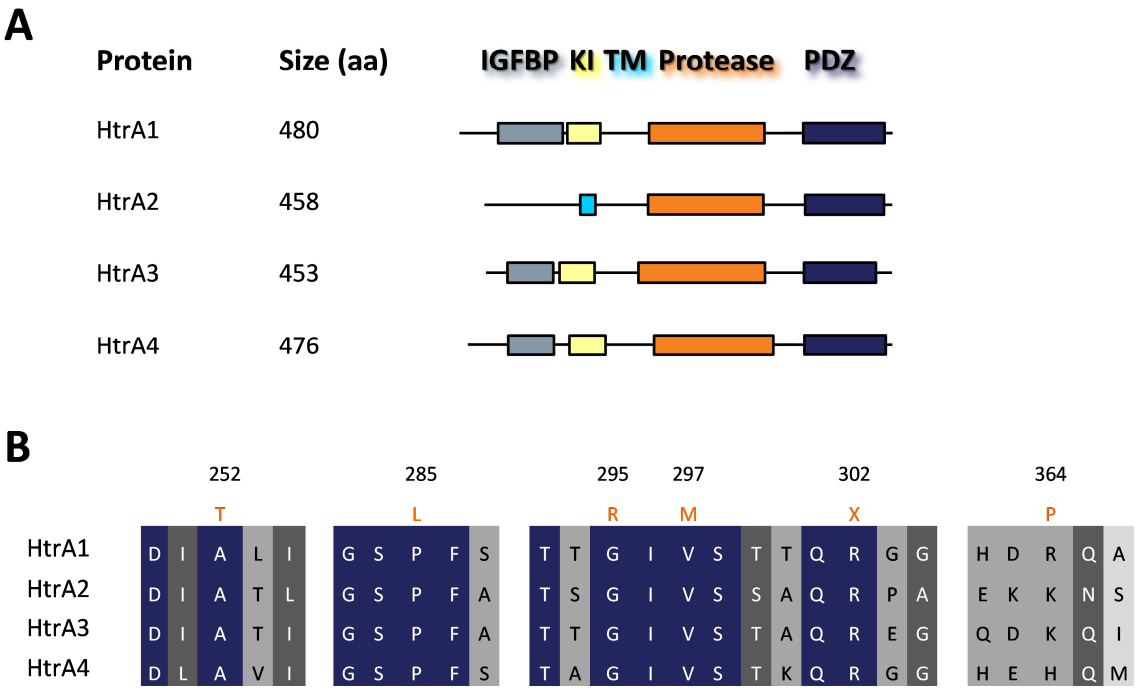

Figure 1.5: Domain organization of HtrA proteases and location of CARASIL mutations within the catalytic domain. (A) Relative positions of high temperature requirement A (HtrA) domains are taken from NCBI. Human HtrA1, 3 and 4 share the same domain architecture including a N-terminal insulin-like growth factor-binding protein module (IGFBP; grey rectangle) and a Kazal-like inhibitor domain (KI; yellow rectangle) (combined these domains are called Mac25), a trypsin-like peptidase domain (Protease; orange rectangle) and a C-terminal PDZ domain (postsynaptic density of 95 kDa, Discs large and zonula occludens 1; dark blue rectangle). HtrA2 lacks the Mac25 domain and possesses a N-terminal transmembrane anchor (TM; turquois rectangle). The PDZ domain mediates protein-protein interactions and binds to a short region of the C-terminus of other specific proteins (Clausen et al., 2002). (B) CARASIL mutations predominantly affect conserved amino acids in the serine protease domain. Sequences of human HtrA1 are shown. Conserved residues are shaded (dark blue, 100 % conserved; dark gray, highly conserved; gray, middle conservation; light grey, low conservation). The mutated amino acids are highlighted in orange. Mutations at these positions are either completely or mainly conserved.

Human *HTRA1* on chromosome 10q26 was originally identified as a gene down-regulated in SV40-transformed fibroblasts two decades ago (Zumbrunn and Trueb, 1996). However, its X-ray crystal structure has been determined only recently (Truebestein et al., 2011). HtrA1 as well as other human HtrAs form pyramidal trimers mediated by interaction between three protease domains (Hansen and Hilgenfeld, 2013). In HtrA1, the catalytic triad forming the active site comprises the residues H220, D250 and S328 (Singh et al., 2011). Mutagenesis of serine 328 to e.g. alanine (S328A) results in a complete loss of catalytic activity.

While most of the ubiquitously expressed protease HtrA1 is secreted into the extracellular space, about 20 % remain in the cytoplasm (Clausen et al., 2011) mainly attached to microtubules (Chien

et al., 2009b). An intracellular HtrA1 substrate has been identified recently: the tumor suppressor protein tuberous sclerosis complex 2 (Campioni et al., 2010). However, as HtrA1 is a predominantly secreted protease, the majority of all so far identified substrates is located extracellularly. Most of them are ECM proteins such as fibronectin, type II collagen, biglycan, clusterin, vitronectin, aggrecan, decorin and fibromodulin (An et al., 2010, Grau et al., 2006, Murwantoko et al., 2004, Tsuchiya et al., 2005), suggesting a role of HtrA1 in promoting extracellular matrix homeostasis.

In addition to CARASIL, HtrA1 has also been implicated in several other disease pathologies. As it is down-regulated in various cancers such as melanomas, ovarian and lung cancer (Esposito et al., 2006, Chien et al., 2009a, Shridhar et al., 2002) and as its overexpression inhibits tumor growth (Baldi et al., 2002), HtrA1 might function as a tumor suppressor. Furthermore, HtrA1 has been reported to be up-regulated in Alzheimer´s disease (Grau et al., 2005) and during osteoarthritis probably affecting the degradation of cartilage (Hu et al., 1998, Milner et al., 2008). Moreover, several studies have reported *HTRA1* as a major candidate within the chromosome region 10q26 linked to age-related macular degeneration (AMD) (Fisher et al., 2005). Finally, HtrA1 has been shown to play a role in cell proliferation, e.g. by processing insulin-like growth factor-binding protein 5 (IGFBP5) and thus releasing IGF1 to stimulate proliferation (Hou et al., 2005).

1.4 Transforming growth factor beta (TGF-β) signaling

During the past decade, a role of HtrA1 in transforming growth factor beta (TGF-β) signaling has emerged. It was reported to bind to various members of the TGF-β superfamily, and to attenuate their signaling activity in cellular reporter assays (Oka et al., 2004, Zhang et al., 2012). HtrA1-mediated TGF-β inhibition was also observed in a chick eye differentiation model (Oka et al., 2004) and during maturation and survival of mouse cortical neurons (Launay et al., 2008). Since TGF-β signaling is crucially involved in various aspects of vascular homeostasis (see below), CARASIL mutations were suspected to interfere with this pathway.

1.4.1 General role

The TGF-β superfamily comprises about 40 members in humans, including the three TGF-β isoforms TGF-β1, 2 and 3, nodal, GDFs, activins, inhibins and BMPs (Ruiz-Ortega et al., 2007). These pluripotent cytokines have important roles as morphogens during embryonic development and in maintaining tissue homeostasis largely via transcriptional regulation of genes involved in cell proliferation and survival, differentiation, apoptosis, cell motility and developmental fate (Moustakas and Heldin, 2009, Shi and Massague, 2003).

Among the superfamily members the three TGF-β ligands TGF-β1, 2 and 3 are subject of an elaborate synthesis and activation mechanism. They are synthesized as dimeric precursor molecules that undergo proteolytic processing in the Golgi apparatus by furin-like convertases (Figure 1.6). The proteolytic fragments, the N-terminal latency associated peptide (LAP) and the C-terminal mature peptide (Dubois et al., 1995, ten Dijke and Arthur, 2007), remain attached through non-covalent bonds forming the small latency complex (SLC), in which the receptor-binding site of mature TGF-β is sequestered by LAP (Annes et al., 2003). After covalent association with a member of the latent TGF-β binding protein family, LTBP-1, LTBP-3 or LTBP-4, the so-called large latency complex (LLC) is secreted (Saharinen et al., 1996, Saharinen and Keski-Oja, 2000). LTBPs mediate LLC attachment to the extracellular matrix by association with ECM proteins such as fibronectin and fibrillin-1 leading to the storage of latent TGF-β in the matrix (Isogai et al., 2003, ten Dijke and Arthur, 2007). TGF-β activation can be mediated by several mechanisms including cleavage of LTBPs by plasmin (Sato and Rifkin, 1989), matrix metalloproteases MMP-2 and MMP-9 (Yu and Stamenkovic, 2000) or BMP1-like proteases (Ge and Greenspan, 2006). This results in the release of mature TGF-β, which in turn binds to a heterotetrameric receptor consisting of two type I and two type II serine/threonine kinase molecules (TGFBRI and II) (Wrana et al., 1992). Their activation results in the downstream phosphorylation of the signal transducers SMAD2 and SMAD3 and their association with SMAD4. The active SMAD complex accumulates in the nucleus where it regulates transcription of several target genes including connective tissue growth factor (CTGF) and plasminogen activator inhibitor-1 (PAI-1) (Chen et al., 2000, Laiho et al., 1986, Shi and Massague, 2003). Of note, the extent and duration of signaling is accurately controlled at different steps during the pathway, including synthesis and activation of latent TGF-β, activation and stability of its receptors and other downstream signaling members (Moustakas and Heldin, 2009).

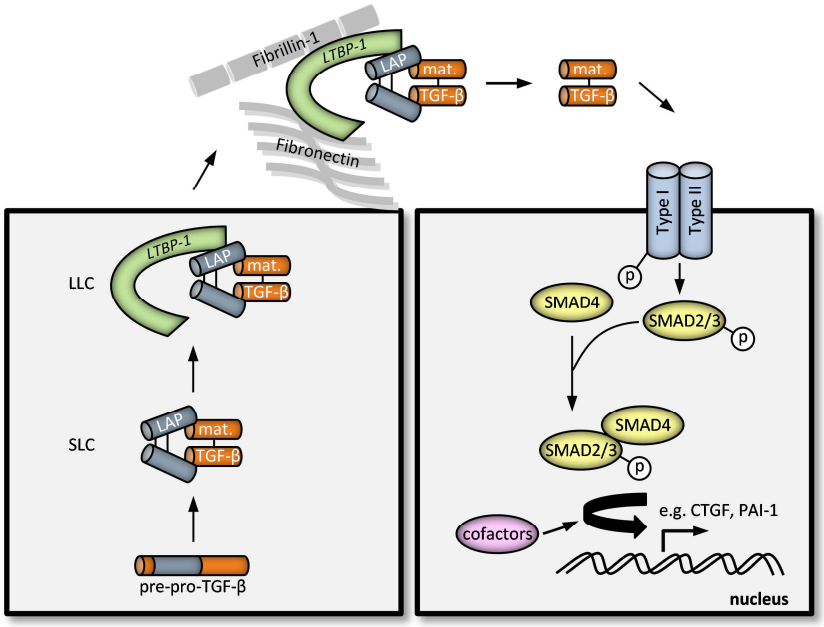

Figure 1.6: TGF-β signaling pathway. Schematic representation of transforming growth factor beta (TGF-β) synthesis, secretion, matrix deposition and signal transduction. See text for details. LAP: latency associated peptide; mat. TGF-β: mature form of TGF-β; LTBP-1: latent TGF-β binding protein; Type I, Type II: type I and type II serine/threonine kinase receptors; P: phosphate; SLC: small latency complex; LLC: large latency complex; CTGF: connective tissue growth factor; PAI-1: plasminogen activator inhibitor-1.

Aberrant TGF-β signaling has been linked to several diseases, such as cancer, autoimmune diseases as well as vascular fibrosis. Moreover, TGF-β participates in disease mechanisms of cardiovascular disorders including hypertension, restenosis, heart failure and atherosclerosis (Ruiz-Ortega et al., 2007). In addition, over the last decades several familial vascular diseases could be linked to TGF-β pathway members in agreement with the key role of TGF-β in blood-vessel morphogenesis and stability (ten Dijke and Arthur, 2007). For instance, TGF-β signaling was found to be enhanced in Marfan syndrome (MFS), a connective tissue disease characterized by aortic root aneurysms and dissections, caused by mutations in *FBN1*, which encodes the ECM component fibrillin-1 (Dietz et al., 1991). Investigation of MFS mouse models such as $Fbn1^{C1039G}$ demonstrated that fibrillin-1 mutations lead to an altered matrix sequestration of the latent LTBP-1/TGF-β complex resulting in an uncontrolled and increased TGF-β activity (Habashi et al., 2006, Neptune et al., 2003). Administration of TGF-β neutralizing antibodies to these mice prevented aortic aneurysms further demonstrating a role of enhanced TGF-β signaling in the disease pathomechanism (Habashi et al., 2006).

1.4.2 Role in CARASIL

Following the identification of *HTRA1* as the gene defective in CARASIL evidence has accumulated supporting a specific role of the TGF-β signaling pathway in the disease pathogenesis. First, increased expression levels of LAP, TGF-β, phosphoSMAD2 and the TGF-β target genes hyaluronan and fibronectin (extra domain-A), were observed in cerebral arteries of two CARASIL patients (A252T, R302X) using *in situ* hybridization or immunohistochemistry (Figure 1.7) (Hara et al., 2009, Shiga et al., 2011). Second, expression levels of the TGF-β target gene noggin were found to be elevated in patient skin fibroblasts (Hara et al., 2009). Third, non-vascular symptoms often observed in CARASIL patients (alopecia, spondylosis) are compatible with dysregulation of TGF-β family member activity in the skin and skeletal system (Botchkarev, 2003, Yoon and Lyons, 2004). In agreement with this, HtrA1-deficient mice displayed elevated trabecular bone mass (Graham et al., 2013). Moreover, TGF-β target genes known to stimulate bone formation were increased after TGF-β induction in HtrA1-deficient embryonic fibroblasts (Graham et al., 2013). Fourth, CARASIL mutations were shown to prevent HtrA1-mediated TGF-β inhibition in a luciferase reporter assay (Hara et al., 2009, Nishimoto et al., 2011) and in fibroblasts from a CARASIL patient carrying the R370X mutation (Shiga et al., 2011). This could be abolished upon restoration of HtrA1 expression (Hara et al., 2009, Shiga et al., 2011).

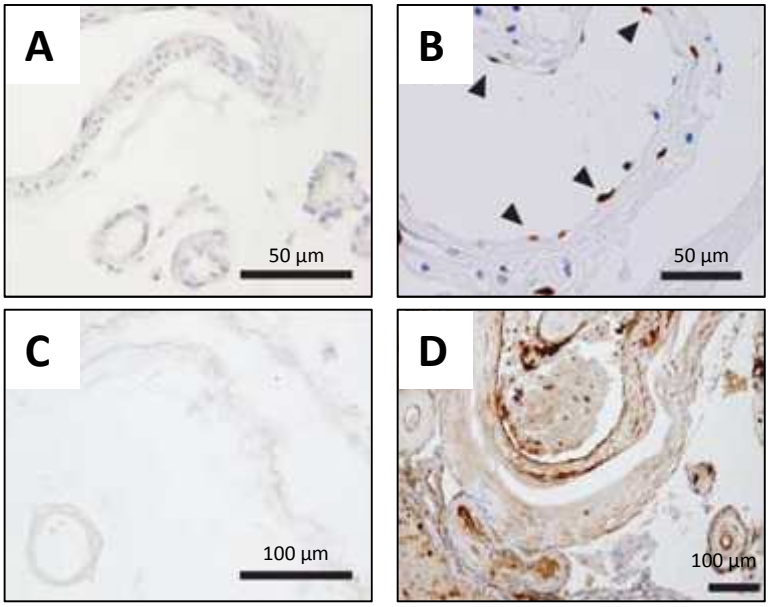

Figure 1.7: Increased TGF-β signaling in cerebral small arteries of a CARASIL patient. (A, B) phosphoSMAD2 staining; (C, D) LAP staining; (A, C) control subject; (B, D) CARASIL (R302X). (B) Increased phosphoSMAD2 immunoreactivity in endothelial cells of a CARASIL patient. Arrowheads indicate nuclei with positive phosphoSMAD2 staining. (D) Increased LAP expression in CARASIL arterial walls. No immunoreactivities were detected in controls (A, C). Adapted from Shiga et al. (2011).

Deregulated TGF-β signaling has also been implicated in sporadic SVD (Thompson and Hakim, 2009). It was reported to be up-regulated in ischemia (Doyle et al., 2010, Klempt et al., 1992) and chronic overproduction of TGF-β might induce microvascular degeneration (Wyss-Coray et al., 2000). Furthermore, TGF-β plays a key role in tissue fibrosis by stimulating expression of ECM components including collagen in myofibroblasts, resulting in ECM overproduction (Ihn, 2002). In addition, TGF-β plays an important role in vasculogenesis, angiogenesis and blood vessel stability (ten Dijke and Arthur, 2007).

The precise molecular mechanisms how HtrA1 interferes with TGF-β signaling have not been fully elucidated. Oka et al. (2004) reported that HtrA1 is co-expressed with TGF-β during embryonic development in mice and demonstrated an interaction between HtrA1 and various TGF-β superfamily members such as TGF-β, bone morphogenetic protein (BMP) 2 and 4, growth differentiation factor (GDF) 5 and 6 and activin, using a GST-pulldown assay (Oka et al., 2004). The authors could also show in luciferase assays and a developmental chick eye model system that HtrA1 inhibits signaling by TGF-β family members. In 2008, Launay et al. reported the degradation of recombinant mature TGF-β1 by HtrA1 *in vitro*. However, Shiga et al. (2011) suggested an alternative mechanism by providing evidence for HtrA1-mediated intracellular cleavage of the latency-associated peptide (LAP) of proTGF-β within the endoplasmic reticulum (ER). Most recently, cleavage of proTGF-β receptors (TGFBRII and TGFBRIII) by HtrA1 was reported (Graham et al., 2013). Irrespective of the mechanism all studies proposed an attenuation of TGF-β signaling by HtrA1 and an increased activity in CARASIL-affected tissues.

1.5 Scope of the thesis

Despite the identification of *HTRA1* as the CARASIL-causing gene the molecular events underlying disease pathogenesis are incompletely understood. An enhancement of TGF-β signaling activity resulting from the lack of HtrA1-mediated proteolytic processing of TGF-β pathway components has been proposed as a crucial step, but none of the proposed substrates (mature TGF-β, pro-TGF-β, type II and type II TGF-β receptors) has undergone a rigorous analysis including e.g. demonstration of processing by endogenous HtrA1. We therefore set out to investigate the consequences of a loss of HtrA1 function in mice as well as human cells by addressing the following questions:

- Is CARASIL pathology recapitulated in HtrA1 knockout mice?

  Embryonic stem cells carrying an interrupted *HTRA1* allele generated by gene trapping had been produced. These cells were intended to be used for the generation of homozygous HtrA1 knockout mice. The analysis plan of these mice included a basic characterization involving embryonic lethality and life expectancy as well as the examination of extraneurological (alopecia, spondylosis) and neurological CARASIL symptoms (white matter changes, smooth muscle cell degeneration).

- What are the consequences of HtrA1 deficiency on TGF-β signaling?

  To address this question, we aimed to design several assays suited for analyzing TGF-β signaling activity in young and aged HtrA1-deficient mice. To analyze effects on a cellular level we sought to generate HtrA1-deficient mouse embryonic fibroblast lines as well as primary skin fibroblasts from CARASIL patients.

- Which HtrA1 substrate might mediate possible effects on the TGF-β pathway?

  To identify physiologically relevant HtrA1 substrates, *in vitro* assays were to be developed to investigate the proteolysis of established (mature TGF-β, pro-TGF-β) and newly identified (latent TGF-β binding protein 1, LTBP-1) substrates in detail. In addition, we aimed to demonstrate substrate processing by endogenous HtrA1 using conditioned supernatants of embryonic fibroblasts.

2 Materials and methods

2.1 Equipment

15 ml falcons	VWR
24-well cell culture dishes	BD Falcon
50 ml falcons	BD Falcon
6-well cell culture dishes	Omnilab
96-well microplates PS, F-bottom	Greiner bio-one
Autoclave VX 150, DX 65	Systec
Biosphere filtertips, extralong (200 µl; 1250 µl)	Sarstedt
Canulas No. 14 BD Microlance™ 3, 23G	BD Medical
Canulas No. 18 BD Microlance™ 3, 25G	BD Medical
Cell scrapers	BD Bioscience
Cell strainers, 40 µm	BD Falcon
Centrifuge Avanti J-26 XP with swinging rotor JS 7.5	Beckmann Coulter
Clean bench HeraSafe KS18	Heraeus
CO_2 incubator HeraCell	Heraeus
Cooling centrifuge Heraeus Megafuge 16R	Thermo Scientific
Centrifuge 5417R, 5415D	Eppendorf
Coverslides 22x50 mm #1	Menzel Glas
Disposable cryotubes, 1.8 ml	Nunc
Filtertips 10 µl E long	Peqlab
Filtertips 10 µl G short	Peqlab
Forceps, scissors	F.S.T.
Freezer -80 C Hera Freeze Top	Thermo Scientific
Incubation shaking cabinet Certomat BS-1	Sartorius
Liquid nitrogen tank Cryoplus 2	Thermo Scientific
Magnetic stirrer KMO 2 basic	IKA
Microscope Axiovert 200M; camera AxioCam MRm	Zeiss
Microscope slides superfrost Plus	Menzel Glas
Microscope Wilovert S	Hund Wetzlar
Microwave	Siemens
Needles with cannula (0,33x12 mm, Myjector U40)	Terumo
PCR machine PTC-200	MJ Reserach
pH-electrode	Schott Instruments
pH-meter Lab 850	Schott Instruments
Pipettor Pipetboy	Integra
Power Supply Power Pac 200	Bio-Rad
Power Supply Power Pac 300	Bio-Rad
Power Supply Power Pac HC	Bio-Rad

Protein LoBind tubes 1.5 ml	Eppendorf
Rocking shaker ST5 CAT	Neolab
Safe lock tubes (0.5 ml; 1.5 ml; 2.0 ml)	Eppendorf
SafeGuard filtertips (20 µl; 200 µl; 1000 µl)	Peqlab
Scale CS Series, 200 g	Ohaus
Shaker ST 5 CAT	Neolab
Sterile disposable pipettes (2 ml; 5 ml; 10 ml; 25 ml)	Sarstedt
Syringe BD Discardit™ II (5 ml; 10 ml)	BD Biosciences
Syringe Inject®-F Luer Duo (1 ml)	B. Braun
Thermo shaker Thriller	Peqlab
TipOne tips (10 µl; 200 µl; 1000 µl)	StarLab
Tissue culture flasks T25	Corning
Tissue culture flasks T80	Nunc
Tissue grinder, Type Potter-Elvehjem, smooth pestle	Wheaton
Vortex genie 2	Scientific Industries
Water bath 1005	GFL
Water purification system Mili-Q (Q-POD)	Milipore

2.2 Chemicals

2-Mercaptoethanol (β-ME) ≥ 99,0 %	Sigma
Acetone	Merck
Acrylamide (Ultra Pure Proto Gel 30 %)	National diagnostics
Agar	Invitrogen
Agarose peqGOLD Universal	Peqlab
Aluminium sulfate hydrate	Sigma
Ammonium persulfate (APS)	Sigma
Ampicillin	Sigma
Boric acid (H_3BO_3)	Sigma
Bovine serum albumin (BSA)	Sigma
Bromophenol blue	Sigma
Coomassie brilliant blue G250	Fluka
Cresyl violet acetate	Sigma
Dimethyl sulfoxide (DMSO)	Sigma
Disodium phosphate (Na_2HPO_4)	Merck
Dithiothreitol (DTT)	Sigma
Ethanol 70 %	Roth
Ethanol 96 %	Roth
Ethanol absolute, for analysis	Merck
Ethylenediaminetetraacetic acid (EDTA)	Roth
Eukitt®	Fluka

Glycerol ≥ 99.5 %	Roth
Glycine	Sigma
Heparin-Natrium-5000	Ratiopharm
HEPES	Roth
Hydrogen chloride (HCl)	Roth
Ketamine hydrochloride Ketavet® 100 mg/ml	Pfizer
Lithium carbonate (Li_2CO_3)	Roth
Luxol® fast blue	Merck
Methanol ≥99 %	Roth
Monopotassium phosphate (KH_2PO_4)	Merck
NP-40	Fluka
Orange G	Sigma
Paraformaldehyde (PFA) 4 % in PBS 7.4	Morphisto
Peptone from casein	Serva
Phosphoric acid	Sigma
Protease inhibitor (cOmplete, Mini, EDTA-free cocktail tablets)	Roche
Select agar	Invitrogen
Skim milk powder	Fluka
Sodium bicarbonate ($NaHCO_3$)	Sigma
Sodium chloride (NaCl)	Roth
Sodium chloride (NaCl) 0.9 %	B. Braun
Sodium deoxycholate	Sigma
Sodium dodecyl sulphate (SDS) Pellets	Serva
Sodium fluoride (NaF)	Sigma
Sodium hydroxide (NaOH)	Roth
Sodium orthovanadate (Na_2VO_4)	Sigma
Tetramethylethylenediamine (TEMED)	Roth
Tris(hydroxymethyl)aminomethane (Tris) HCl	Roth
Tris, Trizma® base	Sigma
Triton X-100	Sigma
Tween-20	Roth
Xylazin 2 %	Albrecht
Xylene cyanole	ICN
Yeast extract	Roth

2.3 DNA techniques

2.3.1 Plasmids

Plasmids used in this thesis are listed in Table 2.1. Details about those plasmids that were generated in this thesis are shown in Table 2.2.

Table 2.1: List of plasmids. Sources: (1) Invitrogen; (2) this thesis, for details see Table 2.2.; (3) N. Beaufort, ISD, Munich, Germany.

Name	Description	Source
pcDNA4_TOA	mammalian expression vector	(1)
pcDNA4_TOA-hHtrA1mycHIS	encodes human HtrA1 WT fused to a C-terminal myc/HIS tag	(2)
pcDNA4_TOA-hHtrA1-S328AmycHIS	contains the mutation S238A in hHtrA1	(2)
pcDNA4_TOA-hHtrA1-A252TmycHIS	contains the mutation A252T in hHtrA1	(2)
pcDNA4_TOA-hHtrA1-G295RmycHIS	contains the mutation G295R in hHtrA1	(2)
pcDNA4_TOA-hHtrA1-V297MmycHIS	contains the mutation V297M in hHtrA1	(2)
pcDNA4_TOA-mHtrA1mycHIS	encodes mouse HtrA1 WT fused to a myc/HIS tag	(2)
pcDNA4_TOA-mHtrA3mycHIS	encodes mouse HtrA3 WT fused to a myc/HIS tag	(2)
pcDNA4_TOA-mHtrA4mycHIS	encodes mouse HtrA4 WT fused to a myc/HIS tag	(2)
pcDNA3-LTBP1S_FL	encodes human LTBP-1S (Jorma Keski-Oja, Helsinki, Finland) fused to a CD5 signal peptide, an N-terminal HA-tag and a C-terminal V5/HIS tag	(3)
ptt5-LTBP1S_ΔC	encodes C-terminally truncated human LTBP-1S (aa 1-689) fused to a C-terminal V5/HIS tag	(3)
pTT5-TGF-β1_V5	encodes human TGF-β1 fused to a C-terminal V5/HIS tag	(3)

Table 2.2: Plasmids generated during this thesis. Primers (see Table 2.3), templates, and restriction sites used for cloning are listed. For construct generation methods see chapter 2.3.5-2.3.12. Generation: (P,OL,D,L) standard PCR, overlapping PCR, digestion of the backbone vector and the PCR product, ligation; (P,D,L) standard PCR, digestion of the backbone vector and the PCR product, ligation; (SM) site-directed mutagenesis.

Name	Primers	Template	Restriction enzymes	Generation
pcDNA4_TOA-hHtrA1	hHtrA1-FBam, hHtrA1-R845; hHtrA1-F845, hHtrA1-Reco	pBSR-hHtrA1 (imaGenes), pcDNA4_TOA	BstEII, XhoI	(P,OL,D,L)
pcDNA4_TOA-hHtrA1mycHIS	hHtrA1-FEco, hHtrA1-RXhoI-o.Stp	pcDNA4_TOA-hHtrA1, pcDNA4_TOA	EcoRI, XhoI	(P,D,L)
pcDNA4_TOA-hHtrA1-S328AmycHIS	hHtrA1-S328A_F, hHtrA1-S328A_R	pcDNA4_TOA-hHtrA1mycHIS	-	(SM)
pcDNA4_TOA-hHtrA1-A252TmycHIS	hHtrA1-A252T_F, hHtrA1-A252T_R	pcDNA4_TOA-hHtrA1mycHIS	-	(SM)
pcDNA4_TOA-hHtrA1-G295RmycHIS	hHtrA1-G295R_F, hHtrA1-G295R_R	pcDNA4_TOA-hHtrA1mycHIS	-	(SM)
pcDNA4_TOA-hHtrA1-V297MmycHIS	hHtrA1-V297M_F, hHtrA1-V297M_R	pcDNA4_TOA-hHtrA1mycHIS	-	(SM)
pcDNA4_TOA-mHtrA1mycHIS	mHtrA1-FEco, mHtrA1-XbaI-o.Stp	pCMV SPORT6 mHtrA1 (Source BioScience), pcDNA4_TOA-hHtrA1mycHIS	EcoRI, XbaI	(P,D,L)
pcDNA4_TOA-mHtrA3mycHIS	F402mHtrA3, R1814mHtrA3	pCR4-TOPO-mHtrA3 (imaGenes), pcDNA4_TOA	XbaI, XhoI	(P,D,L)
pcDNA4_TOA-mHtrA4mycHIS	F89mHtrA4, R1537mHtrA4	pCR4-TOPO-mHtrA4 (imaGenes), pcDNA4_TOA	XbaI, XhoI	(P,D,L)

2.3.2 Oligonucleotides

If not stated otherwise, oligonucleotides were designed with CLC DNA Workbench and manufactured by Metabion, Martinsried, Germany.

Table 2.3: List of oligonucleotides.

Name	Sequence	Application
hHtrA1-RXhoI-o.Stp	5´-GCCTCGAGTGGGTCAATTTCTTCGGGA -3´	cloning
hHtrA1-FEco	5’-GAGAATTCGTCGCCATGCAGATCCC-3’	cloning
F402mHtrA3	5´-GCCTCGAGTTCGGGCCTCGGTATC-3´	cloning

Name	Sequence	Application
R1814mHtrA3	5´-GCTCTAGACATGACCACCTCAGGGA-3´	cloning
F89mHtrA4	5´-GCCTCGAGGCCGCCATGAGCTTCCAGCGGT-3´	cloning
R1537mHtrA4	5´-GCTCTAGAATTGATTATTTCAGGTGTGAC-3´	cloning
hHtrA1-FBam	5´-GAGGATCCGTCGCCATGCAGATCCCG-3´	cloning
hHtrA1-F845	5´-CCAAAATCAAGGATGTGGATGAGAAAGCAGACATC-3´	cloning
hHtrA1-R845	5´-GATGTCTGCTTTCTCATCCACATCCTTGATTTTGG-3	cloning
hHtrA1-REco	5´-GCGAATTCCTATGGGTCAATTTCTTCGG-3´	cloning
mHtrA1-FEco	5´-GAGAATTCTCGGAGTCGTCATGCAGT-3´	cloning
mHtrA1-XbaI-o.Stp	5´-GCTCTAGAGTAGGGGTCGATTTCTTCAGG-3´	cloning
TF1102-5´	5´-AGGGTCTCAAGTATCCAGGTTG-3´	genotyping
TF1102-3´	5´-CCAGAAATAAGACTCGGACTCA-3´	genotyping
LTR-rev	5´-ATAAACCCTCTTGCAGTTGCATC-3´	genotyping
mHtrA1OKA3_F	5´-CAGCTGCCACCGTCTGTC-3´	genotyping
mHtrA1OKA3_R	5´-GGCACAGGTTGGTGTAGGTC-3´	genotyping
Oka Neo for	5´-CTTGGGTGGAGAGGCTATTC-3´	genotyping
Oka Neo rev	5´-AGGTGAGATGACAGGAGATC-3´	genotyping
F358-mouse	5´-GGTAGCGACGCCAAGACCTACACCA-3´	HtrA1 mRNA analysis
F471-mouse	5´-AGGGCAGGAAGATCCCAA-3´	HtrA1 mRNA analysis
R764-mouse	5´-TTCCCTGGTGGTCAATCT-3´	HtrA1 mRNA analysis
R1005-mouse	5´-GTTAATCCCAATCACCTCGCCATCC-3´	HtrA1 mRNA analysis
rt-mHtrA1_F	5´-GGCGAGGTGATTGGGATTAA-3´	HtrA1 mRNA analysis/real-time PCR
rt-mHtrA1_R	5´-TCCGTTGATGCTGATGATG-3´	HtrA1 mRNA analysis/real-time PCR
qRT_m_ACTA2_f	5´-CCAGCACCATGAAGATCAAG-3´	real-time PCR
qRT_m_ACTA2_r	5´-CTTCGTCGTATTCCTGTTTGC-3´	real-time PCR
mActinb_#63_F	5´-GGATGCAGAAGGAGATTACTGC-3´	real-time PCR
mActinb_#63_R	5´-CCACCGATCCACACAGAGTA-3´	real-time PCR
mCTGF#71-F	5´-TGACCTGGAGGAAAACATTAAGA-3´	real-time PCR
mCTGF#71-R	5´-AGCCCTGTATGTCTTCACACTG-3´	real-time PCR
mHtrA3_#22_F	5´-AAGCGCTTCATTGGCATC-3´	real-time PCR
mHtrA3_#22_R	5´-TGCTGACCGCTGGAAAGT-3´	real-time PCR
mHtrA4_#66_F	5´-TCCCTGATGTGAGTTCTGGA-3´	real-time PCR
mHtrA4_#66_R	5´-CAATTACATCATGGTCTCTCAACC-3´	real-time PCR
mPAI-1_#80_F	5´-CCTCCTCATCCTGCCTAAGTT-3´	real-time PCR
mPAI-1_#80_R	5´-GGCCAGGGTTGCACTAAAC-3´	real-time PCR
h_bActin_qRT_f	5´-AGAGCTACGAGCTGCCTGAC-3´	real-time PCR
h_bActin_qRT_r	5´-CGTGGATGCCACAGGACT-3´	real-time PCR
hCTGF_#71_F	5´-AGCTGACCTGGAAGAGAACATT-3´	real-time PCR
hCTGF_#71_R	5´-GCTCGGTATGTCTTCATGCTG-3´	real-time PCR
hPAI-1_2_F	5´-CTCCTGGTTCTGCCCAAGTT-3´	real-time PCR
hPAI-1_2_R	5´-GAGAGGCTCTTGGTCTGAAAG-3´	real-time PCR
Oligo dT (15)	5´-TTTTTTTTTTTTTTT-3´	cDNA synthesis

2.3.3 RNA isolation and cDNA synthesis

Up to 25 mg mouse tissue was homogenized in a TissueLyser LT (Qiagen) with a 5 mm metal-ball (Qiagen) for 3 min at 50 hertz in 350 µl (aorta, isolated brain vessels) or 600 µl (brain, heart, kidney, lung) RLT buffer (Qiagen) with 40 mM DTT. After centrifugation for 3 min at 16300 g, total RNA was isolated from the supernatant using the RNeasy Mini kit (Qiagen) according to the manufacturer's protocol. Total RNA from MEF cells was isolated using 350 µl RLT buffer (Qiagen) with 40 mM DTT without preceding homogenization using the RNeasy Mini kit (Qiagen). For genomic DNA removal the RNase-Free DNase Set (Qiagen) was used during RNA purification according to the manufacturer's specifications. The concentration and quality of RNA was checked using the Nanodrop ND-1000 (Peqlab) or the Qubit 2.0 Fluorometer (Life Technologies) and loading each RNA sample on an electrophoresis gel. 250-1000 ng of RNA (brain, heart, kidney, lung, MEF cells) or 13.2 µl of eluted RNA (aorta, isolated brain vessels) in a total volume of 20 µl were used for the cDNA synthesis using the primer Oligo dT (15) (see Table 2.3) and the Omniscript RT kit (Qiagen).

2.3.4 Quantitative real-time PCR

For real-time PCR reactions 1.25 % (brain, heart, kidney, lung, MEF cells) or 6.25 % (aorta, isolated brain vessels) of the cDNA were mixed with Brilliant II SYBR Green QPCR Master Mix (Agilent Technologies). Primers were designed with the CLC DNA Workbench or primer sequences were acquired from Roche Universal Probe Library to amplify regions of mRNA transcripts between 80-150 bp in length (see Table 2.3). To minimize interference caused by contaminant genomic DNA, primer pairs were separated by intron sequences of at least 1000 bp. PCR reactions were run on the Stratagene Mx3000P real-time PCR system (Agilent Technologies) and analyzed with MxPro QPCR Software (Agilent Technologies). Melting curves made at the end of every run confirmed the presence or deficiency of PCR products. Samples were run in duplicates or triplicates and expression levels, normalized to β-Actin or GAPDH, were determined by the comparative CT method (Livak and Schmittgen, 2001).

Table 2.4: Real-time PCR program.

Step	Temperature	Period
Denaturation	95 °C	10 min
40 cycles:		
Denaturation	95 °C	30 s
Annealing	60 °C	1 min
Elongation	72 °C	1 min
Melting curve:		
	55-95 °C	continuously

2.3.5 PCR

Standard PCR was performed to amplify a certain DNA sequence with DNA polymerase and buffers purchased from Life Technologies.

Table 2.5: PCR reaction mix.

Component	Volume
2 U/µl AccuPrime DNA Polymerase	0.5 µl
5x AccuPrime Buffer B	5 µl
Template	30 ng
Forward primer (10 µM)	0.5 µl
Reverse primer (10 µM)	0.5 µl
H_2O_{DI}	ad 25 µl

Reaction was performed in a thermocycler using the following program:

Table 2.6: PCR program.

Step	Temperature	Period
Denaturation	95 °C	3 min
30 cycles:		
Denaturation	95 °C	30 s
Annealing	50-60 °C	30 s
Elongation	72 °C	1 min / kb
Elongation	72 °C	10 min
Storage	4 °C	infinite

PCR products were purified using the QIAquick PCR Purification kit (Qiagen) according to the manufacturer's specifications.

2.3.6 Site-directed mutagenesis

Oligonucleotides for site-directed mutagenesis were designed with the help of the QuikChange Primer Design Program (Agilent Technologies). Mutations were inserted using the QuikChange Lightning Site-Directed Mutagenesis kit (Agilent Technologies) according to the manufacturer's protocol.

2.3.7 Agarose gel electrophoresis

TBE buffer:
89 mM Boric acid, 2 mM EDTA, 89 mM Trizma® base, pH 8.0

DNA loading buffer (6x):
60 % glycerol, 60 mM EDTA, 0.025 % (w/v) Xylene Cyanol, 0.025 % (w/v) Orange G, 10 mM Trizma® Hydrochloride, pH 7.6

Gel electrophoresis was applied for the analytical and preparative separation of DNA and RNA. Depending on fragment size, 0.7 - 2 % (w/v) agarose was dissolved in TBE buffer, heated in the microwave and 1:10000 SYBR® Safe DNA Gel stain (Life Technologies) was added. DNA- or RNA-samples were mixed with 1x DNA loading buffer and electrophoresis was performed in TBE buffer using PerfectBlue gelsystems (Peqlab) with a constant voltage of 80 volt (small chambers) or 100 volt (large chambers) for 1 h. As a molecular marker peqGOLD 50 bp DNA ladder (Peqlab, 50-1000 bp) or peqGOLD DNA ladder mix (Peqlab, 100-10000 bp) was used. The fluorescence signal

was detected with the Fusion FX7 (Vilber Lourmat). An alternative system to analyze PCR fragments was applied using the QIAxcel Advanced System (Qiagen) and the QIAxcel DNA Screening Gel Cartridge (Qiagen) according to the manufacturer's specifications.

2.3.8 Restriction enzyme treatment

Analytical or preparative DNA restriction was carried out with restriction enzymes and buffers purchased from NEB (see Table 2.2). The type of buffer and the temperature of incubation were recommended by the manufacturer. The amount of enzyme was calculated depending on the amount of DNA. Restriction fragments obtained were analyzed and purified by DNA extraction using the GeneJET Gel Extraction kit (Fermentas) according to the manufacturer's specifications.

Table 2.7: Restriction enzyme treatment.

Component	Volume
Restriction enzyme 1	10 U
Restriction enzyme 2 (optional)	10 U
Restriction buffer	3 µl
DNA	500 ng (preparative digestion)
	1000 ng (analytical digestion)
10x BSA (optional)	3 µl
H_2O_{DI}	ad 30 µl

2.3.9 Vector dephosphorylation

To avoid religation of linearized plasmids with compatible ends, 5´ phosphate groups from restricted DNA were removed by adding Antarctic Phosphatase (NEB) to the restricted DNA (see chapter 2.3.8) according to the manufacturer's protocol.

2.3.10 DNA ligation

Ligation was performed adding 1 µl *T4* DNA Ligase (NEB), 2 µl ligase buffer (NEB) and H_2O_{DI} up to a volume of 20 µl to the DNA. Restricted plasmid DNA and the DNA fragment were ligated in a molar ratio of 1:3 for 1 h at room temperature.

2.3.11 Transformation of competent bacteria

Luria-Bertani broth (LB medium):
1 % (w/v) peptone, 0.5 % (w/v) NaCl, 0.5 % (w/v) yeast extract, pH 7.0, autoclaved

LB_{amp} medium:
LB medium; after cooling the autoclaved medium to about 50 °C, 100 µg/ml ampicillin was added.

LB_{amp} agar plates:
LB medium, 1.5 % (w/v) agar; after cooling the autoclaved medium to about 50 °C, 100 µg/ml ampicillin was added.

50 µl of competent *E. coli* DH5α cells were mixed with 100 ng DNA or 2 µl ligation mix and incubated for 30 min on ice. Then cells were heated for 90 s at 42 °C and subsequently cooled on ice for 5 min. 200 µl LB medium was added to the cell suspension followed by incubation at 37 °C for 1 h. 100 µl of the outgrowth was spread on LB_{amp} agar plates. After incubation overnight at 37 °C, colonies were picked and further incubated overnight at 37 °C in 4 ml or 100 ml LB_{amp} medium under gentle shaking.

2.3.12 DNA isolation from bacteria

Isolation of plasmid-DNA was carried out using commercially available anion-exchange columns. For small amounts of plasmid-DNA (4 ml LB medium), the NucleoSpin Plasmid kit (Macherey-Nagel) was used according to the manufacturer´s instructions. DNA was eluted in 30 µl elution buffer. For plasmid-DNA isolation from 100 ml overnight cultures, the NucleoBond Xtra Midi kit (Macherey-Nagel) was used according to the manufacturer´s instructions. DNA was eluted in 500 µl elution buffer. The concentration and quality of DNA was checked using the Nanodrop ND-1000 (Peqlab). Before the plasmid was sent for sequencing to GATC Biotech AG (Konstanz, Germany), analytical restriction analysis was carried out to ensure the correct build-up of the plasmid (see chapter 2.3.8).

2.4 Mouse techniques

2.4.1 Strains

Table 2.8: Mouse strains used in this thesis.

Strain name	Nomenclature	Gene	Mutation	Source / Reference
HtrA1$^{-/-}$(gt)	HtrA1$^{Gt(OST394864)Lex}$	HtrA1; location: Chr7:130936111-130985660 bp, + strand; genetic position: Chr7, 73.2 cM	Gene trap OST394864	Lexicon Genetics; Taconic
HtrA1$^{-/-}$(tm)	HtrA1^{tm1Ybf}	HtrA1; location: Chr7:130936111-130985660 bp, + strand; genetic position: Chr7, 73.2 cM	Targeted mutation: insertion, intragenic deletion	Yingbin Fu (Jones et al., 2011)

2.4.2 Isolation of genomic DNA from mouse tissue

Isolation of genomic DNA was performed by incubation of mouse tail biopsies or ear mark tissue with 50 mM NaOH at 97 °C for 30 min. Samples were neutralized with 30 µl 1M Trizma® hydrochloride, pH 7.0.

2.4.3 PCR genotyping

For PCR genotype analysis of the two mouse strains the respective primers were used (see Table 2.3). Sequences of oligonucleotides were either recommended by Taconic (HtrA1(gt) strain) or designed with the CLC DNA Workbench (HtrA1(tm) strain). The PCR products represented either the wild-type HtrA1 locus (HtrA1(gt) strain: 434 bp; HtrA1(tm) strain: 297 bp) or the mutant locus (HtrA1(gt) strain: 281 bp; HtrA1(tm) strain: 280 bp). The respective PCRs were performed with DNA polymerase and buffers purchased from Fermentas using the following components and the following programs (see Table 2.9 for the HtrA1(gt) mouse PCR and Tables 2.10 and 2.11 for the HtrA1(tm) mouse PCR).

Table 2.9: PCR reaction mix and program for the combined detection of the wild-type and mutant locus of HtrA1(gt) mice.

Component	Volume
5 U/µl Taq DNA polymerase	0.5 µl
10X Taq Buffer with KCl	5 µl
25 mM $MgCl_2$	6.5 µl
10 mM dNTPs	1 µl
Tissue lysate	3 µl
TF1102-3´	1 µl
TF1102-5´	1 µl
LTR-rev	1 µl
H_2O_{DI}	31 µl

Step	Temperature	Period
Denaturation	95 °C	10 min
30 cycles:		
Denaturation	95 °C	2 min
Annealing	65 °C	1 min
Elongation	72 °C	30 s
Elongation	72 °C	10 min
Storage	4 °C	infinite

Table 2.10: PCR reaction mix and program for the detection of the wild-type locus of HtrA1(tm) mice.

Component	Volume
5 U/µl Taq DNA polymerase	0.5 µl
10X Taq Buffer with KCl	5 µl
DMSO	5 µl
25 mM $MgCl_2$	3.5 µl
10 mM dNTPs	1 µl
Tissue lysate	3 µl
mHtrA1OKA3_F	1 µl
mHtrA1OKA3_R	1 µl
H_2O_{DI}	30 µl

Step	Temperature	Period
Denaturation	95 °C	10 min
35 cycles:		
Denaturation	95 °C	30 s
Annealing	60 °C	45 s
Elongation	72 °C	1 min
Elongation	72 °C	10 min
Storage	4 °C	infinite

Table 2.11: PCR reaction mix and program for the detection of the mutant locus of HtrA1(tm) mice.

Component	Volume
5 U/µl Taq DNA polymerase	0.5 µl
10X Taq Buffer with KCl	5 µl
5 x Q-Solution (Qiagen)	10 µl
25 mM $MgCl_2$	3.5 µl
10 mM dNTPs	1 µl
Tissue lysate	3 µl
Oka Neo for	1 µl
Oka Neo rev	1 µl
H_2O_{DI}	25 µl

Step	Temperature	Period
Denaturation	95 °C	10 min
35 cycles:		
Denaturation	95 °C	30 s
Annealing	58 °C	1 min
Elongation	72 °C	2 min
Elongation	72 °C	10 min
Storage	4 °C	infinite

2.4.4 Isolation of mouse tissue

Ketamine/Xylazine anaesthesia:
0.6 ml Ketamine 10 %, 0.2ml Xylazine 2 %, 0.2 ml 0.9 % NaCl solution; injection per mouse: 0.3-0.4 ml (6-8 mg/kg Xylazine, 90-120 mg/kg Ketamine)

PBS:
154 mM NaCl, 9.5 mM Na_2HPO_4, 1.7 mM KH_2PO_4, pH 7.4

Heparin perfusion:
5 ml 25 units Heparin followed by 5 ml 12.5 units Heparin and 10 ml PBS

Mice were deeply anesthetized with Ketamine/Xylazine and perfused transcardially with either Heparin solutions (see above) or with 20-30 ml PBS. Lung, liver, kidney, heart, spleen, aorta and brain were harvested and immediately frozen on dry ice. All organs were stored at -80 °C.

2.4.5 Isolation of mouse serum

Mice were deeply anesthetized with Ketamine/Xylazine. Blood samples were collected from the right ventricle of the heart and were allowed to clot for 2 h at room temperature before being centrifuged for 20 min at 2000 g. Serum was removed and stored immediately at -80 °C.

2.4.6 Isolation of mouse brain vessels

Frozen mouse brain tissue was minced with a scalpel and homogenized in 15 ml cold Minimal Essential Media (MEM, Gibco®, Life Technologies) with 40-50 up-and-down strokes in a

Potter-Elvehjem tissue grinder. Equal volume of 30 % Ficoll® 400 (Sigma) in MEM was added and the suspension was centrifuged for 20 min at 6000 g and 4 °C. The supernatant was discarded and the pellet was resuspended in 1 % BSA in PBS. Then, the suspension was poured through a 40 µm nylon mesh and extensively washed with PBS. Microvessels were collected in PBS by inversion of the nylon mesh. The purity of the vessels was checked under the microscope and the suspension was centrifuged for 5 min at 3000 g and 4 °C.

2.5 Cell culture

2.5.1 Cell lines

Table 2.12: Cell lines used in this thesis. Description: (1) Mouse embryonic fibroblasts derived from HtrA1$^{+/+}$(gt) embryos (see chapter 2.4.1), immortalized through serial passaging; (2) Mouse embryonic fibroblasts derived from HtrA1$^{-/-}$(gt) embryos (see chapter 2.4.1), immortalized through serial passaging.

Cell line	Description	Source / Reference
HEK293T	Human embryonic kidney cells	laboratory´s cell line collection
MFB-F11	Mouse embryonic fibroblasts derived from TGF-β1$^{-/-}$ embryos stably transfected with reporter plasmids consisting of TGF-β responsive SMAD-binding elements coupled to a secreted alkaline phosphatase reporter gene (pSBE-SEAP).	(Tesseur et al., 2006)
WT1(gt)	(1)	this study
WT2(gt)	(1)	this study
WT3(gt)	(1)	this study
WT4(gt)	(1)	this study
WT272(gt)	(1)	this study
WT1o(gt)	(1)	this study
WT2o(gt)	(1)	this study
KO1(gt)	(2)	this study
KO2(gt)	(2)	this study
KO3(gt)	(2)	this study
KO272(gt)	(2)	this study
KO1o(gt)	(2)	this study
KO2o(gt)	(2)	this study

Cell line	Description	Source / Reference
WT(tm)	Mouse embryonic fibroblasts derived from HtrA1$^{+/+}$(tm) embryos (see chapter 2.4.1), immortalized through serial passaging during this thesis.	kindly provided by M. Ehrmann, University Duisburg-Essen, Germany
KO(tm)	Mouse embryonic fibroblasts derived from HtrA1$^{-/-}$(tm) embryos (see chapter 2.4.1), immortalized through serial passaging during this thesis.	kindly provided by M. Ehrmann, University Duisburg-Essen, Germany
WT/WT	Human skin fibroblasts derived from a 45 year old male control	kindly provided by D. Werring; UCL Institute of Neurology, National Hospital for Neurology and Neurosurgery, London, Great-Britain
A321T/E42fs	Human skin fibroblasts derived from a 29-year-old Romanian female CARASIL patient carrying two heterozygous *HTRA1* mutations: c.961G>A (aa substitution p.A321T) mutation in exon 4 and a G deletion c.126delG (frameshift p.E42fs; introduction of a stop codon at position 214) in exon 1; showed severe diffuse leukoencephalopathy, subcortical infarcts, degenerative disc disease	kindly provided by A. Federico, University of Siena, Italy (Bianchi et al., 2014)
A173T/A173T	Human skin fibroblasts derived from a 34-year-old Pakistani female CARASIL patient carrying a homozygous *HTRA1* mutation: c.517G>A (aa substitution p.A173T) mutation in exon 2; showed confluent T2 hyperintensities in periventricular, deep and subcortical cerebral WM and in the brainstem; multiple lesions in the corpus callosum and periventricular WM; arteriolosclerosis; minor non-compressive spondylosis	kindly provided by D. Werring; UCL Institute of Neurology, National Hospital for Neurology and Neurosurgery, London, Great-Britain

2.5.2 Mouse embryonic fibroblasts

PBS (sterile):
154 mM NaCl, 9.5 mM Na_2HPO_4, 1.7 mM KH_2PO_4, pH 7.4, autoclaved

Medium:
Dulbecco's Modified Eagle Medium (DMEM), high glucose, GlutaMAX™ Supplement (Gibco®, Life Technologies)

Supplements:
Fetal bovine serum (FBS) (Gibco®, Life Technologies)
Penicillin/streptomycin (p/s) (100 U/ml penicillin, 100 µg/ml streptomycin) (Gibco®, Life Technologies)

Mouse embryonic fibroblasts (MEF) were derived from 13.5-15.5 days post coitus embryos. Embryos were dissected from maternal tissue in sterile PBS followed by decapitation and removal of organs. The embryos were then placed in a petri dish with DMEM supplemented with 10 % FBS

and 2 % p/s and minced with a scissor. After incubation in a humidified 37 °C incubator containing 5 % CO_2 for 2 days, medium was changed and cells were grown to 80-90 % confluence. MEF cells were split every 3 days (see chapter 2.5.3) and a defined number of cells was seeded into T80 flasks. Cells were immortalized through serial replating of the cells. During the rapid growth phase of the culture (the first 5-7 passages), cells were split twice a week 1:3 to 1:5. As the MEF cells entered crisis, cells were split 1:2 or merely replated. Starting at passage 10 immortalized cells began to overgrow the culture. Immortalized cells were split two or three times a week.

2.5.3 Cell cultivation

Medium:
Dulbecco's Modified Eagle Medium (DMEM), high glucose, GlutaMAX™ Supplement (Gibco®, Life Technologies)

Supplements:
Fetal bovine serum (FBS) (Gibco®, Life Technologies)
Penicillin/streptomycin (p/s) (100 U/ml penicillin, 100 µg/ml streptomycin) (Gibco®, Life Technologies)

0.05 % Trypsin-EDTA 1x (Gibco®, Life Technologies)

All cell lines were maintained in DMEM supplemented with 10 % FBS and 1 % p/s in a humidified 37 °C incubator containing 5 % CO_2. Cells were split at 80–90 % confluence (2-3 times a week). After washing with PBS, cells were trypsinized for 2 min at 37 °C. Detached cells were centrifuged for 5 min at 400 g. Then, cell pellets were resuspended and an appropriate amount of cells were seeded in fresh medium. Cells were tested frequently for mycoplasma using the Venor GeM OneStep kit (Minerva Biolabs) or the MycoAlert™ PLUS Mycoplasma Detection kit (Lonza).

2.5.4 Cell transfection

Cells were counted using a TC20™ Automated Cell Counter (Bio-Rad) or a Neubauer chamber and a defined number was seeded into well plates. After overnight incubation, cells were washed with PBS and serum-free medium was added for 2 h. Transfection was performed with Lipofectamine® 2000 (Life Technologies) or FuGENE® HD Transfection Reagent (Roche) according to the manufacturer´s manual. Following culturing for 24 h or 48 h in serum-free DMEM, medium was collected and centrifuged 10 min at 1000 g to eliminate cell debris. Cells were washed with PBS and collected in PBS followed by centrifugation for 10 min at 1000 g.

2.5.5 Cell cryoconservation

Freezing medium:
FBS containing 10 % DMSO

For long term storage of cell lines, cells were trypsinized and pelleted (see chapter 2.5.3) and resuspended in freezing medium. The suspension was then transferred into a cryovial and allowed to slowly cool down overnight at -80 °C using a freeze-box (Mr. Frosty, Nalgene®). Finally, cryovials were transferred into a liquid nitrogen tank. If needed, cell suspensions were thawed by short incubation of the vial at 37 °C. After adding DMEM, cells were centrifuged and seeded with fresh medium into a new flask.

2.5.6 Generation of cells and conditioned media from MEF cells

Preparation of cells and conditioned medium for real-time PCR (chapter 2.3.4), total protein lysates (chapter 2.6.2), proteolysis assay (chapter 2.6.7), TGF-β ELISA (chapter 2.6.8) and active TGF-β measurement (chapter 2.6.9):

Cells were counted using a TC20™ Automated Cell Counter (Bio-Rad) or a Neubauer chamber and a defined number was seeded into well plates. After overnight incubation, cells were washed with PBS and serum-free medium was added for 2 h. Following culturing for 24 h, 48 h or 72 h in fresh serum-free DMEM, medium was collected and centrifuged 10 min at 1000 g to eliminate cell debris. Media were directly analyzed or concentrated 10- to 20-fold by spinning 10 min at 4000 g and 4 °C using Amicon Ultra-15 Centrifugal Filter Unit with Ultracel-3 membrane (Millipore). Cells were washed with PBS and collected in PBS followed by centrifugation for 10 min at 1000 g.

Preparation of TGF-β1 stimulated MEF cells:

Cells were counted and a defined number was seeded into well plates. After overnight incubation, cells were washed with PBS and serum-free medium was added for 10 h. Then, medium was exchanged to fresh serum-free DMEM with 1 or 10 ng/ml recombinant Human TGF-beta 1 (R&D Systems). Following culturing for 12 h, cells were washed with PBS and collected in PBS followed by centrifugation for 10 min at 1000 g.

2.6 Protein analysis methods

2.6.1 Antibodies

The monoclonal rat anti-HtrA1(16C8) antibody was generated in collaboration with Dr. Elisabeth Kremmer, HelmholtzZentrum, Munich, Germany. Rats were immunized with a synthetic HtrA1 peptide corresponding to aa 155–170 of the human sequence and a C-terminal cysteine residue (CGQGQEDPNSLRHKYNC). Hybridoma cell supernatants were used undiluted for Western blotting.

Table 2.13 and Table 2.14 list all primary and secondary antibodies that were used for Western blotting.

Table 2.13: Primary antibodies used for Western blotting.

Antibody	Type	Dilution	Source
β-Actin	rabbit polyclonal	1:1000	SIGMA
HtrA1(16C8)	rat monoclonal	pure	E. Kremmer, HelmholtzZentrum, Munich, Germany
HtrA1(ΔMac)	rabbit polyclonal	1:1000	kindly provided by S. Fauser, University Cologne, Germany, (Vierkotten et al., 2011)
Myc(9E10)	mouse monoclonal	1:5000	Hybridoma Bank, Iowa, USA
Phospho-Smad2 (Ser465/467) (138D4)	rabbit monoclonal	1:500	Cell Signaling
α-Smooth Muscle Actin-Cy3™	mouse monoclonal	1:1000	SIGMA
TGF-β1	rabbit polyclonal	1:2000	Torrey Pines Biolabs
V5	mouse monoclonal	1:5000	Life Technologies

Table 2.14: Secondary antibodies used for Western blotting.

Antibody	Conjugate	Dilution	Source
Goat anti-mouse	HRP	1:10000	DAKO
Goat anti-rabbit	HRP	1:10000	DAKO
Rabbit anti-goat	HRP	1:10000	DAKO
Rabbit anti-rat	HRP	1:10000	DAKO

2.6.2 Cell total protein lysates

10x Protease inhibitor (PI):
1 protease inhibitor tablet in 1 ml H_2O_{DI}

SMAD lysis buffer:
100 mM NaCl, 2mM EDTA, 50 mM NaF, 20 mM $Na_4P_2O_7$, 2 mM Na_3VO_4, 0.1 % SDS, 0.5 % sodium deoxycholate, 1 % Triton-X 100, 10 % glycerol, 1 x PI, 10 mM Trizma® base, pH 7.6

TNT lysis buffer:
50 mM Tris-HCl, 200 mM NaCl, 0.5 % NP-40, 1x PI, pH 8.0

Cells were washed with PBS and collected in PBS followed by centrifugation for 10 min at 1000 g. Pellet was lysed in SMAD lysis buffer for phosphoSMAD2 analysis or in TNT lysis buffer and incubated on ice for 20 min. Cell debris was removed by centrifugation for 10 min at 16300 g and 4 °C. Total protein concentration of phosphoSMAD2 analysis lysates could not be determined because of incompatibilities of buffer components with available protein quantification assays.

2.6.3 Mouse tissue protein lysates

Tissue lysates:

10x Protease inhibitor (PI):
1 protease inhibitor tablet in 1 ml H_2O_{DI}

Homogenisation Buffer:
150 mM NaCl, 50 mM Trizma® base, pH 7.4; supplemented with 1 x PI, 50 mM NaF, 20 mM $Na_4P_2O_7$, 2 mM Na_3VO_4

10 x detergent:
10 % NP-40, 5 % SDS, 150 mM NaCl, 50 mM Trizma® base, pH 7.4

Up to 50 mg mouse tissue was homogenized in a TissueLyser LT (Qiagen) with a 5 mm metal-ball (Qiagen) for 3 min at 50 hertz in 495 µl homogenisation buffer. After addition of 55 µl 10 x detergent, tissue was incubated on ice for 20 min. Lysates were centrifuged for 20 min at 16300 g and 4 °C and pellets were discarded.

Isolated vessel lysates:

10x Protease inhibitor (PI):
1 protease inhibitor tablet in 1 ml H_2O_{DI}

RIPA:
150 mM NaCl, 50 mM Trizma® base, 0.1 % SDS, 1 % NP-40, 0.5 % Sodium deoxycholate, pH 7.4; supplemented with 1 x PI, 50 mM NaF, 20 mM $Na_4P_2O_7$, 2 mM Na_3VO_4

5x Loading buffer:
30 % glycerol, 6 % (w/v) SDS, 500 mM DTT, 0.03 % (w/v) bromophenol blue, 375 mM Trizma® base, pH 6.8

Isolated vessels from one hemisphere were homogenized in a conical tissue grinder (Wheaton) in 80 µl RIPA with 30-40 up-and-down strokes. Vessels were incubated on ice for 1 h and lysates were centrifuged for 20 min at 16300 g and 4 °C. Pellets were resuspended in 50 µl RIPA with 1 x loading buffer, incubated over night at room temperature and centrifuged for 30 min at 16300 g and 11 °C. Lysates were collected and stored at -20 °C.

2.6.4 Protein quantification

Protein concentrations of cell and tissue lysates were determined using the Pierce™ BCA Protein Assay kit (Thermo Scientific) according to the manufacturer´s protocol. Absorbance at 562 nm was measured with a Multiskan RC plate reader (Thermo / LabSystems). Standards and samples were measured in duplicates. Protein concentrations in conditioned MEF cell media was measured with a Qubit 2.0 Fluorometer (Life Technologies) using the manufacturer´s manual.

2.6.5 SDS-PAGE

4x Lower Tris:
0.4 % (w/v) SDS, 1.5 M Trizma® base, pH 8.8

4x Upper Tris:
0.4 % (w/v) SDS, 0.5 M Trizma® base, pH 6.8

1x Running buffer:
25 mM Trizma® base, 192 mM glycine, 1 % (w/v) SDS

5x Loading buffer:
30 % glycerol, 6 % (w/v) SDS, 500 mM DTT, 0.03 % (w/v) bromophenol blue, 375 mM Trizma® base, pH 6.8

Protein lysates containing equal amounts of protein and conditioned media were size-fractioned by denaturing SDS-polyacrylamide gel electrophoresis (SDS-PAGE) in a discontinuous system with a 1.0 mm thick stacking and separating gel (see Table 2.15) in 1x running buffer. Protein lysates and conditioned media were mixed with 5x loading buffer and boiled for 5 min at 95 °C before loading onto the gel. 5 µl Precision Plus Protein All Blue Standards (Bio-Rad) was used as a molecular

weight marker and electrophoresis was performed with the Mini-Protean® Tetra Cell system (Bio-Rad) at 80-120 V.

Table 2.15: Composition of SDS-polyacrylamide gels.

Solution	10 % Separating gel	12.5 % Separating gel	Stacking gel
H_2O_{DI}	2.44 ml	1.9 ml	1.47 ml
Acrylamide	2 ml	2.54 ml	0.276 ml
4x Lower Tris	1.5 ml	1.5 ml	-
4x Upper Tris	-	-	556 µl
APS	50 µl	50 µl	23 µl
TEMED	5 µl	5 µl	2.3 µl

2.6.6 Western blotting

Blotting buffer:
192 mM glycine, 20 % methanol, 25 mM Trizma® base, pH 8.3

1x TBST
150 mM NaCl, 0.2 % Tween-20, 10 mM Trizma® base, pH 8.0

Blocking solution:
4 % (w/v) skim milk powder in 1x TBST buffer

After SDS-PAGE, proteins were transferred to an Immobilion-P Membrane (Millipore). The membrane was shortly immersed in methanol and incubated for 5 min together with the gel in blotting buffer. The protein-transfer was performed by electro-blotting for 1 h at 125 milliampere per membrane using blotting buffer in a Trans-Blot SD Semi-Dry Transfer Cell (Bio-Rad). As a loading control proteins were visualized by staining of the membrane with Ponceau-S Solution (Sigma). Afterwards, membranes were blocked for 1 h in blocking solution at room temperature to inhibit unspecific binding. After incubation with the primary antibody diluted in blocking solution overnight at 4 °C, membranes were washed in 1x TBST followed by incubation with the horseradish peroxidase (HRP) conjugated secondary antibody in blocking solution for 1 h at room temperature or overnight at 4 °C. Then, membranes were washed again with 1x TBST and developed using the Immobilon Western Chemiluminescent HRP Substrate (Millipore) according to the manufacturer's instructions. The chemiluminescence signal was detected with the Fusion FX7 (Vilber Lourmat). The antibodies used for Western blotting and the respective dilutions are indicated in Tables 2.13 and 2.14. For quantification, the densities of the bands were determined using the software ImageJ.

2.6.7 Proteolysis assay

Denatured BSA and cell-derived HtrA1:

Coomassie brilliant blue (CBB) solution:
5 % Aluminium sulphate, 10 % Ethanol, 0.02 % Coomassie brilliant blue G250, 2 % ortho-Phosphoric acid

0.4 mg/ml BSA, 1.5 mM DTT in PBS was added to conditioned medium from vector, wild-type or mutant HtrA1 transfected HEK293T cells and samples were incubated for 24 h at 37 °C. After SDS-PAGE (see chapter 2.6.5), gels were stained with CBB solution.

LTBP-1 or TGF-β1 and cell-derived HtrA1:

Conditioned medium from LTBP-1 or TGF-β1 transfected HEK293T cells was mixed with one volume of medium from vector, wild-type or mutant HtrA1-transfected HEK293T cells or of concentrated medium from MEF cells and samples were incubated for 24 h (72 h for MEF cells) at 37 °C. In some assays, 5 mM EDTA or 5 µM NVP-LBG976 was added.

2.6.8 ELISA for TGF-β

Activation solutions:
1 N HCl
1.2 N NaOH, 0.5 HEPES

TGF-β1 concentration was quantified with TGF-beta 1 Quantikine ELISA kit (R&D Systems) using the manufacturer's protocol. To activate latent TGF-β1 to the immunoreactive form, samples were acidified followed by neutralization. After incubation of 50 µl MEF cell culture medium or 10 µl blood serum with 10 µl or 2.5 µl HCl for 10 min, samples were neutralized with 10 µl or 2.5 µl NaOH. TGF-β1 concentration of the activated samples was either measured undiluted (MEF cell culture medium) or diluted 60-fold (blood serum). Absorbance at 562 nm and 420 nm was measured with a Multiskan RC plate reader (Thermo / LabSystems).

2.6.9 Active TGF-β measurement

In order to measure active TGF-β in conditioned MEF cell media, an assay using fibroblasts derived from TGF-$\beta1^{-/-}$ mice (MFB-F11 cells), kindly provided by Ina Tesseur (Stanford University School of Medicine, Stanford, CA), was applied. These cells were transfected with a reporter plasmid containing TGF-β responsive SMAD-binding elements driving the expression of secreted alkaline phosphatase (SEAP) (Tesseur et al., 2006). $3x10^4$ MFB-F11 cells per 96-well were seeded and incubated overnight. After washing with PBS and incubation of MFB-F11 cells in serum-free DMEM

for 2 h, 50 µl of heat activated (10 min at 80 °C) conditioned MEF cell medium, that was collected after 24 h, 48 h or 72 h, was added to MFB-F11 cells. SEAP activity was measured after 24 h using the Great EscAPe™ SEAP Chemiluminescence kit 2.0 (Clontech) with a GloMax-Multi+ Detection System (Promega). The relative amount of bioactive TGF-β (fold induction) is determined based on the baseline measurement (no TGF-β).

2.7 Histological stainings of mouse brain cryosections

2.7.1 Antibodies

Table 2.16 and Table 2.17 list the primary and secondary antibodies that were used for histological stainings.

Table 2.16: Primary antibodies used for immunofluorescence stainings.

Antibody	Type	Dilution	Source
Collagen type IV	goat polyclonal	1:400	Southern Biotech
Laminin	rabbit polyclonal	1:50	Dako
Phospho-Smad2 (Ser465/467) (138D4)	rabbit monoclonal	1:50	Cell Signaling
α-Smooth Muscle Actin-Cy3™	mouse monoclonal	1:500	SIGMA

Table 2.17: Secondary antibodies used for immunofluorescence stainings.

Antibody	Conjugate	Dilution	Source
Donkey anti-rabbit	Cy3 (red)	1:100	Jackson
Donkey anti-goat	Cy2 (green)	1:100	Jackson
Goat anti-rabbit	Alexa Fluor 488 (green)	1:100	Invitrogen

2.7.2 Immunofluorescence stainings

Histo blocking buffer:
5 % (w/v) BSA in 1x PBS

Dilution buffer:
0.2 % BSA in 1x PBS

Serial coronal mouse brain sections were prepared using a cryostat (CM1950, Leica) in 7 µm thickness and stored at -80 °C until further use. Sections were thawed to room temperature for 15 min and then fixed for 15 min with PFA under gentle agitation. After washing with PBS, sections were blocked with histo blocking buffer for 1h at room temperature. For the detection of phosphoSMAD2, sections were additionally permeabilized by adding 0.1 % Triton-X to the histo blocking buffer. Primary antibodies were diluted in dilution buffer and sections were incubated with the antibodies overnight at 4 °C. After washing with PBS, sections were incubated with the fluorescence coupled secondary antibody in dilution buffer for 1.5 h at room temperature and washed again. Sections were mounted in ProLong® Gold Antifade Reagent with DAPI (Life Technologies) with coverslips. The antibodies and the respective dilutions are indicated in Tables 2.16 and 2.17. Regions of interest were analyzed with the Axiovert 200M Fluorescence Microscope (Zeiss). Quantitative comparisons on sections from mutant and wild-type mouse brains were performed in parallel using the same settings of digital images for each brain region. Quantification of immunofluorescence stainings was performed using the software ImageJ. Collagen IV-, phosphoSMAD2- and α-SMA-immunopositive area was expressed as a percentage of the total image area.

For the detection of α-SMA, cryo sections derived from 20-26 old HtrA1$^{+/+}$(gt) and HtrA1$^{-/-}$(gt) mouse brains taken -0.50 to 1.20 mm to the midline (in total 3 areas) according to the mouse brain atlas (Paxinos and Franklin, 2001) were probed with an α-SMA antibody and co-stained with laminin (one section per mouse per area).

For the detection of collagen IV and phosphoSMAD2, brain sections derived from 20-26 old HtrA1(gt) animals taken -1.50 to 1.70 mm to the midline (in total 6 areas) according to the mouse brain atlas (Paxinos and Franklin, 2001) were probed with a collagen IV or phosphoSMAD2 antibody (one section per mouse per area).

2.7.3 Klüver-Barrera Luxol fast blue staining

Luxol solution:
0.1 % Luxol fast blue in 95 % Ethanol, after dissolution addition of 0.0005 % acetic acid; filtration.

Cresyl violet solution:
0.1 % Cresyl violet acetate in H_2O_{DI}, after dissolution addition of 0.001 % acetic acid; filtration.

Lithium Carbonate solution:
0.025 % Lithium Carbonate in H_2O_{DI}

Serial coronal mouse brain sections were prepared using a cryostat (CM1950, Leica) in 7 µm thickness and stored at -80 °C until further use. Sections taken -2.30 to 1.10 mm to the midline according to the mouse brain atlas (Paxinos and Franklin, 2001) were thawed to room temperature for 15 min and then dipped for 30 s in 96 % Ethanol. After staining of myelin sheaths with Luxol solution for 1 h at room temperature under gentle stirring, sections were rinsed with H_2O_{DI} and differentiated for 30 s in Lithium Carbonate solution and 30 s in 70 % Ethanol. Sections were washed again in H_2O_{DI} and cell bodies were stained with Cresyl violet solution for 10 min at room temperature. Sections were washed with H_2O_{DI}, dipped for 5 s in 96 % Ethanol and for 10 s in 99 % Ethanol and finally mounted in Eukitt® (Fluka) with coverslips. Regions of interest were analyzed with the Axio Imager.M2 Microscope (Zeiss). Comparisons on sections from mutant and wild-type mouse brains (two sections per mouse per area, in total 5 areas) were performed in parallel using the same settings of digital images for each brain region. Alterations in myelin structure were determined semi-quantitatively by visual inspection of stained sections: 1, structured organization of myelin sheaths; 2, partially disorganized myelin sheath; 3, disorganization of myelin sheaths. Vacuolisation was also determined semi-quantitatively by visual inspection: 1, no vacuoles; 2, a few vacuoles; 3, several vacuoles.

2.8 Statistical analysis

Quantitative data are represented as mean values and standard error of the mean (SEM) of the indicated number of experiments. Statistical analysis was performed applying the Mann-Whitney Test with the SigmaPlot 12.5 Software. Significance is depicted with stars: *: $p < 0.05$; **: $p < 0.01$; ***: $p < 0.001$.

3 Results

3.1 Description of HtrA1$^{-/-}$ mice

In 2009, Hara et al. demonstrated that loss-of-function mutations in the *HTRA1* gene cause the recessively inherited small vessel disease (SVD) CARASIL. The same group proposed that the transforming growth factor beta (TGF-β) signaling pathway plays a key role in CARASIL pathogenesis. To learn more about the molecular mechanisms underlying this disorder, especially the link between HtrA1 and TGF-β, HtrA1 knockout (HtrA1$^{-/-}$) mice, that have not been characterized in literature at the beginning of this thesis, were analyzed. Initially, a newly generated mouse strain carrying an *HTRA1* allele interrupted by gene trapping (gt) was available (HtrA1(gt) mice). During the course of this thesis we got access to a second HtrA1 null strain created previously through targeted mutation (tm) (Jones et al., 2011, Zhang et al., 2012). This strain (HtrA1(tm) mice) was used to verify and complement the results of the trapped strain.

3.1.1 The HtrA1(gt) strain

A mouse embryonic stem (ES) cell clone (129/SvEvBrd strain) carrying one *HTRA1* allele interrupted by the insertion of the OmniBank® Gene Trapping vector VICTR 48 within the first intron had been generated as part of a high-throughput gene trapping approach (see also chapter 2.4.1) (Zambrowicz et al., 2003). Microinjection of ES cells into C57BL/6J blastocysts and subsequent breeding of chimeras with wild-type mice (C57BL/6J strain) resulted in the generation of heterozygous offspring with a mixed genetic background (129/SvEvBrd and C57BL/6J). These mice were obtained from Lexicon Genetics/Taconic (Woodlands, TX; New York) and bred to homozygosity.

VICTR 48 contains a splice acceptor (SA) followed by a neomycin selection marker (NEO) and a transcript-terminating polyadenylation signal (pA) (Figure 3.1 A). Thus, a transcript driven by the *HTRA1* promoter that encodes only the first *HTRA1* exon and the NEO sequence is generated from the trapped allele (Figure 3.1 A, left transcript). Exons 2-9 are not included in this *HTRA1* transcript resulting in a loss of HtrA1 protein function. However, together with the partial first exon of the murine Bruton's tyrosine kinase (BTK) gene they are part of a transcript initiated by the ES cell-specific phosphoglycerate kinase (PGK) promoter which is used for the identification of sequence tags from the mutated genes. The presence of termination codons in all three reading frames prevents the translation of *HTRA1* exons (Figure 3.1 A, right transcript).

Genotyping of HtrA1(gt) mice was performed by PCR using the primer pairs depicted in Figure 3.1 A (grey arrows). Amplification resulted in the generation of a 434 bp fragment for the wild-type (WT) locus and a 281 bp fragment for the mutant locus (Figure 3.1 B).

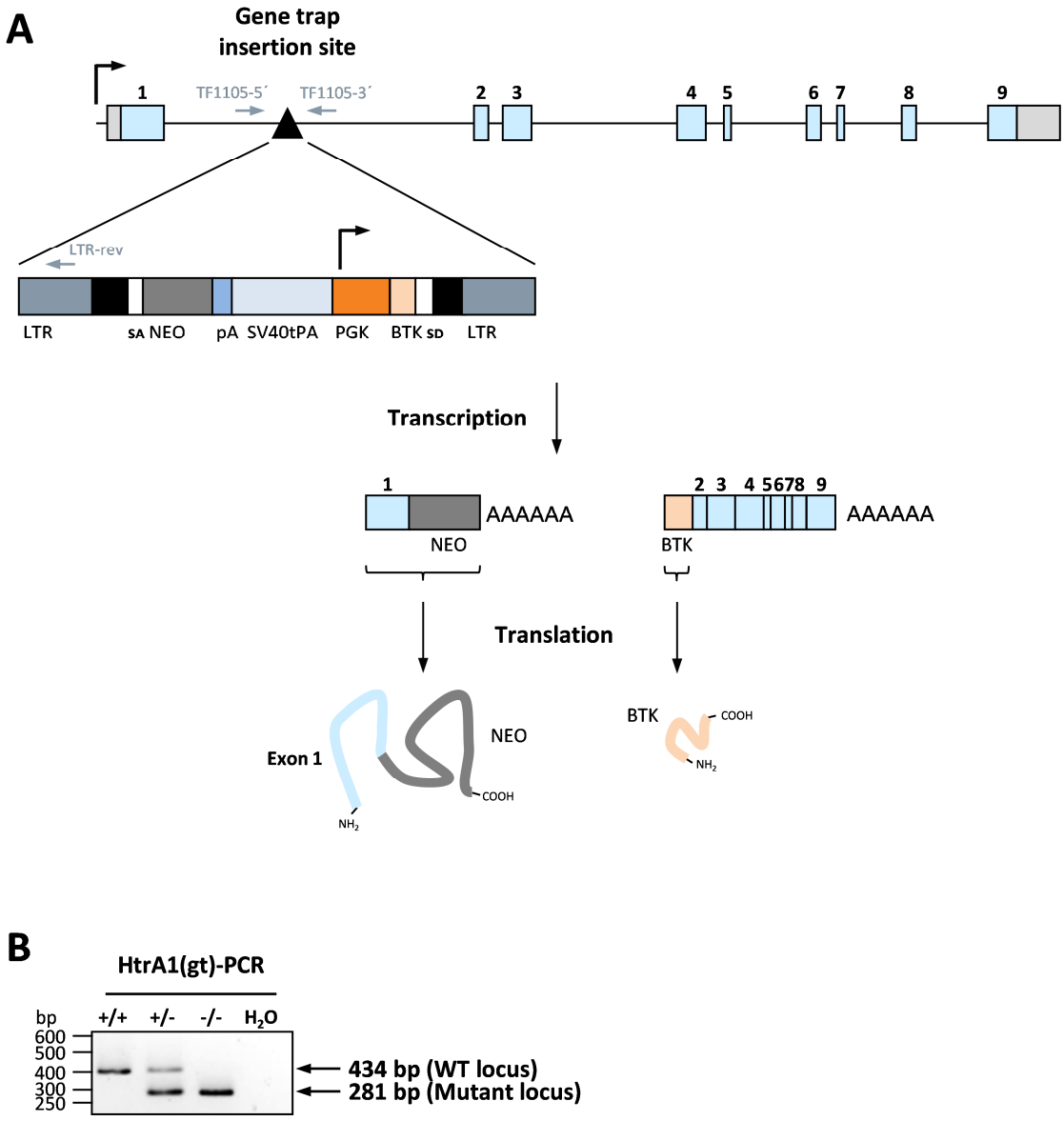

Figure 3.1: Genomic structure followed transcription and translation, and genotyping of the mouse *HTRA1* gene in HtrA1$^{-/-}$(gt) mice. (A) Depicted are *HTRA1* exons (light blue boxes numbered 1-9) and localization of the OmniBank® Gene Trapping vector VICTR 48 (black triangle) containing a splice acceptor (SA) and splice donor site (SD). LTR: long terminal repeat; NEO: neomycin-resistance cassette; pA: polyadenylation signal; SV40tPA: SV40 polyadenylation signal; PGK: phosphoglycerate kinase 1 promoters; BTK: Bruton´s tyrosine kinase exon 1; light grey boxes: untranslated region; black arrows: promoter; grey arrows: primers used for genotyping. Upon transcription two primary transcripts occur, the first contains *HTRA1* exon 1 and NEO, the second *BTK* (contains stop codons in all reading frames) and *HTRA1* exons 2-9. Translated is only the first transcript, while the second one contains only parts of BTK. Curved lines depict proteins. (B) Genotyping by PCR revealed a wild-type (WT) band of 434 bp (primers TF1102-5´and TF1102-3´) and a mutant band of 281 bp (primers TF1102-5´ and LTR-rev; see Table 2.3). +/+: wild-type; +/-: heterozygous; -/-: knockout.

We verified inactivation of the trapped allele on mRNA level by PCR with different primer pairs (arrows, Figure 3.2 A). Using primers spanning exons 1 through 6 including the gene trap insertion site, a band of 672 bp was amplified in kidney tissues derived from HTRA1$^{+/+}$(gt) and HTRA1$^{+/-}$(gt) mice (Figure 3.2 B, left panel). However, no transcript was detected in HTRA1$^{-/-}$(gt) mice demonstrating the interruption of the trapped allele. Similar results were obtained with primer pairs spanning exons 2 through 6 (middle panel, Figure 3.2 B), or exons 6 through 9 (right panel, Figure 3.2 B) yielding PCR products of 559 bp and 309 bp. This was confirmed in other tissues including brain and lung (see Fig. 3.3).

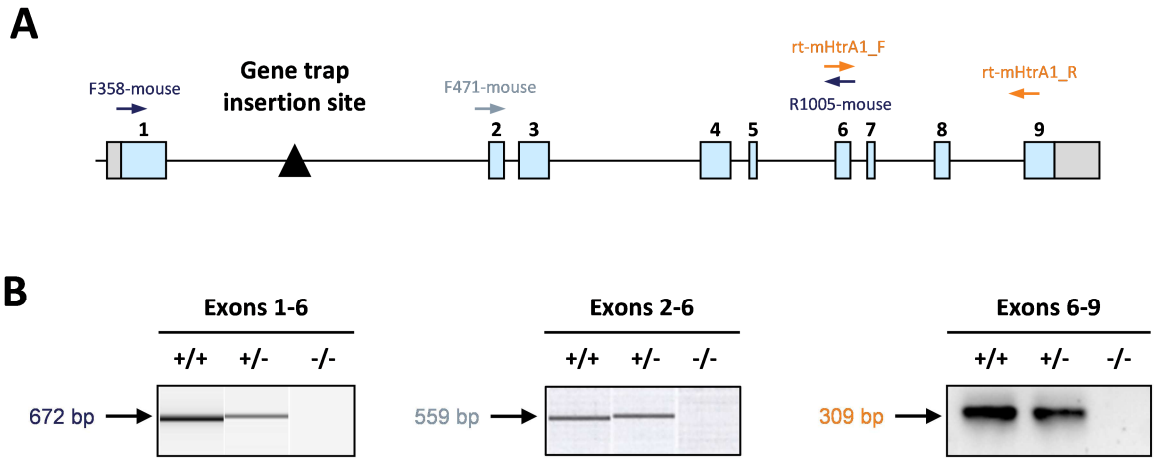

Figure 3.2: Loss of HtrA1 mRNA expression in HtrA1$^{-/-}$(gt) mice. (A) Genomic structure of the mouse *HTRA1* gene with exons depicted as light blue boxes. Arrows indicate the position of the primers (see Table 2.3); the black triangle represents the localization of the gene trapping vector. (B) HtrA1 mRNA expression was analyzed in kidney samples using three different primer pairs. None of them amplified a detectable band in HtrA1$^{-/-}$(gt) mice. Exon 1-6 and 2-6 fragments were visualized by the QIAxcel capillary electrophoresis system (Qiagen), exon 6-9 fragments by regular agarose gel electrophoresis.

To quantify HtrA1 mRNA expression levels, real-time PCR was performed on brain, kidney and lung samples using primers spanning exons 6 to 9. While no transcripts were detected in homozygous knockout mice, HtrA1 mRNA expression was reduced to about 50 % in heterozygous mice (Figure 3.3 A). A verification of HtrA1 deficiency in mouse tissues on protein level was only possible upon combined immunoprecipitation/immunoblotting performed by N. Beaufort (ISD, Munich) due to low HtrA1 expression levels in the wild-type mice (Beaufort et al., 2014). In cell lysates and concentrated supernatants of mouse embryonic fibroblasts HtrA1 protein was detected by common Western blotting (see chapter 3.4.3.1) and the knockout validated.

HtrA3 and HtrA4 share extensive homology with HtrA1 (see Figure 1.5) and might have redundant activities (Clausen et al., 2002). We investigated their mRNA expression levels by real-time PCR in brain tissue and observed no significant changes (Figure 3.3 B). These data demonstrated the absence of compensation on mRNA level in HtrA1(gt) deficient mice.

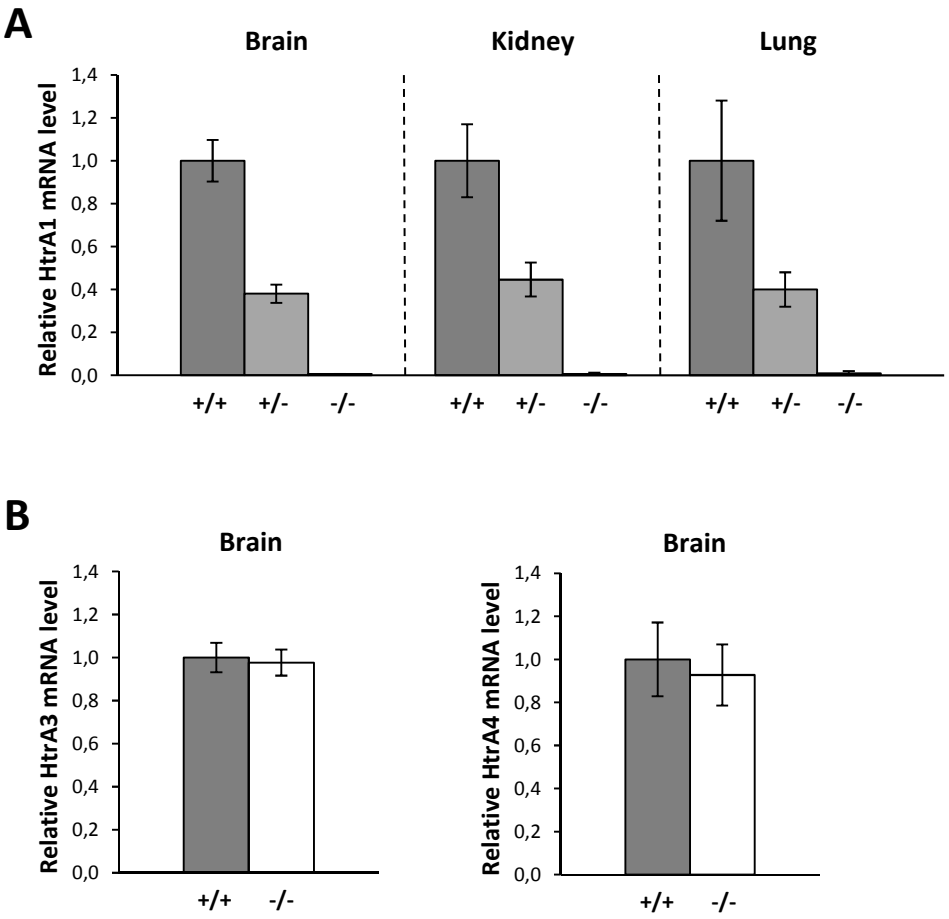

Figure 3.3: HtrA1, HtrA3 and HtrA4 mRNA expression analysis in HtrA1(gt) mice. (A) Relative HtrA1 mRNA levels from brain, kidney and lung samples isolated from HtrA1(gt) mice were determined by real-time PCR (β-Actin was used for normalization) using primers spanning exon 6 to 9. n=3. (B) HtrA3 or HtrA4 mRNA levels of brain samples isolated from HtrA1(gt) mice were normalized to β-Actin mRNA levels. n=6; results are expressed as mean ±SEM and are not significant as determined by Mann-Whitney Rank Sum Test

3.1.2 The HtrA1(tm) strain

During the course of this thesis we got access to a second HtrA1 knockout mouse model (HtrA1(tm); see also chapter 2.4.1), which had previously been generated by C. Oka (Nara Institute of Science and Technology, Japan) (Jones et al., 2011, Zhang et al., 2012). This strain provided us with the opportunity to confirm findings in an independent model. In contrast to HtrA1(gt) mice, this strain had been backcrossed over several generations. To precisely determine the homogeneity of the genetic background, 1449 SNP (single nucleotide polymorphism) markers across 19 autosomes as well as the X chromosome were genotyped representatively in two animals (Taconic, New York). They were found to be 98.3 and 99.1 % identical to the C57BL/6J strain

demonstrating a fairly homogenous genetic background equivalent to approximately six backcrosses (Markel et al., 1997).

This strain had been created by homologous recombination with a gene targeting vector containing an IRES-lacZ reporter element as well as a neomycin-resistance sequence (NEO) followed by a transcript-terminating polyadenylation signal (pA) which causes the exclusion of most of exon 1 sequence including the ATG initiation codon (Figure 3.4 A). Thus, no HtrA1 protein can be translated from the transcript driven by the endogenous *HTRA1* promoter.

Genotyping of HtrA1(tm) mice was performed by PCR using primer pairs located within exon 1 (WT allele) and the NEO cassette (mutant allele) resulting in fragment sizes of 297 bp and 280 bp respectively (Figure 3.4 B).

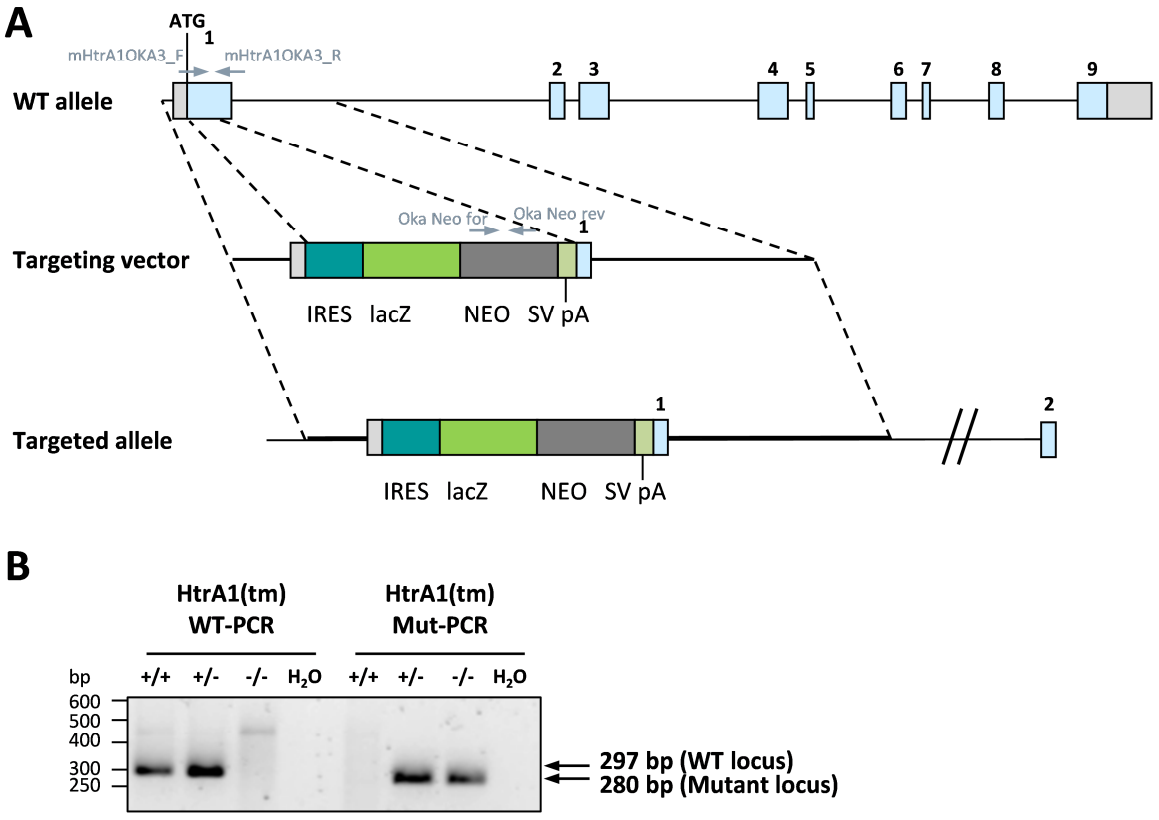

Figure 3.4: Genomic structure and genotyping of the mouse *HTRA1* gene in HtrA1$^{-/-}$(tm) mice (adapted from Jones et al. (2011)). (A) Depicted are *HTRA1* exons (light blue boxes numbered 1-9) and the targeting vector containing an IRES-lacZ reporter element, a neomycin-resistance sequence (NEO) and a SV polyadenylation signal (pA). Light grey boxes: untranslated region; grey arrows: primers used for genotyping. (B) Genotyping by PCR revealed a WT band of 297 bp and a mutant band of 280 bp (for primers see Table 2.3)

Like in HtrA1(gt) mice, inactivation of the targeted allele was verified on mRNA level by real-time PCR using primers spanning exons 6 to 9. Again, no HtrA1 transcripts were detected in lung

samples of HtrA1$^{-/-}$ animals (Figure 3.5 A). Furthermore, HtrA3 and HtrA4 mRNA levels were not elevated in HtrA1$^{-/-}$(tm) mice but even reduced (Figure 3.5 B).

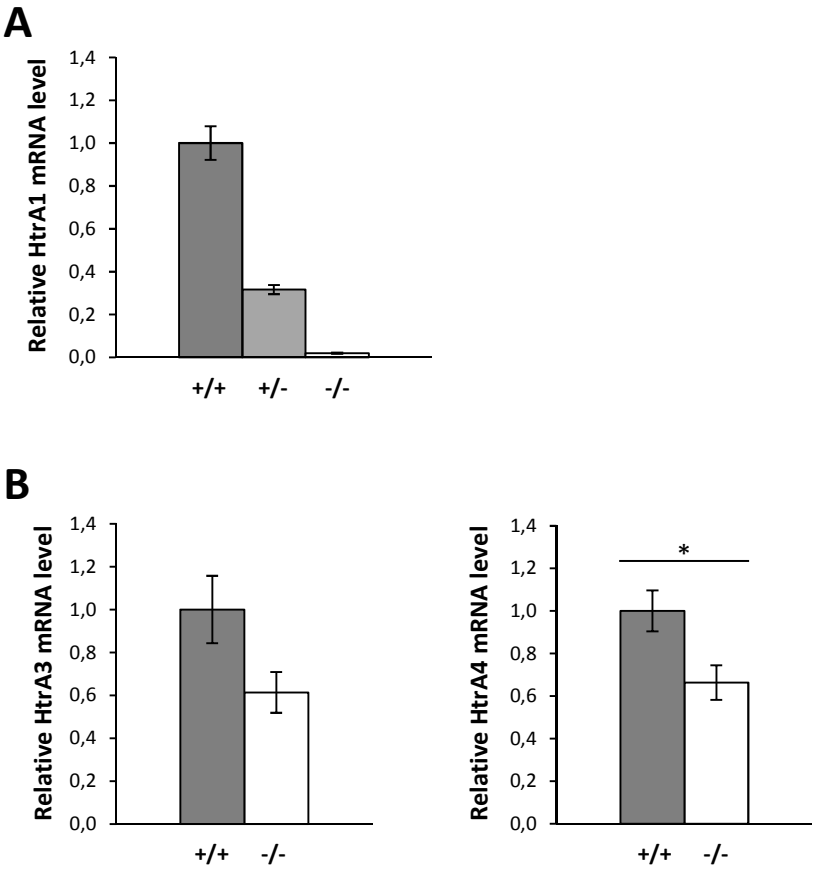

Figure 3.5: HtrA1, HtrA3 and HtrA4 mRNA expression analysis in HtrA1(tm) mice. (A) Relative HtrA1 mRNA levels of lung samples isolated from HtrA1(tm) mice were determined by real-time PCR (β-Actin was used for normalization) using primers spanning exons 6 to 9. n=3-4. (B) HtrA3 or HtrA4 mRNA levels of brain samples isolated from HtrA1(tm) mice were normalized to β-Actin mRNA levels. n=7-9; results are expressed as mean ±SEM; * $p < 0.05$, Mann-Whitney Rank Sum Test.

In summary, these data demonstrated the absence of HtrA1 expression in the HtrA1(gt) as well as HtrA1(tm) mouse strain. Furthermore, no signs of compensation by other HtrA family members were observed. We therefore continued by analyzing the consequences of HtrA1 deficiency.

The results presented in the following sections were obtained with HtrA1(gt) mice unless stated otherwise.

3.1.3 Basic characterization of HtrA1$^{-/-}$ mice

Our initial analyses performed on adult animals (see chapter 3.1.1 and 3.1.2) indicated that HtrA1-deficient mice are viable. To confirm this statistically the genotypes of 100 offspring from heterozygous parents were determined (Table 3.1). The numbers obtained were in agreement with a Mendelian distribution demonstrating the absence of embryonic lethality.

Table 3.1: Mendelian inheritance of HtrA1 mice. The numbers represent the percentages of genotypes determined from 100 individuals with heterozygous parents.

Genotype	+/+	+/-	-/-
Inheritance HtrA1	25 %	53 %	22 %

Furthermore, breeding of homozygous mice produced normal litter sizes demonstrating no impairment of fertility.

Next, we analyzed the body weight of 10 and 24 months old mice. Neither in male nor in female HtrA1$^{-/-}$ animals differences were observed relative to wild-type animals (Figure 3.6).

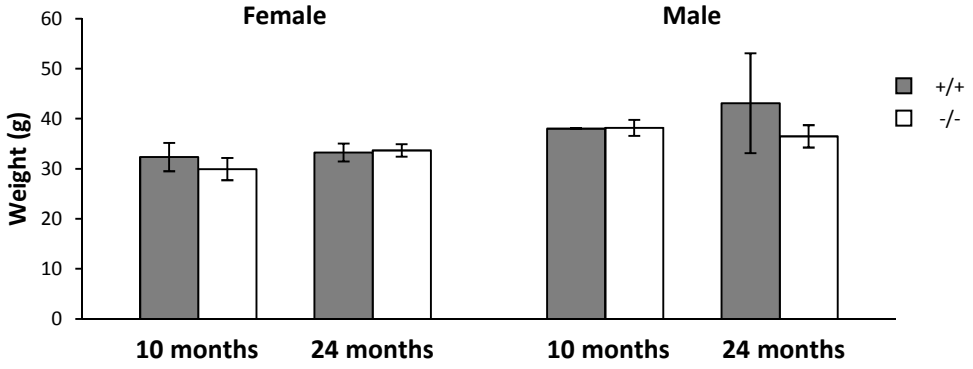

Figure 3.6: Body weight of HtrA1$^{-/-}$ mice was similar to age-matched wild-type littermates. Body weight of 10 months (n=4) or 24 months old (n=4-6) female and 10 months (n=1-5) or 24 months old (n=2-4) male HtrA1 mice was measured. Results are expressed as mean ±SEM and are not significant as determined by Mann-Whitney Rank Sum Test.

In order to assess the survival over time, a Kaplan-Meier curve was generated (Figure 3.7). Mice sacrificed at specific time points were not included. Even though a higher lethality was observed for HtrA1$^{-/-}$ mice in the first year, this finding was not significant. Overall, the lifespan of HtrA1-deficient animals was comparable to that of wild-type littermates.

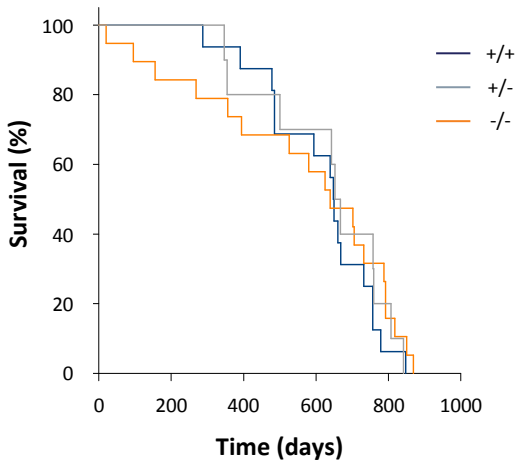

Figure 3.7: Kaplan-Meier survival curve. The x-axis depicts the age of the mice in days. The y-axis depicts the fraction of survival in %. n=10-19; ANOVA on Ranks statistical test found no significant difference between the three groups.

In summary, HtrA1$^{-/-}$ mice did not show abnormalities with respect to embryonic and adult survival, inheritance, litter size or body weight.

3.2 Analysis of extraneurological CARASIL symptoms

Typical extraneurological manifestations of CARASIL patients are spondylosis, kyphosis and alopecia (Fukutake, 2011, Yanagawa et al., 2002). Thus, we investigated these features in aged HtrA1$^{-/-}$(tm) mice.

3.2.1 No alopecia in HtrA1$^{-/-}$ mice

Behavior-associated hair loss (so-called “overgrooming” or whisker/hair and fur trimming, nibbling as well as eating) has long been observed in laboratory mice (Long, 1972, Sarna et al., 2000, Strozik and Festing, 1981), and alopecia is common in mouse and human aging (Novak and Meyer, 2009, Trifunovic et al., 2004). Nevertheless, we analyzed alopecia in 19-20 months old HtrA1(tm) mice by visual inspection. Quantification was performed by photographing the animals and ranking the degree of hair loss on a scale from 0 (no alopecia) to 3 (severe alopecia). Figure 3.8 A shows examples of mice with completely intact fur (left pictures) as well as of mice with areas of alopecia (right pictures). Especially hair loss at the area around the nose, which is typical for laboratory mice, was found in almost all animals (Figure 3.8 B). When hair loss was evaluated separately at the body, head and snout, HtrA1$^{-/-}$ mice did not show alopecia to a stronger degree compared to their

heterozygous or wild-type littermates (Figure 3.8 C). However, due to the difficulty of assessing specific hair loss, the relevance of this analysis should not be considered too high.

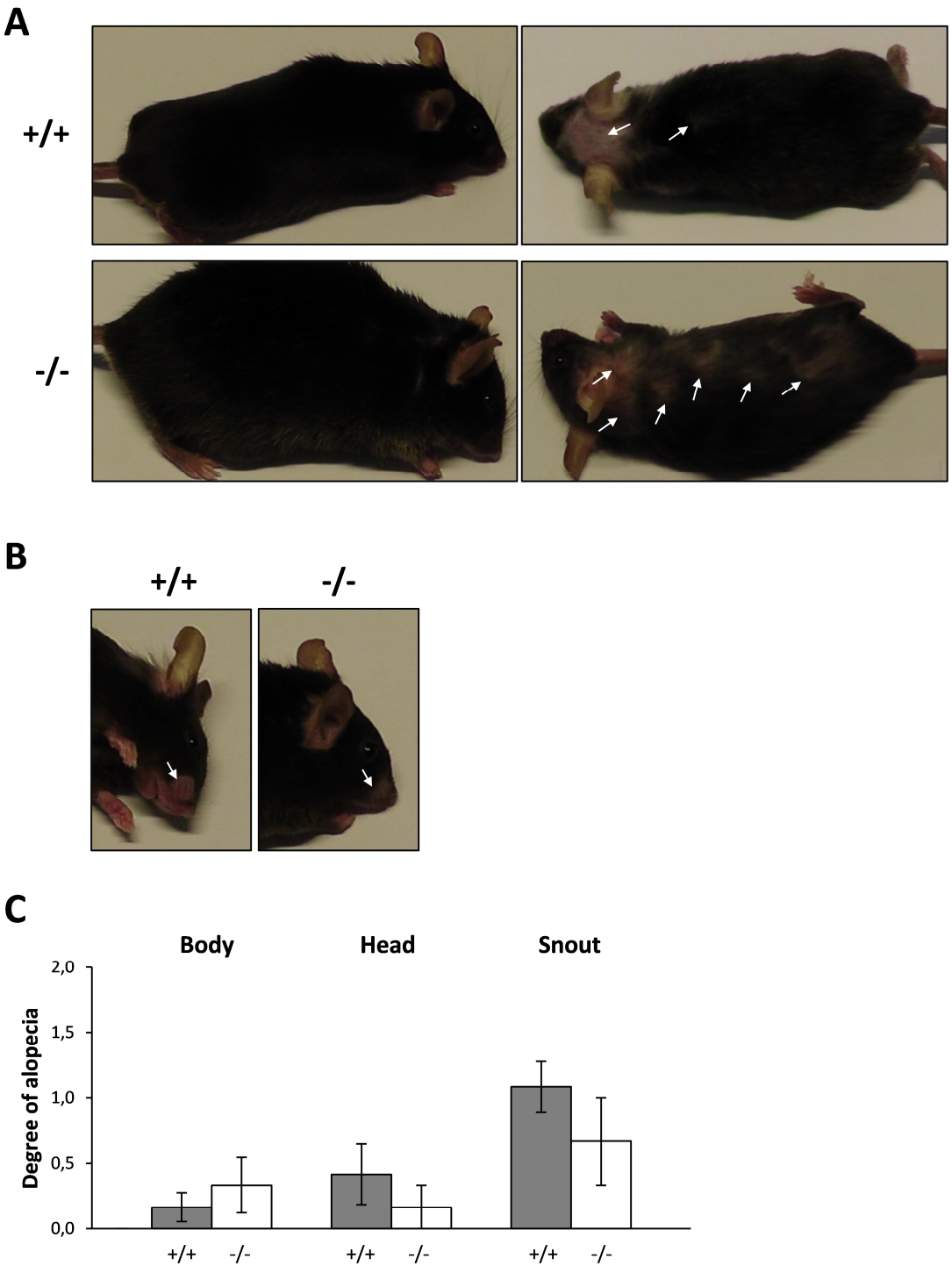

Figure 3.8: Alopecia in HtrA1(tm) mice. 19-20 months old mice were photographed and evaluated for alopecia by visual inspection. (A, B) Arrows indicate areas of hair loss at the whole body (A) or at the snout (B). (C) Quantification of alopecia. Severity of alopecia was evaluated semi-quantitatively on a scale from 0 (no alopecia) to 3 (severe alopecia). n=6-12; results are expressed as mean ±SEM and are not significant as determined by Mann-Whitney Rank Sum Test.

3.2.2 No spondylosis in HtrA1$^{-/-}$ mice

To investigate skeletal abnormalities, 18-19 months old HtrA1(tm) mice were checked for dysmorphology by X-ray examination in a Faxitron MX-20 (collaboration with the German Mouse Clinic, Neuherberg, Germany). The following parameters were screened: skull shape; orbit; mandible, maxilla, teeth; vertebrae (cervical, thoracic, lumbar, sacral and caudal; for number and shape); scapulas, clavicle, humerus, ulna, radius; ribs (for number and shape); pelvis; femur (for diameter and shape); tibia, fibula; digits (for number and completeness); and joints. HtrA1$^{-/-}$ mice did not show abnormalities concerning any of these parameters. In addition, no spondylotic differences between wild-type and knockout animals were detected (Figure 3.9 A). Some animals displayed kyphosis (Figure 3.9 B, C), a well-known aging-related phenotype in humans and rodents (Katzman et al., 2010, Trifunovic et al., 2004), and/or scoliosis (Figure 3.9 D), conditions that are associated with spondylosis. However, these alterations were observed in animals of all genotypes and no significant differences could be found in HtrA1-deficient mice.

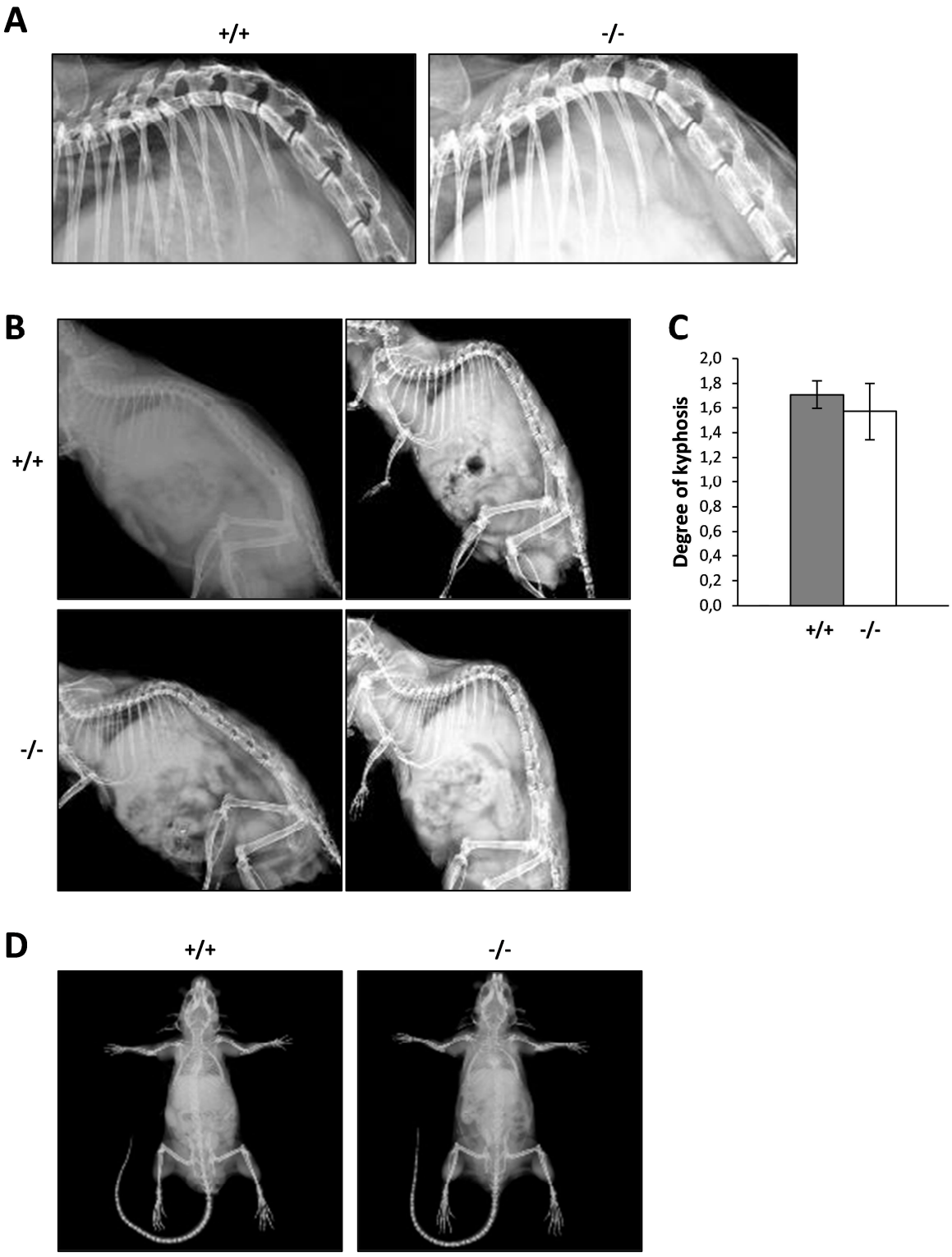

Figure 3.9: X-ray analysis. 18-19 months old HtrA1(tm) mice were analyzed by X-ray. (A) No spondylosis deformans in HtrA1(tm) mice. (B, D) Some animals showed kyphosis (B, right panels), normal spine shape (B, left panels) and/or scoliosis (D) in a genotype independent manner. (C) Quantification of kyphosis. Severity of kyphosis was evaluated semi-quantitatively by visual inspection of X-ray pictures: 0, no kyphosis; 3, severe kyphosis. n=7-12; results are expressed as mean ±SEM; * $p < 0.05$, Mann-Whitney Rank Sum Test.

3.3 Analysis of cerebral CARASIL symptoms

3.3.1 Reduction of cerebral α-smooth muscle actin (α-SMA) expression in HtrA1$^{-/-}$ mice

CARASIL represents an arteriopathy characterized by the loss of vascular smooth muscle cells (vSMCs) in cerebral small vessels (Oide et al., 2008). To investigate whether this pathological feature is recapitulated in HtrA1-deficient mice, we quantified mRNA levels of the vSMC marker α-smooth muscle actin (α-SMA) in brains from 2, 12 and 18-26 months old mice by real-time PCR. While α-SMA mRNA was similar in 2 months old HtrA1$^{+/+}$ and HtrA1$^{-/-}$ mice, we found a trend towards lower levels in 12 months old HtrA1$^{-/-}$ animals (Figure 3.10). In 18-26 months old mice, we detected a significant reduction of ~50 % in Htra1-deficient animals.

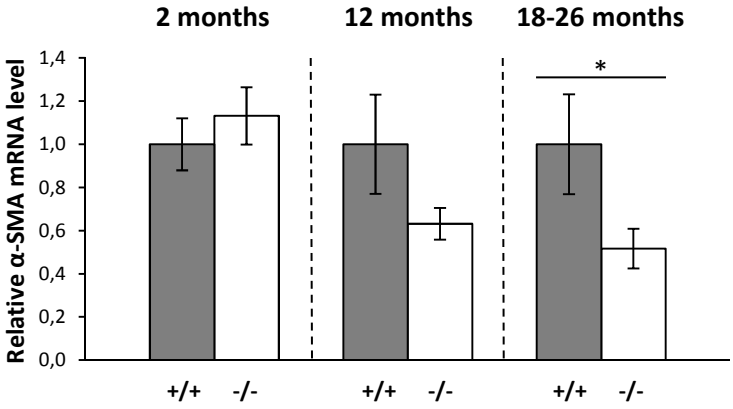

Figure 3.10: Decreased cerebral α-SMA mRNA expression in aged HtrA1$^{-/-}$ animals. α-smooth muscle actin (α-SMA) mRNA levels of brain samples isolated from 2, 12 and 18-26 months old HtrA1 mice were determined by real-time PCR and normalized to β-Actin. 2 months: n=4-7; 12 months: n=5-6; 18-26 months: n=7-10; results are expressed as mean ±SEM; * $p < 0.05$ Mann-Whitney Rank Sum Test.

Next, we examined α-SMA protein levels by quantification of Western blot signals normalized to β-Actin (same mice that were used for mRNA analysis were partially also used for further α-SMA studies). In 2 months old knockout mice we detected increased α-SMA expression levels (Figure 3.11). In contrast, a reduction was observed in 12 and 20-26 months old HtrA1$^{-/-}$ animals. These results are similar to those observed by real-time PCR and show that aged HtrA1-deficient mice display less α-SMA expression.

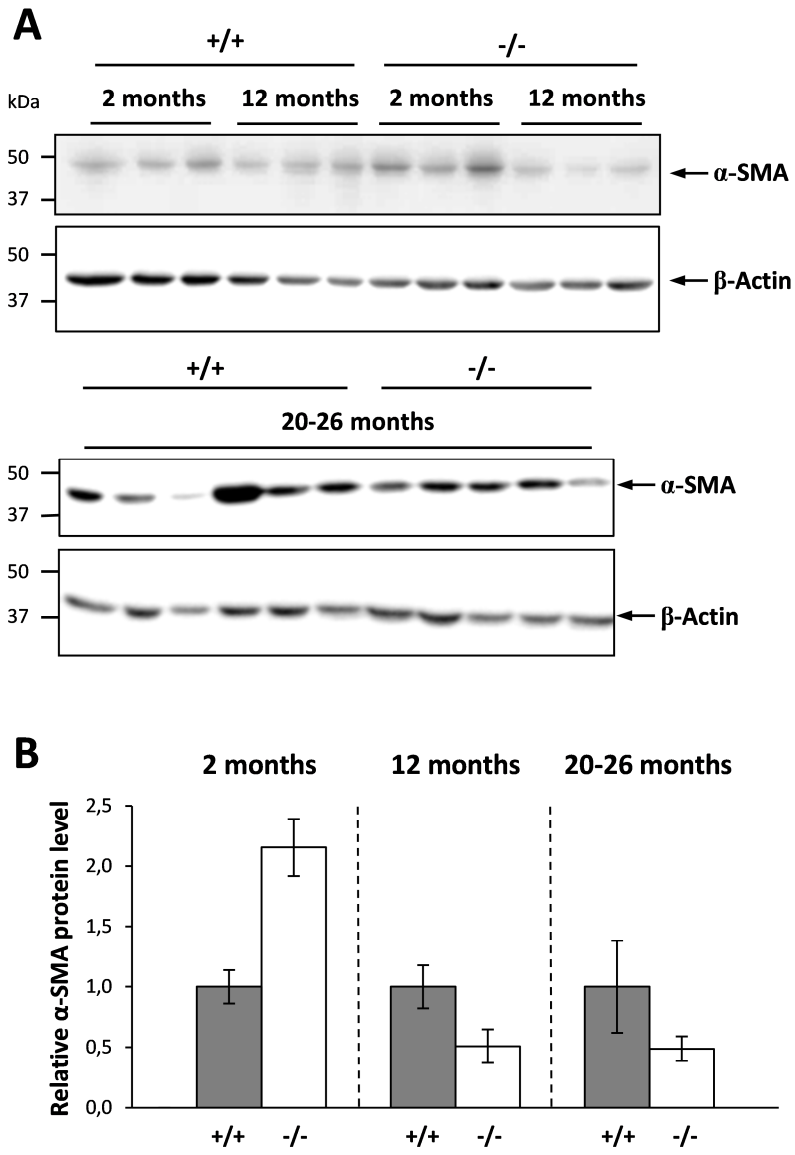

Figure 3.11: Reduction of α-SMA protein expression in brains of aged HtrA1$^{-/-}$ mice. (A) α-SMA protein levels were analyzed by immunoblotting of equal amounts of brain samples derived from 2, 12 or 20-26 months old HtrA1 mice using an α-SMA antibody (42 kDa; upper panels). Detection of β-Actin expression (42 kDa; lower panels) was used for normalization. (B) α-SMA protein levels were normalized to β-Actin. 2 months, 12 months: n=3; 20-26 months: n=6; results are expressed as mean ±SEM and are not significant as determined by Mann-Whitney Rank Sum Test.

To further investigate this finding, we probed cerebral coronal cryo sections derived from the 20-26 months old animals that also underwent α-SMA mRNA and protein analysis with an α-SMA antibody and co-stained with laminin to visualize the vessels (one section per mouse per area, in total 2 areas). Figure 3.12 depicts representative images showing α-SMA expressing vessels in a larger magnification (Figure 3.12 A) and a lower magnification (Figure 3.12 B). Upon quantification of total stained area (Figure 3.12 C) and the number of α-SMA immunopositive vessels per picture

(0.6 mm^2; taken with a 10 x objective; Figure 3.12 D) we found a significant difference between wild-type and knockout mice in the corpus callosum (cc) and a clear trend in the cortex: cerebral α-SMA immunopositive areas in the vessels as well as the vessel number were decreased in knockout animals.

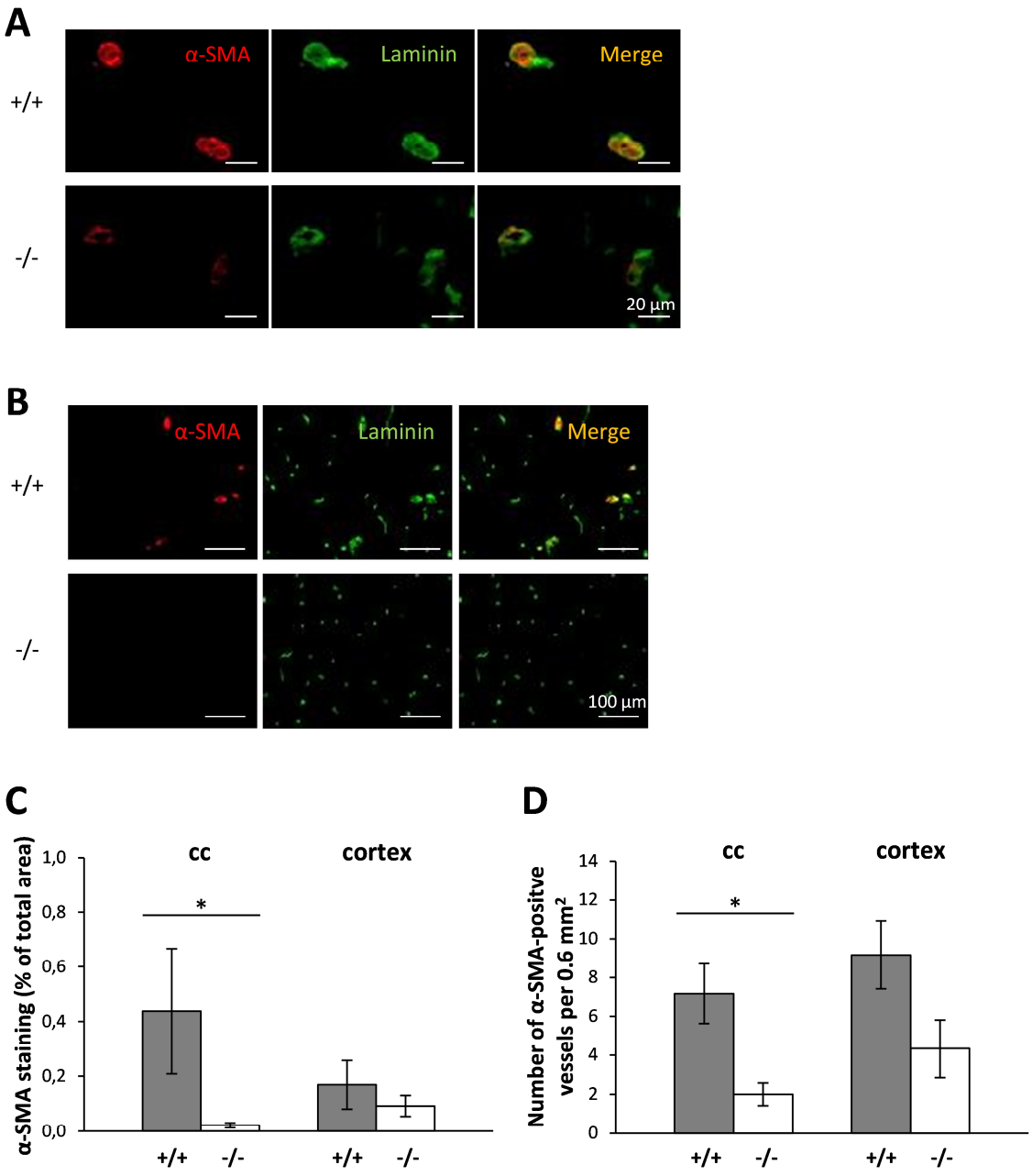

Figure 3.12: Decreased α-SMA levels in aged HtrA1 knockout animals demonstrated by immunohistochemistry. (A, B) One brain hemisphere per 20-26 months old HtrA1 mouse was cut coronally and sections were stained with an α-SMA antibody (red) and co-stained with an Laminin antibody (green). Pictures show representative α-SMA stainings of vessels of the corpus callosum taken with a 40 x objective (A) or with a 10 x objective (B). (C) Quantification of the α-SMA immunopositve area in the corpus callosum (cc) and cortex of 20-26 months old HtrA1$^{-/-}$ compared to HtrA1$^{+/+}$ mice expressed as a percentage of the total image area. (D) Number of α-SMA immunopositve vessels per image (0.6 mm^2; taken with a 10 x objective; counted manually, false-positive background-artifacts were excluded by co-localization with the laminin staining) in the cc and cortex of 20-26 months old HtrA1$^{-/-}$ compared to HtrA1$^{+/+}$ mice. n=6; results are expressed as mean ±SEM; * $p < 0.05$, Mann-Whitney Rank Sum Test.

In summary, α-smooth muscle actin expression is reduced in aged HtrA1$^{-/-}$ mouse brains on mRNA and protein level.

3.3.2 Decreased cerebral type IV collagen expression in aged HtrA1$^{-/-}$ mice

Another characteristic feature of CARASIL is a reduced immunoreactivity of the basal lamina protein type IV collagen in the cerebrovasculature (Oide et al., 2008). In order to evaluate collagen IV expression in our mouse model, we measured its protein levels in various brain regions of aged animals via immunohistochemistry (one brain section per mouse per area, in total 6 areas). As CARASIL is primarily a disease of the WM (Fukutake, 2011), mainly these regions were investigated separately (anterior commissure, anterior part; corpus callosum including forceps minor of the corpus callosum; internal capsule; fimbria of the hippocampus), but also two grey matter regions (cortex; hippocampus). Figure 3.13 A shows representative type IV collagen stainings from the corpus callosum of an HtrA1$^{+/+}$ (upper panels) and HtrA1$^{-/-}$ (lower panels) mouse brain. After quantification, a reduction was observed in HtrA1-deficient animals in most areas, but significance was reached only in cc, aca and cortex (Figure 3.13 B). However, counting the number of collagen IV immunopositive vessels per picture revealed no differences indicating a decrease of basal lamina thickness per vessel (Figure 3.13 C). Note, that the vascular density is higher in the cortex than in the white matter regions. This can be explained by the fact that neurons, mainly present in grey matter regions including the cortex, have a far higher demand of oxygen and nutrients than white matter regions and thus are better supplied with blood (Cavaglia et al., 2001).

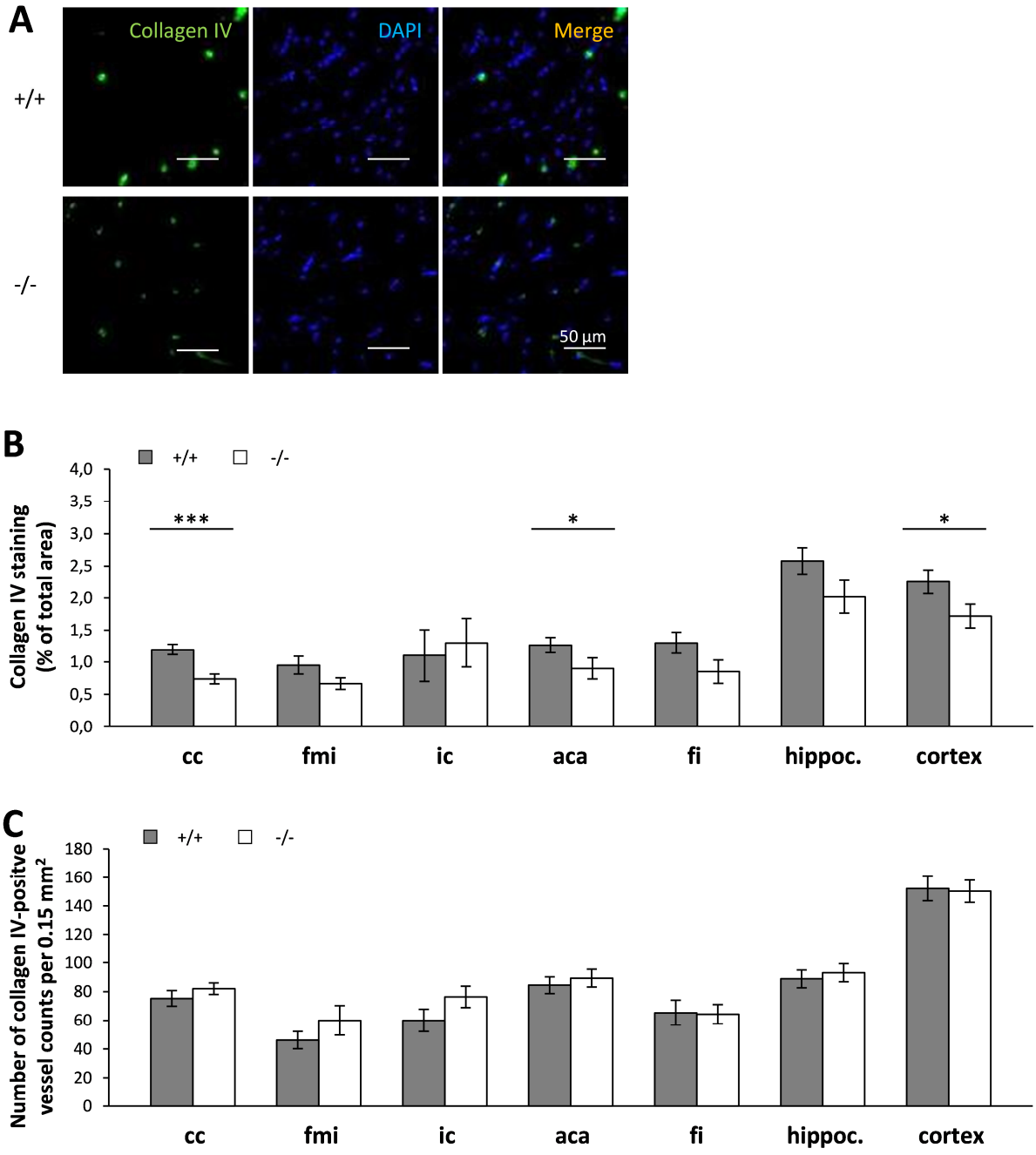

Figure 3.13: Aged HtrA1$^{-/-}$ mouse brains show a reduced type IV collagen expression. (A) Brain sections of 20-26 months old HtrA1 mice were stained with collagen IV antibody (green) and nuclei were visualized with DAPI (blue). Pictures show a representative staining of the corpus callosum. (B) Quantification of the collagen IV immunoreactive area in the corpus callosum (cc), forceps minor of the corpus callosum (fmi), internal capsule (ic), anterior commissure, anterior part (aca), fimbria of the hippocampus (fi), hippocampus (hippoc.) or cortex of 20-26 months old HtrA1$^{-/-}$ compared to HtrA1$^{+/+}$ mice expressed as a percentage of the total image area. (C) Number of collagen IV immunopositve vessel counts per image (0.15 mm^2; taken with a 20 x objective) in different brain areas of 20-26 months old HtrA1$^{-/-}$ compared to HtrA1$^{+/+}$ mice. n(animals)=6; n(evaluated sections per genotype)=6-34; results are expressed as mean ±SEM; * $p < 0.05$, *** $p < 0.001$, Mann-Whitney Rank Sum Test.

3.3.3 No white-matter vacuolization but diffuse demyelination in HtrA1$^{-/-}$ mouse brains

The most characteristic MRI finding in CARASIL patient brains are white-matter lesions (Fukutake and Hirayama, 1995). In mice such lesions can be visualized histologically by Klüver-Barrera Luxol fast blue staining followed by quantification of brain vacuolization as demonstrated in the CADASIL mouse model (Joutel et al., 2010). We therefore stained coronal cryo sections of 20-26 months old HtrA1 animals with Klüver-Barrera Luxol fast blue staining to visualize lesions, white matter structure and myelin (two sections per mouse per area, in total 5 areas). The regions of interest (corpus callosum; internal capsule; anterior commissure, anterior part) were analyzed separately and images were evaluated semi-quantitatively with respect to the presence of vacuoles by visual inspection (see chapter 2.7.3). We hardly detected any vacuoles in the investigated brain regions of transgenic mice as well as of age-matched non-transgenic littermates (Figure 3.14). Figure 3.14 A shows representatively the occurrence of very few lesions (arrows) in the corpus callosum of an HtrA1$^{+/+}$ and an HtrA1$^{-/-}$ mouse. However, HtrA1$^{-/-}$ mice did not display a higher number of vacuoles than their wild-type littermates (Figure 3.14 B).

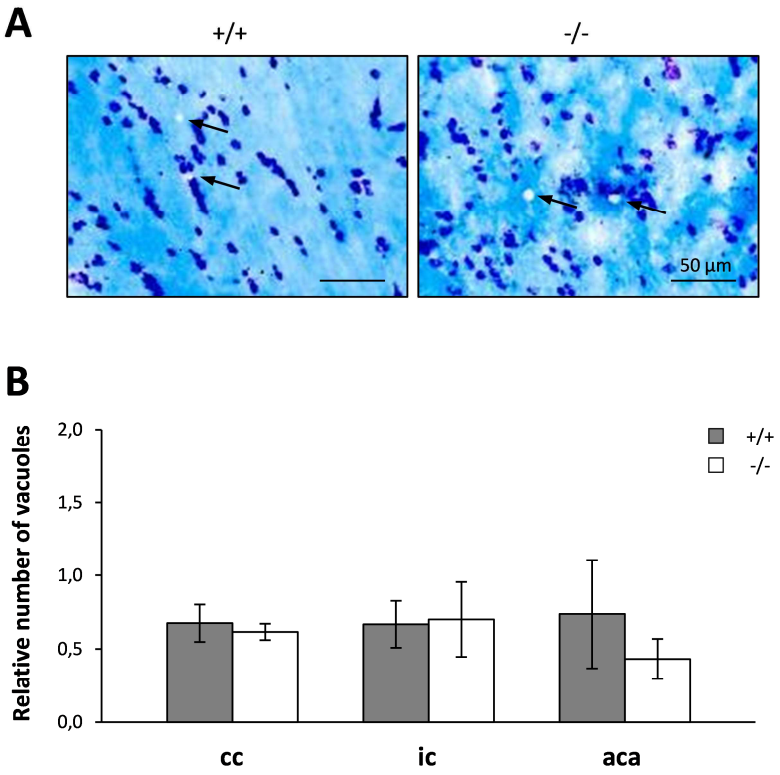

Figure 3.14: White-matter vacuolization in HtrA1 mice. (A) Brain sections of 20-26 months old HtrA1 mice were stained with Klüver-Barrera Luxol fast blue staining (myelin appears in blue, nuclei in purple). Pictures show representative stainings of the corpus callosum. Arrows indicate the position of the vacuoles. (B) Semi-quantitative quantification of vacuoles in the corpus callosum (cc), internal capsule (ic) and anterior commissure, anterior part (aca) by visual inspection: 0, no vacuoles; 1, a few vacuoles; 2, several vacuoles. n(animals)=6; cc: n(evaluated pictures per mouse)=16-22; ic: n(evaluated pictures per mouse)=1-4; aca: n(evaluated pictures per mouse)=2-4; results are expressed as mean ±SEM and are not significant as determined by Mann-Whitney Rank Sum Test.

Moreover, as diffuse myelin loss in the cerebral WM is also typical for CARASIL patients (Arima et al., 2003), we investigated the structure of myelin sheaths upon Klüver-Barrera Luxol fast blue staining of coronal sections of 20-26 months old mice. We found disorganized myelin fibers with diffuse demyelination in HtrA1$^{-/-}$ mouse brains (Figure 3.15 A; see also Figure 3.14 A), that was significant after quantification (Figure 3.15 B). In contrast, control mice showed nearly intact myelin.

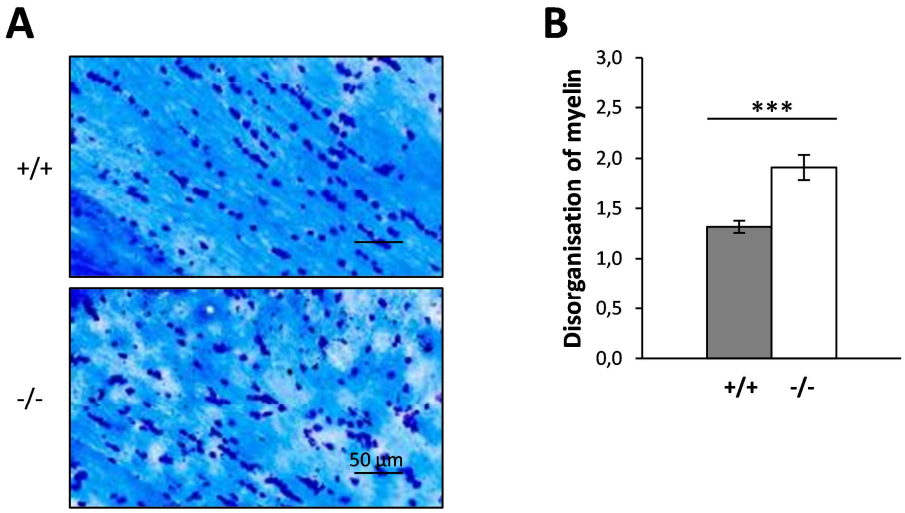

Figure 3.15: Disorganized myelin sheaths with diffuse demyelination in HtrA1$^{-/-}$ mice. (A) Brain sections of 20-26 months old HtrA1 mice were stained with Klüver-Barrera Luxol fast blue staining; myelin appears in blue, nuclei in purple. Pictures show a representative staining of the corpus callosum. (B) Quantification of disorganized myelin sheaths in the corpus callosum of 20-26 months old HtrA1$^{-/-}$ compared to HtrA1$^{+/+}$ mice. Alterations in myelin structure were determined semi-quantitatively by visual inspection of stained sections: 1, structured organization of myelin sheaths; 2, partially disorganized myelin sheaths; 3, disorganization of myelin sheaths. n(animals)=6; n(evaluated pictures per mouse)=20; results are expressed as mean ±SEM; *** $p < 0.001$, Mann-Whitney Rank Sum Test.

In summary, the histological examination of brains from aged HtrA1$^{-/-}$ mice provided evidence for white matter changes and a reduction of vessel marker proteins indicating the presence of pathological alterations similar to those observed in CARASIL patients.

3.4 Consequences of HtrA1 deficiency on TGF-β signaling

HtrA1 has previously been associated with the transforming growth factor beta (TGF-β) signaling pathway (Launay et al., 2008, Oka et al., 2004). Accordingly, TGF-β activity was reported to be altered in cerebral arteries of CARASIL patients (Hara et al., 2009, Shiga et al., 2011). Therefore, we set out to analyze the consequences of HtrA1 deficiency on TGF-β signaling in HtrA1$^{-/-}$ mice.

3.4.1 Decreased TGF-β signaling in brains of HtrA1$^{-/-}$ mice

The TGF-β life cycle consists of various phases including ligand synthesis and secretion, storage within the extracellular matrix, release of the active ligand and activation of an intracellular signaling cascade resulting in transcriptional alterations (see Figure 1.6). Therefore, pathway activity was examined at several levels.

First, we analyzed SMAD2 phosphorylation, an intracellular indicator of TGF-β activity (see chapter 1.4), by Western blotting using an antibody recognizing the phosphorylated forms of SMAD2 (~60 kDa) and SMAD3 (~50 kDa). In brain lysates of aged mice, a single band of ~60 kDa was observed indicating the presence of predominantly SMAD2 (Figure 3.16 A). In the representative blot shown, the phosphoSMAD2 signal was decreased in all three HtrA1$^{-/-}$ animals tested. Quantification of the signals from 6 mice per group and normalization to β-Actin showed that this reduction is significant (Figure 3.16 B). Total SMAD2 levels could not be clearly detected in these samples. However, SMAD2 mRNA analysis revealed that expression levels were similar in brains of HtrA1$^{+/+}$ and HtrA1$^{-/-}$ mice (Figure 3.16 C).

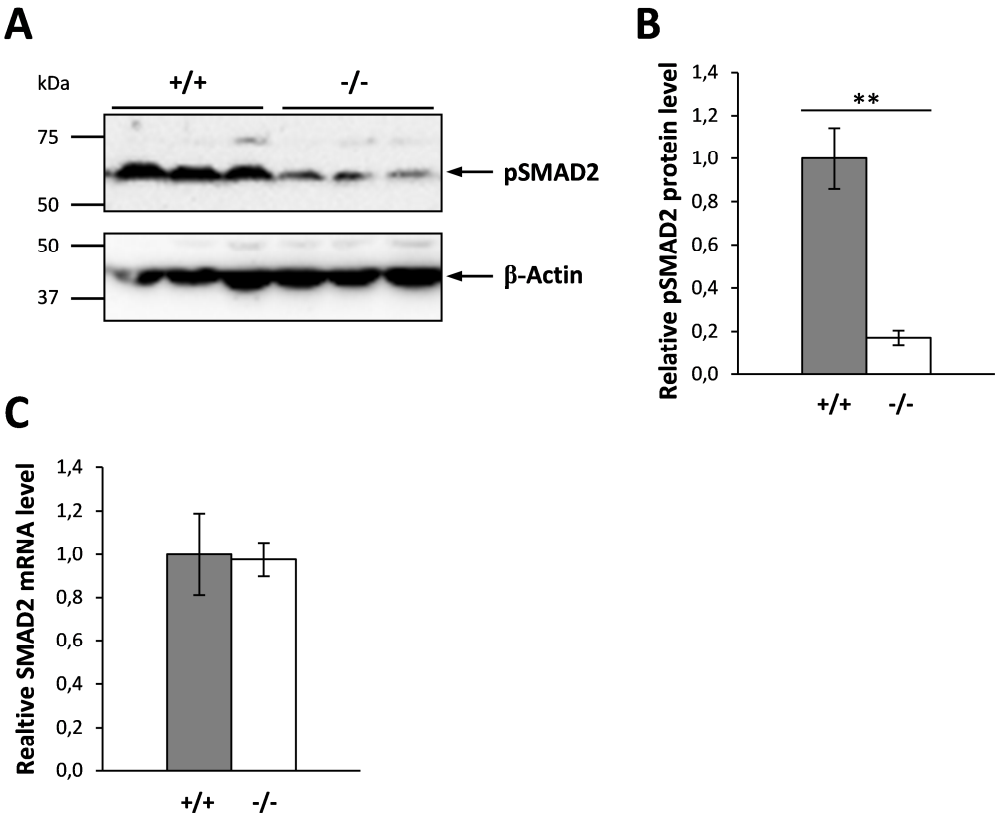

Figure 3.16: Decreased phosphorylation of SMAD2 in HtrA1$^{-/-}$ mouse brains. (A, B) PhosphoSMAD2 levels (60 kDa) were analyzed by immunoblotting of brain lysates derived from 20-26 months old HtrA1 mice using a phosphoSMAD2 antibody (A, representative blot) and normalized to β-Actin (42 kDa) (B). (C) Relative SMAD2 mRNA levels from mouse brains used for phosphoSMAD2 analysis were determined by real-time PCR (β-Actin was used for normalization). n=6; results are expressed as mean ±SEM; ** $p < 0.01$, Mann-Whitney Rank Sum Test.

To allow the localization of the phosphoSMAD2 signal within mouse brains we performed immunohistological stainings. We probed coronal cryo sections from different regions of HtrA1$^{+/+}$ and HtrA1$^{-/-}$ mouse brains with a phosphoSMAD2 antibody (one section per mouse per area, in

total 5 areas; n(WT, KO)=5-6). As damages in CARASIL brains are predominantly detected in WM regions, they were mainly investigated (anterior commissure, anterior part; corpus callosum including forceps minor of the corpus callosum; internal capsule; fimbria of the hippocampus), but also two grey matter regions (cortex; hippocampus). Figure 3.17 A shows a representative phosphoSMAD2 staining taken from corpus callosum of an HtrA1$^{+/+}$ (upper images) and an HtrA1$^{-/-}$ mouse brain (lower images). Phosphorylated SMAD2 translocates to the nucleus, thus the phosphoSMAD2 staining (in red) co-localizes with the nuclear DAPI staining (in blue). As the corpus callosum is a white matter region, labeled cells likely represent predominantly glial cells such as astrocytes and oligodendrocytes. Upon quantification, a significant decrease in phosphoSMAD2 staining was observed in HtrA1-deficient mice (Figure 3.17 B). A similar result was obtained in the forceps minor, internal capsule and cortex. While a trend was seen in the anterior commissure, no clear differences were seen in hippocampal regions.

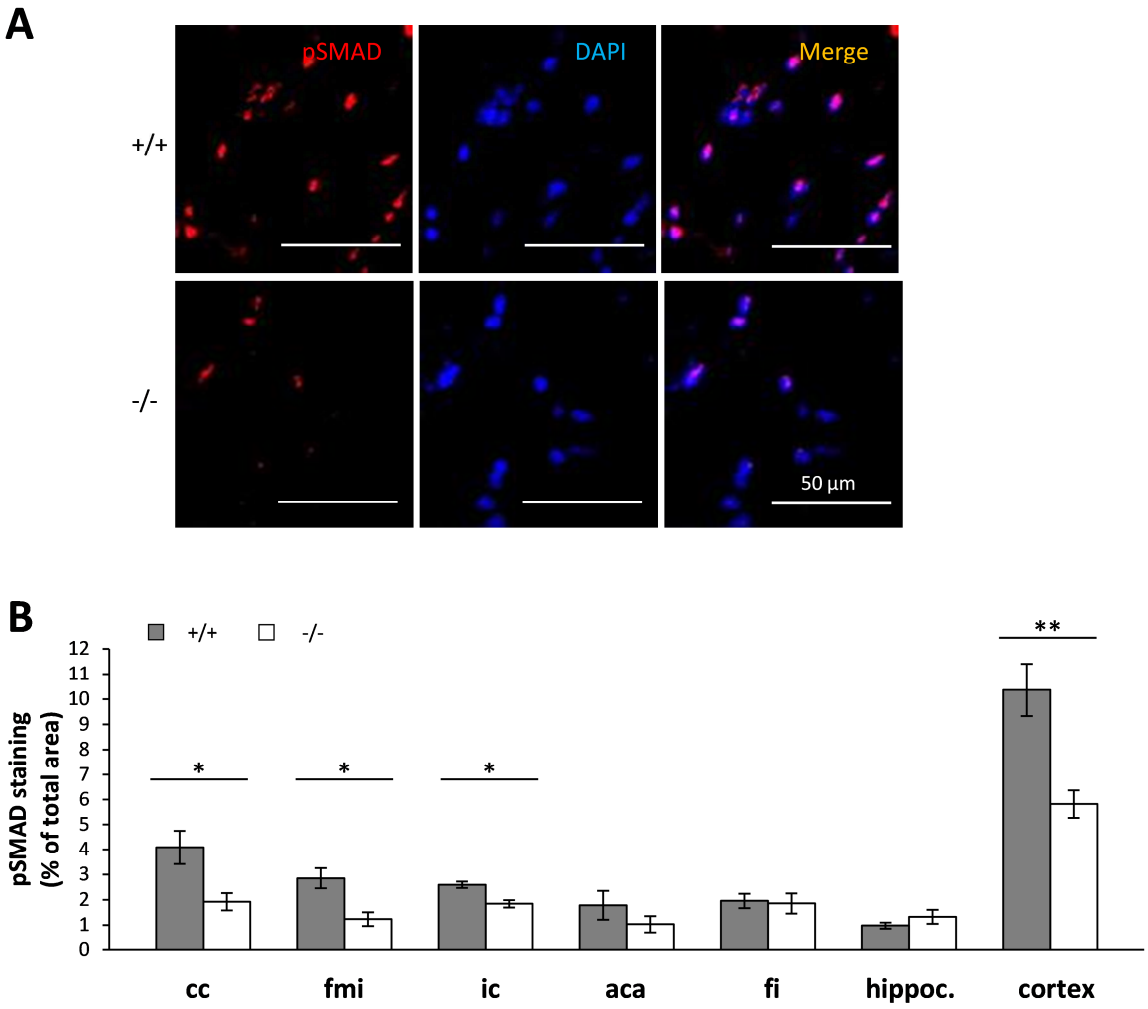

Figure 3.17: Reduced phosphoSMAD2 levels in HtrA1-deficient brains detected by immunohistochemistry. (A) Brain sections of 20-26 months old HtrA1 mice were stained with phosphoSMAD2 antibody (red) and nuclei were visualized with DAPI (blue). Pictures show representative phosphoSMAD2 stainings of the corpus callosum. (B) Representative quantification of the phosphoSMAD2 immunopositve area in the corpus callosum (cc), forceps minor of the corpus callosum (fmi), internal capsule (ic), anterior commissure, anterior part (aca), fimbria of the hippocampus (fi), hippocampus (hippoc.) or cortex of 20-26 months old HtrA1$^{-/-}$ compared to HtrA1$^{+/+}$ mice expressed as a percentage of the total image area. n=5-6; results are expressed as mean ±SEM; * $p < 0.05$, ** $p < 0.01$ Mann-Whitney Rank Sum Test.

In order to confirm these effects on a different TGF-β pathway level, we analyzed mRNA levels of connective tissue growth factor (CTGF), a well-known TGF-β target gene with an important role in angiogenesis (Chen et al., 2000), in whole mouse brains. Again a significant reduction was observed in aged (18-26 months) HtrA1$^{-/-}$ mice (Figure 3.18). A similar result was obtained in younger mice with a significant decrease at 2 months of age and a clear trend at 12 months ($p = 0.052$). This not only confirmed reduced TGF-β signaling activity upon HtrA1 ablation, but also indicated a dysregulation already at a very young age.

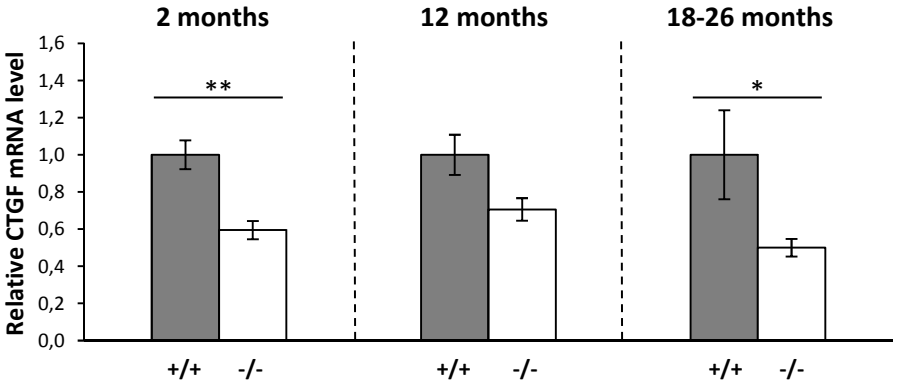

Figure 3.18: Decreased TGF-β target gene expression in HtrA1$^{-/-}$ mouse brains. Relative connective tissue growth factor (CTGF) mRNA levels from 2, 12 and 18-26 months old HtrA1 mouse brains were determined by real-time PCR and normalized to β-Actin. 2 months: n=4-7; 12 months: n=5-6; 18-26 months: n=7-10; results are expressed as mean ±SEM; * $p < 0.05$, ** $p < 0.01$ Mann-Whitney Rank Sum Test.

We further investigated whether the observed effect on TGF-β signaling is systemic or restricted to brain tissue. Blood serum obtained from young and aged mice was analyzed for circulating TGF-β1 concentrations using an ELISA. A similar analysis had been performed previously in a mouse model for Marfan syndrome (Matt et al., 2009), a hereditary connective tissue disorder also associated with a TGF-β dysregulation (Judge et al., 2004, Ng et al., 2004). In contrast to this study, we were unable to detect significant differences in blood TGF-β1 levels between 6 months old HtrA1$^{-/-}$(tm) or 20-26 months old HtrA1$^{-/-}$(gt) and age-matched wild-type littermates (Figure 3.19). Note, that TGF-β1 concentrations increased with age, an effect that was also seen by Matt et al. (2009).

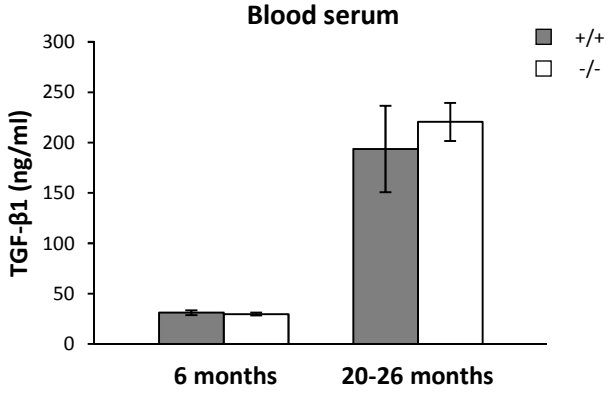

Figure 3.19: TGF-β concentration in serum of HtrA1$^{-/-}$ mice is not altered compared to HtrA1$^{+/+}$ mice. Total TGF-β1 concentrations in ng/ml were determined in serum from 6 months old HtrA1(tm) mice (n=7-10) and 20-26 months old HtrA1(gt) animals (n=5-6) using an ELISA. Results are expressed as mean ±SEM and are not significant as determined by Mann-Whitney Rank Sum Test.

Next, we analyzed TGF-β target gene expression in non-cerebral mouse tissue by quantifying CTGF and PAI-1 (plasminogen activator inhibitor-1) mRNA levels in lung, a heavily vascularized organ, and aorta, the largest artery of the body. Although in three of the four tissue-target gene combinations a trend towards reduced levels in HtrA1$^{-/-}$ mice versus wild-type mice was observed, differences were not significant (Figure 3.20).

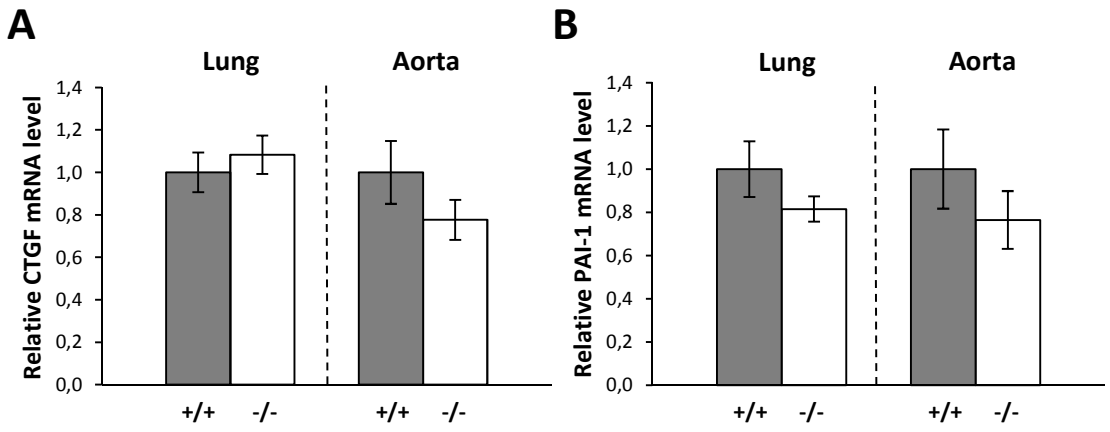

Figure 3.20: TGF-β target gene expression in lung and aorta samples of HtrA1$^{-/-}$ mice similar to HtrA1$^{+/+}$ mice. Relative connective tissue growth factor (CTGF) (A) and plasminogen activator inhibitor-1 (PAI-1) (B) mRNA levels of lung and aorta samples isolated from 6 months old HtrA1(tm) animals were determined by real-time PCR (β-Actin was used for normalization). Lung: n=7-10; aorta: n=6; results are expressed as mean ±SEM and are not significant as determined by Mann-Whitney Rank Sum Test.

In summary, these data indicated decreased TGF-β signaling in HtrA1 knockout mice, an effect apparently restricted to brain tissue.

3.4.2 Decreased TGF-β signaling in isolated brain vessels of HtrA1$^{-/-}$ mice

3.4.2.1 Isolation of brain vessels

Since CARASIL is a vascular disorder we sought to localize the observed TGF-β signaling alterations to cerebral vessels. In collaboration with A. Joutel (University Paris Diderot, France) we established a protocol (illustrated in Figure 3.21 A) to isolate microvessels including pial and intraparenchymal arteries, veins and capillaries from mouse brains with high purity (see chapter 2.4.6). The quality of the preparation was monitored by microscopy (Figure 3.21 B). Depending on the subsequent analysis, vessels were processed for mRNA or protein isolation. Figure 3.21 C demonstrates the strong enrichment of the vascular SMC marker α-smooth muscle actin (α-SMA) in the preparations. The protein yield obtained from different vessel preparations were very low and variable (between 20 and 90 µg per hemisphere) limiting subsequent analyses.

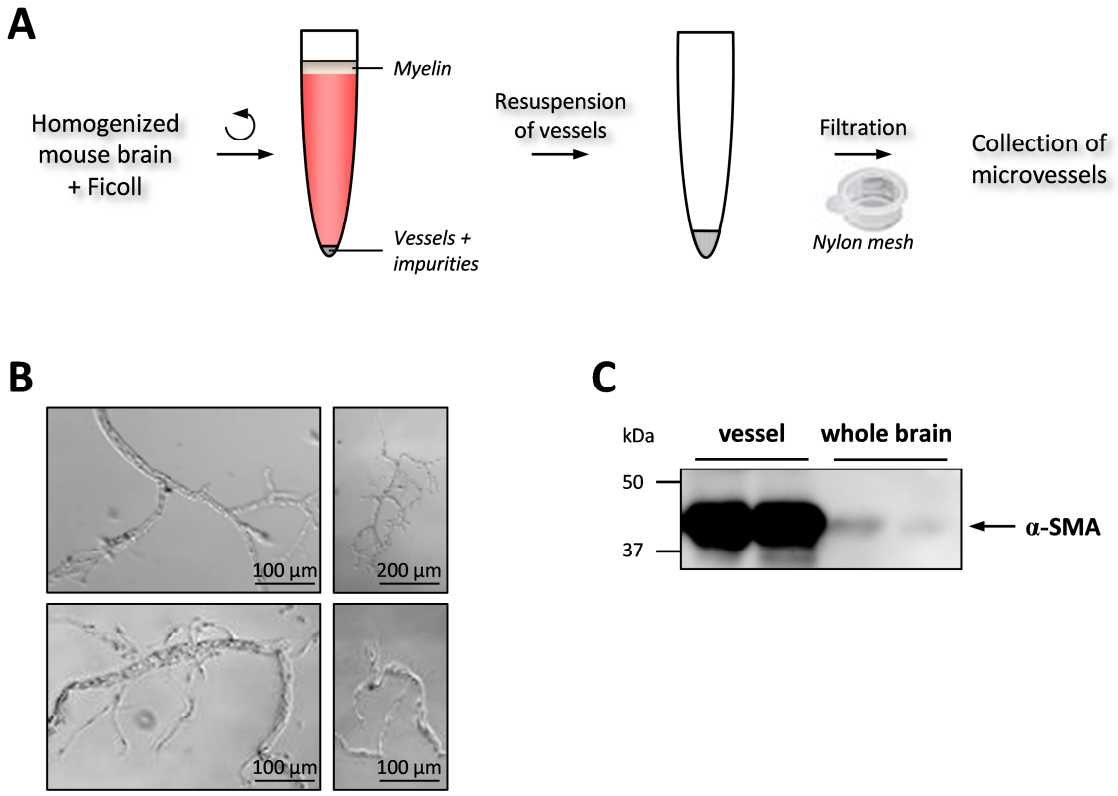

Figure 3.21: Isolation of cerebral microvessels. (A) Schematic diagram of the isolation of vessels from mouse brain. Brain material was homogenized with a smooth pestle to leave blood vessels intact. Myelin was removed by Ficoll density gradient centrifugation yielding a vessel pellet. Tissue debris still present in this fraction was removed by resuspending the pellet and abundant washing on a 40-µm nylon mesh. Purified microvessels were collected by inversion of the mesh. The conus depicts a falcon. (B) Microscopic examination of mouse brain vessels without cell debris. (C) α-SMA protein levels were analyzed by immunoblotting of 5 µg isolated vessel lysates (two bands on the left side) and 5 µg whole brain lysates (two bands on the right side) using an α-SMA antibody (42 kDa).

3.4.2.2 Analysis of TGF-β signaling

To analyze TGF-β signaling in isolated cerebral vessels, we first investigated the intracellular phosphoSMAD2 levels by immunoblotting. In brain vessels of 6 months old HtrA1$^{-/-}$(tm) mice a strong reduction in the phosphoSMAD2 signal compared to wild-type vessels was observed (Figure 3.22 A). Due to the limited amount of material, equal loading of samples could not always be achieved. However, quantification of the phosphoSMAD2 signals and normalization to β-Actin levels demonstrated the significance of this observation (Figure 3.22 B). We also performed real-time PCR studies on mRNA preparations of isolated microvessels. For both analyzed TGF-β target genes, CTGF and PAI-1, we observed a significant reduction in vessels from HtrA1$^{-/-}$ mice (Figure 3.22 C, D) confirming decreased TGF-β signaling as observed by phosphoSMAD2 analysis.

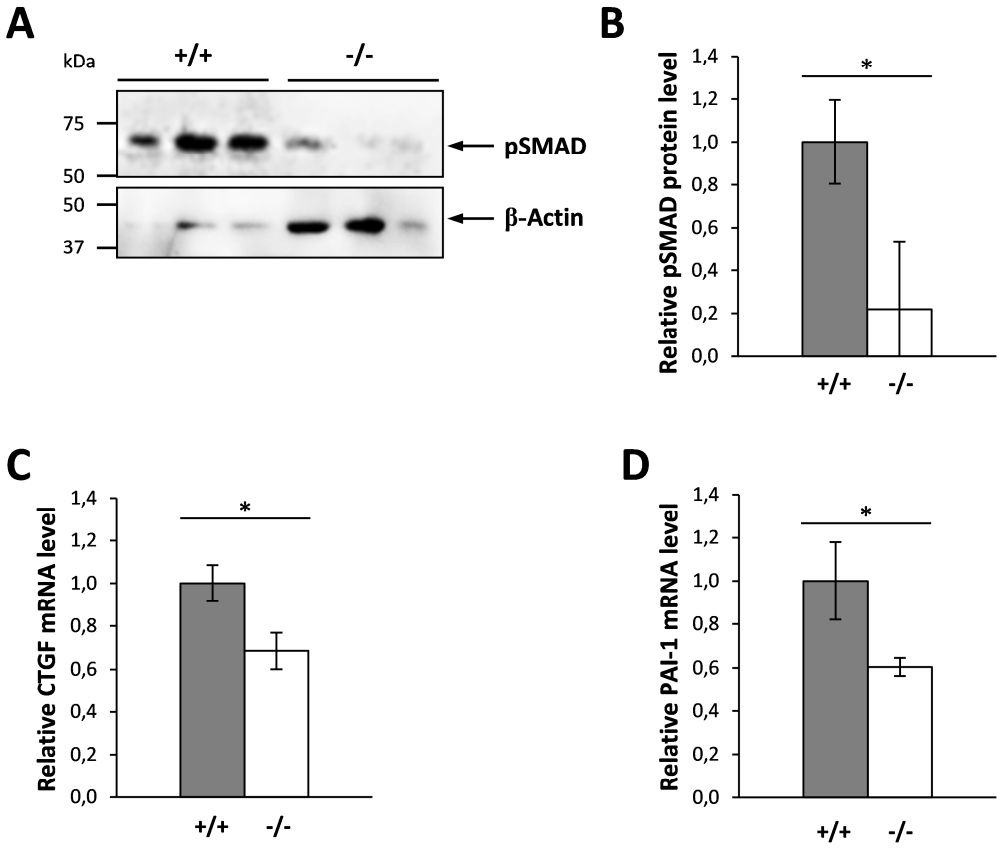

Figure 3.22: Reduced TGF-β1 signaling in isolated brain vessels derived from HtrA1$^{-/-}$ mice. (A, B) Phosphorylation of SMAD2 in cerebral blood vessels. PhosphoSMAD2 levels were analyzed by immunoblotting of microvessels isolated from 6 months old HtrA1(tm) mice using a phosphoSMAD2 antibody (A, representative blot) and normalized to β-Actin (42 kDa) (B); n=4-6. Relative CTGF (C) and PAI-1 (D) mRNA expression from brain vessels were determined by real-time PCR and normalized to β-Actin. n=7-10; results are expressed as mean ±SEM; * $p < 0.05$ Mann-Whitney Rank Sum Test.

Thus, a reduction of TGF-β pathway activity can specifically be observed in brain microvessels from young HtrA1$^{-/-}$ mice (6 months old) confirming our findings from whole brain analysis. Furthermore, as for this analysis HtrA1(tm) mice were used, we could demonstrate a decrease of TGF-β signaling in the cerebral tissue of two different HtrA1$^{-/-}$ mouse models.

3.4.3 Loss of HtrA1 function results in reduced TGF-β signaling in mouse embryonic and human dermal fibroblasts

To study the effects of HtrA1 deficiency on TGF-β in a homogenous cell population under well-defined culture conditions, mouse embryonic fibroblasts (MEF) were used, a popular mouse cell model (Sharpless, 2006) previously applied to study the TGF-β pathway (Graham et al., 2013, Tesseur et al., 2006). Since a serum starvation step, which is detrimental to primary MEF cells, is

often required to measure TGF-β effects, we decided to generate MEF cell lines by serial passaging and spontaneous immortalization.

3.4.3.1 Isolation and immortalization of MEF cells

MEF cells were isolated from 13.5-15.5 days old embryos and propagated in culture (see chapter 2.5.2). Spontaneous immortalization has been described to occur during serial passaging with high frequency resulting from a stochastic genetic event. While the majority of immortalized MEF cell loose either the "Guardian of the Genome" p53 (Lane, 1992), or $p19^{ARF}$ function (Kamijo et al., 1997), various other genetic events can contribute to immortalization (Frank et al., 2000, Jacobs et al., 1999, Kamijo et al., 1999, Sharpless et al., 2001).

Figure 3.23 shows representative growth curves of two $HtrA1^{+/+}$(gt) and two $HtrA1^{-/-}$(gt) MEF cell lines. Within the first 5-7 passages (15-20 days in culture) cells go through a rapid growth phase, before they enter a crisis phase in which they hardly grow or some cells even die. After a lag phase (up to 300 days) cultures start to proliferate again, likely due to a few transformed cells overgrowing the rest of the culture. In total, we isolated and immortalized seven $HtrA1^{+/+}$(gt) and six $HtrA1^{-/-}$(gt) MEF cell lines and immortalized one $HtrA1^{+/+}$(tm) and one $HtrA1^{-/-}$(tm) MEF cell line.

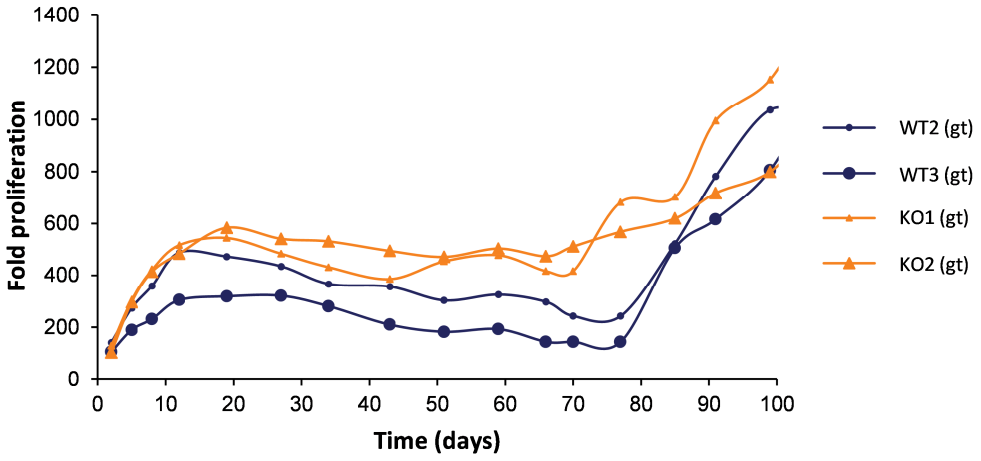

Figure 3.23: Representative growth curves of two wild-type and two knockout HtrA1(gt) mouse embryonic fibroblast lines. Primary HtrA1(gt) MEF cells were isolated from 14.5 days post coitus embryos and immortalized through serial replating as described in chapter 2.5.2. The fold proliferation was calculated with the formula: [((number of harvested MEF cells)-(number of seeded MEF cells))x100]/(number of seeded MEF cells).

The loss of *HTRA1* expression in these lines was confirmed by real-time PCR (Figure 3.24 A). Moreover, HtrA1 deficiency could be demonstrated for the first time on protein level. While immunoblotting of cell lysates detected a ~50 kDa band in wild-type cells, albeit at low intensity (Figure 3.24 B), no signal was observed in $HtrA1^{-/-}$ cells. Even more convincing was the analysis of

10-fold concentrated culture medium which revealed a strong, single band confirming expression and efficient secretion of HtrA1 in MEF cells. This band was not present in HtrA1$^{-/-}$(tm) and HtrA1$^{-/-}$(gt) cells demonstrating the absence of HtrA1 in both mouse models. Compared to HtrA1$^{+/+}$(gt) MEF cells, more HtrA1 protein was found in the conditioned medium of HtrA1$^{+/+}$(tm) MEF cells and less in the lysates probably due to variable expression levels between different cell lines (see chapter 3.4.4) and unequal HtrA1 ratio in lysate and medium (30 µg whole protein of cell lysates were loaded for HtrA1(gt) MEF cells, and only 20 µg were loaded for HtrA1(tm) MEF cells). The ~25 and 75 kDa bands in the lysate of HtrA1(tm)$^{+/+}$ cells likely represent unspecific bands due to crossreactivities of the antibody, while the ~30 kDa band in the HtrA1(tm)$^{+/+}$ cell medium probably results from autodegradation.

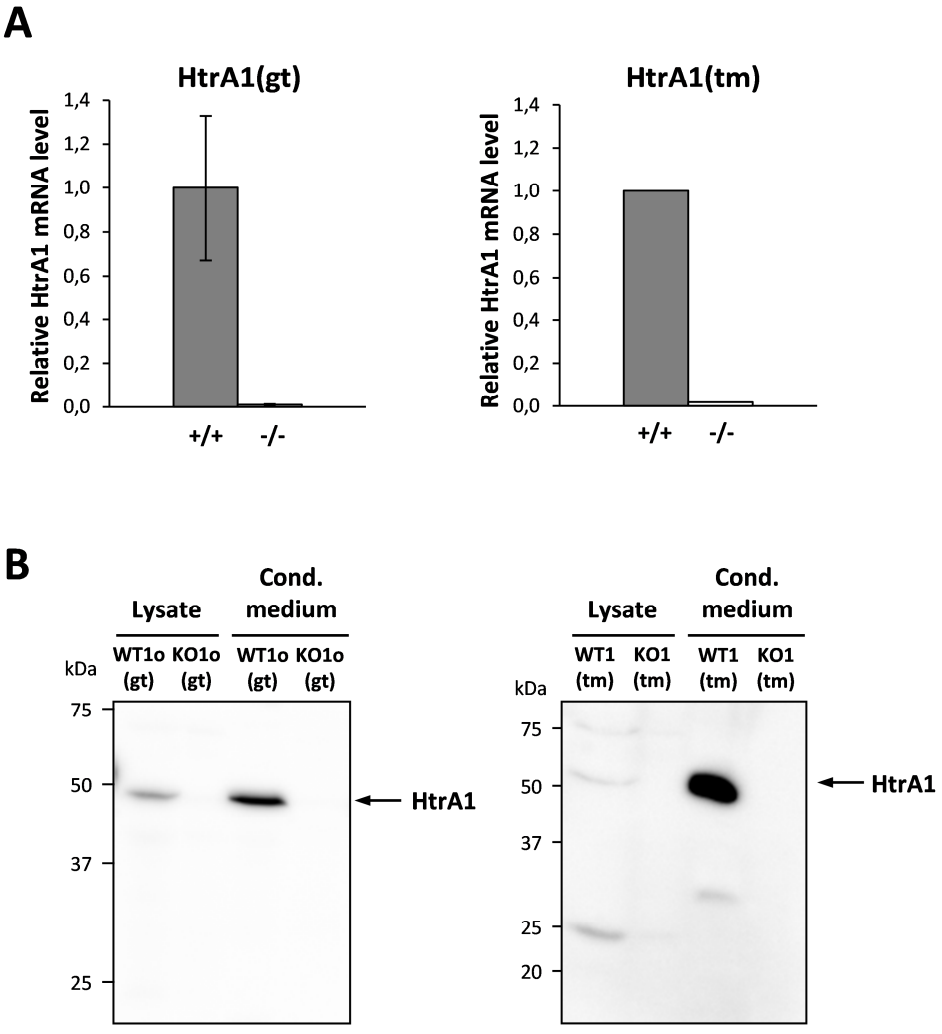

Figure 3.24: HtrA1 expression in HtrA1$^{+/+}$ and HtrA1$^{-/-}$ MEF cells. (A) Relative mRNA levels from 7 HtrA1$^{+/+}$(gt) and 6 HtrA1$^{-/-}$(gt) cell lines (left diagram) or 1 HtrA1$^{+/+}$(tm) and 1 HtrA1$^{-/-}$(tm) (right diagram) cell line were determined by real-time PCR (right diagrams; used primers: rt-mHtrA1_F and rt-mHtrA1_R). The equal expression of the housekeeping gene β-Actin in all cDNA samples guaranteed the correct isolation of RNA and translation to cDNA (data not shown); results are expressed as mean ±SEM. (B) Protein levels were analyzed by immunoblotting of 30 µg HtrA1(gt) (left panel) or 20 µg HtrA1(tm) (right panel) cell lysates and 20 µl 10-fold concentrated medium using the HtrA1(ΔMac) antibody.

Similar to mouse brain tissue, we investigated possible compensatory effects by the HtrA family members HtrA3 and HtrA4 using real-time PCR. As observed before, their mRNA expression levels were rather reduced than elevated in HtrA1$^{-/-}$ MEF cells (Figure 3.25).

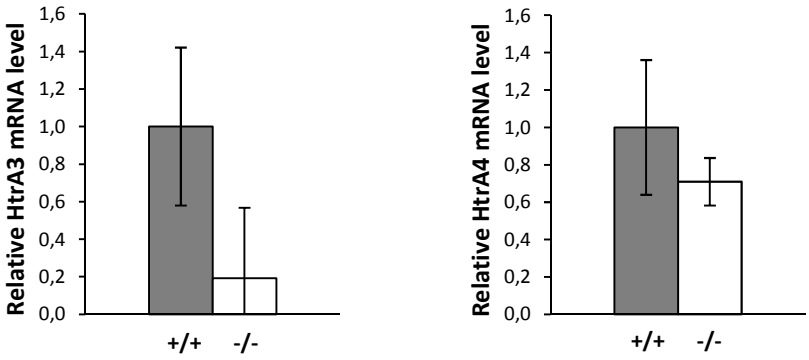

Figure 3.25: HtrA3 and HtrA4 do not compensate for missing HtrA1 on mRNA expression level in MEF cells. HtrA3 and HtrA4 mRNA levels of MEF cells isolated from HtrA1(gt) embryos were determined by real-time PCR and normalized to β-Actin mRNA levels. n=7-8; results are expressed as mean ±SEM and are not significant as determined by Mann-Whitney Rank Sum Test.

Having confirmed HtrA1 deficiency in our MEF cell lines, we turned to the investigation of the TGF-β pathway.

3.4.3.2 Decreased TGF-β signaling in HtrA1$^{-/-}$ MEF cells

In a first step, we quantified TGF-β1 levels in conditioned media collected 48 h after starvation from immortalized MEF cell lines using an enzyme-linked immunosorbent assay (ELISA) (see chapter 2.5.6 and 2.6.8) and found them significantly reduced to about 50 % in HtrA1$^{-/-}$ medium (Figure 3.26 A). In order to correct for cell seeding number variations we normalized total TGF-β levels to whole protein amount in the medium and obtained similar results (Figure 3.26 B, values at 48 h). Moreover, relative TGF-β concentrations in conditioned media collected after different time points (24 h, 48 h and 72 h) increased over time in HtrA1$^{+/+}$ as well as in HtrA1$^{-/-}$ medium and TGF-β levels were significantly decreased in HtrA1$^{-/-}$ medium at each time point.

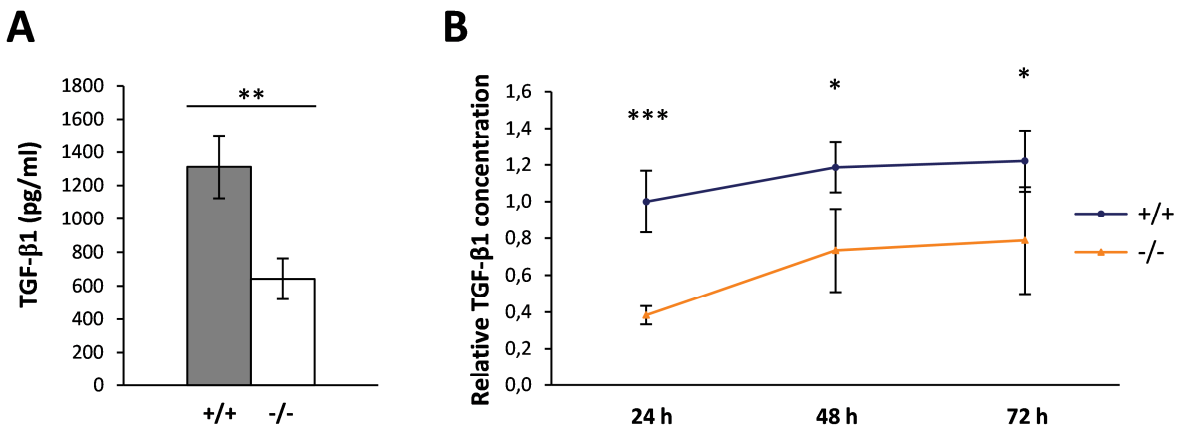

Figure 3.26: TGF-β1 protein levels measured via ELISA are decreased in HtrA1$^{-/-}$ MEF cell media. (A) Total TGF-β1 protein concentrations in pg/ml were determined in supernatants from HtrA1(gt) and HtrA1(tm) MEF cell lines collected after 48 h using an ELISA. (B) TGF-β1 protein levels in supernatants from HtrA1(gt) and HtrA1(tm) MEF cell lines collected after 24 h, 48 h and 72 h were normalized to whole protein amount in the media. n=7-8; results are expressed as mean ±SEM; * $p < 0.05$, ** $p < 0.01$, *** $p < 0.001$ Mann-Whitney Rank Sum Test.

Since only a fraction of TGF-β present in body fluids is signaling-competent, we measured bioactive TGF-β present in the MEF cell medium by a highly sensitive and specific bioassay. It is based on a reporter cell line (MFB-F11) in which the secreted alkaline phosphatase (SEAP) gene is under the control of a minimal promoter containing a TGF-β-responsive SMAD binding element (SBE) (Tesseur et al., 2006). The line was generated by stable transfection of a secreted alkaline phosphatase (SEAP) reporter construct into TGF-β1$^{-/-}$ MEF cells (see chapter 2.5.6 and 2.6.9). Upon stimulation with active TGF-β MFB-F11 cells secrete SEAP whose activity can be measured using a chemiluminescence assay (Figure 3.27 A). In order to assess the sensitivity and linearity of the assay, we stimulated MFB-F11 cells with increasing amounts of recombinant TGF-β1. SEAP activity showed a dose-dependent response to TGF-β1 ranging from 1 pg/ml to 1 ng/ml (Figure 3.27 B) (Tesseur et al., 2006), a range in which concentration of bioactive TGF-β in MEF media was expected (see Figure 3.26 A). Applying this bioassay to MEF cell media conditioned for 48h, we detected significantly decreased TGF-β levels in HtrA1$^{-/-}$ MEF cell media compared to wild-type media (Figure 3.27 C) even after normalization of SEAP activity to total protein amount present in the medium (Figure 3.27 D). Similar results were obtained using the bioassay and MEF media collected after 24 h and 72 h (data not shown).

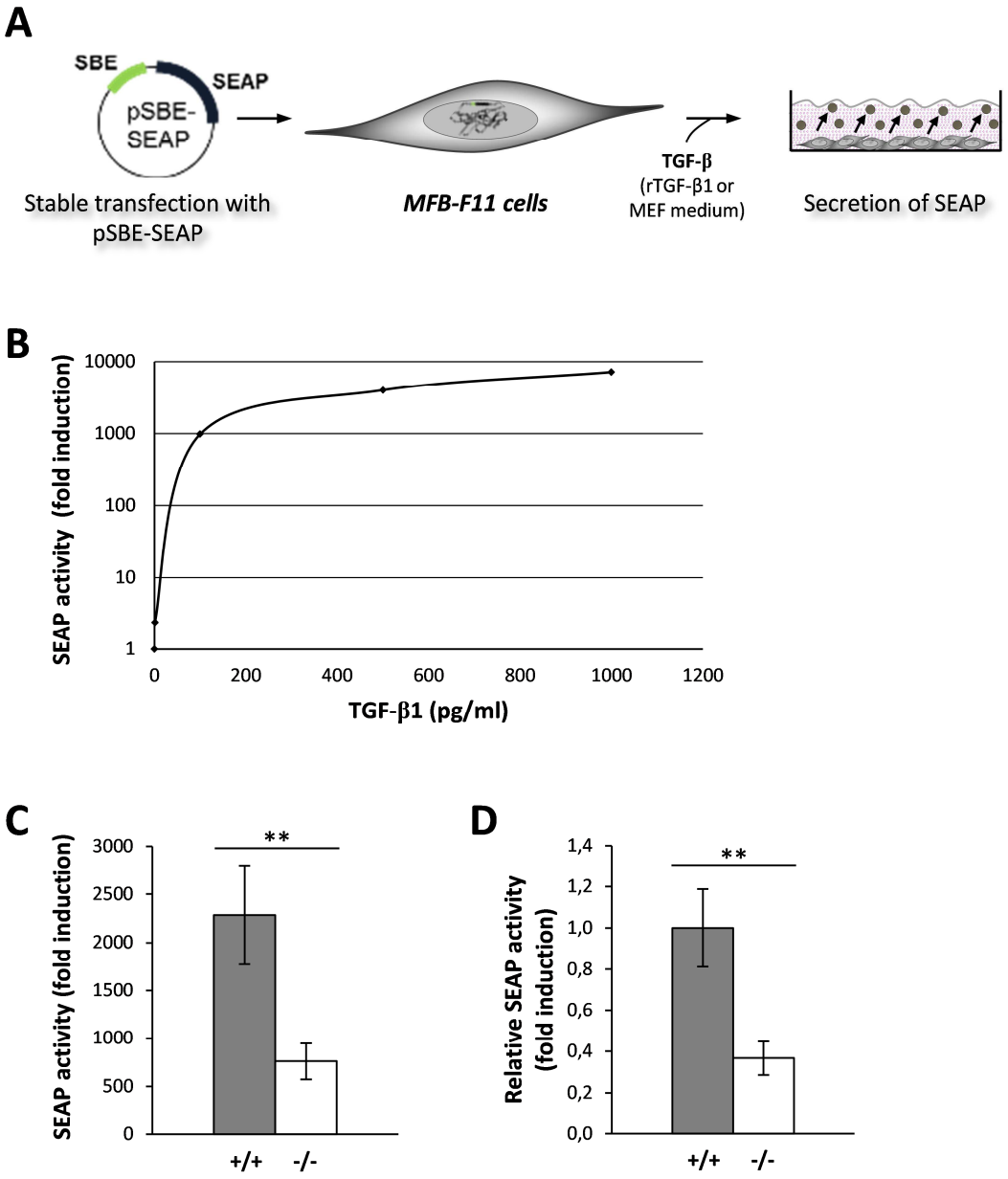

Figure 3.27: Reduced TGF-β1 bioactivity in HtrA1$^{-/-}$ MEF cell media. (A) Scheme of a bioassay to measure active TGF-β1. Mouse embryonic fibroblasts derived from TGF-β1$^{-/-}$ embryos (MFB-F11) were stably transfected with the reporter plasmid pSBE-SEAP consisting of TGF-β responsive SMAD-binding elements (SBE, depicted in light green) coupled to a secreted alkaline phosphatase (SEAP, dark green hemicycle) reporter gene (Tesseur et al., 2006). After seeding and overnight incubation of MFB-F11 cells, recombinant TGF-β1 (rTGF-β1) or conditioned MEF cell medium was added to MFB-F11 cells. SEAP activity was measured after 24 h using a Chemiluminescence kit. (B) TGF-β1 dose-dependently induces SEAP reporter activity in MFB-F11 cells. SEAP activity was measured in the conditioned media of MFB-F11 cells that were cultured with the indicated concentrations of rTGF-β1. Note the logarithmic scale (C) Conditioned medium from HtrA1(gt) and HtrA1(tm) MEF cell lines collected after 48 h activates the TGF-β-responsive reporter cell line MFB-F11, inducing expression of alkaline phosphatase activity. (D) SEAP activity in supernatants from HtrA1(gt) and HtrA1(tm) MEF cell lines collected after 48 h was normalized to whole protein amount in the media. The relative amount of bioactive TGF-β (fold induction) was determined based on the baseline measurement (no TGF-β). n=7-8; results are expressed as mean ±SEM; ** $p < 0.01$ Mann-Whitney Rank Sum Test.

To examine intracellular TGF-β pathway activity we analyzed SMAD2 phosphorylation by immunoblotting of MEF cell lysates. In HtrA1$^{-/-}$ cells clearly reduced phosphoSMAD2 levels were detected (Figure 3.28 A, depicted by a specific ~60 kDa phosphoSMAD2 band). After correction to β-Actin, we detected a significant reduction of phosphoSMAD2 levels to ~30 % (Figure 3.28 B), while SMAD2 mRNA levels were not different in both MEF cell types (data not shown).

Finally, we examined the mRNA expression of the TGF-β target genes PAI-1 and CTGF. We observed a strong reduction by ~90 % of both mRNA levels in HtrA1$^{-/-}$ MEF cells. While the decrease in PAI-1 expression was significant, that of CTGF was not due to a large standard deviation (Figure 3.28 C, D). It is striking, that in HtrA1$^{-/-}$ cells the target gene mRNA levels are stronger reduced than the TGF-β concentration, the TGF-β bioactivity and the phosphoSMAD2 levels. This finding results from the fact, that we found large variations between individual MEF cell lines. However, as the tendency observed in all assays was the same, we think that these differences are not of physiological importance.

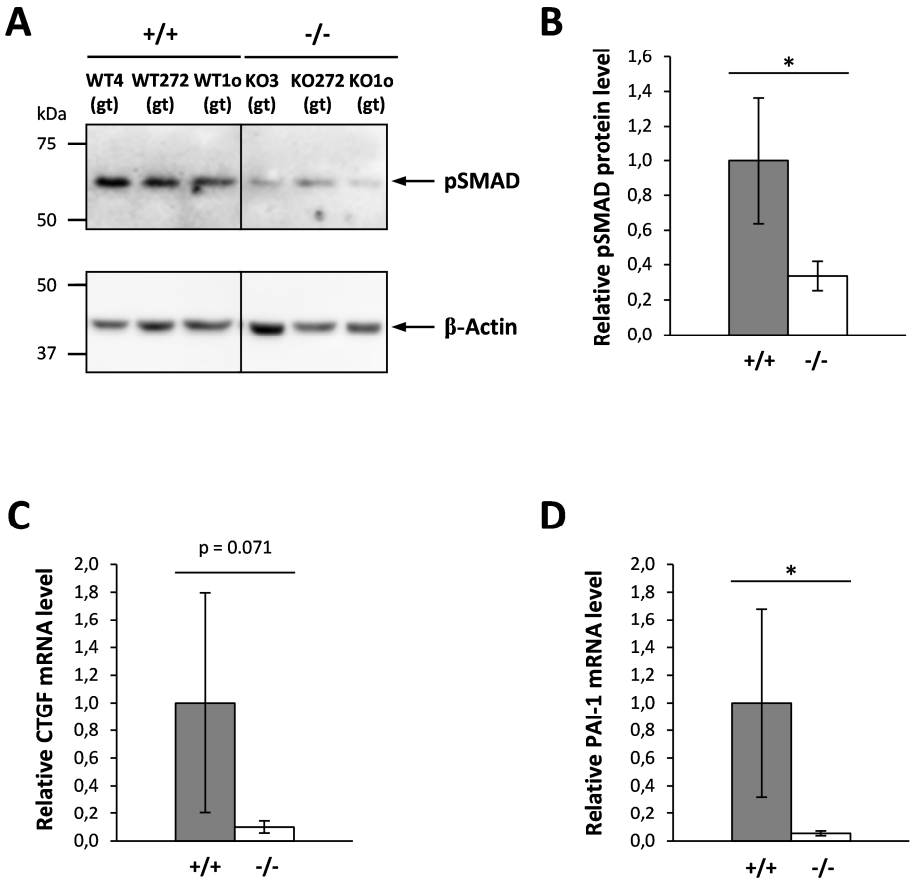

Figure 3.28: HtrA1 deficiency causes reduced TGF-β1 signaling in MEF cells. (A, B) Phosphorylation of SMAD2 in MEF cell lysates. PhosphoSMAD2 levels were analyzed by immunoblotting of MEF cells isolated from HtrA1 mice using a phosphoSMAD2 antibody (A, representative blot) and normalized to β-Actin (42 kDa) (B); n=5-7. Relative CTGF (C) and PAI-1 (D) mRNA levels from MEF cells were determined by real-time PCR (β-Actin was used for normalization). n=7-8; results are expressed as mean ±SEM; * $p < 0.05$ Mann-Whitney Rank Sum Test.

To rule out that HtrA1$^{-/-}$ MEF cells are for some reasons non-responsive to TGF-β activation, we stimulated HtrA1$^{+/+}$ and HtrA1$^{-/-}$ MEF cells with recombinant TGF-β1 and again analyzed SMAD2 phosphorylation (Figure 3.29 A) as well as CTGF and PAI-1 mRNA expression levels (Figure 3.29 B, C). Although the induction range between the individual cell lines varied strongly (see the large SEM bars in Figure 3.29 B; C), we found that each wild-type as well as each knockout cell line could be induced upon TGF-β1 stimulation.

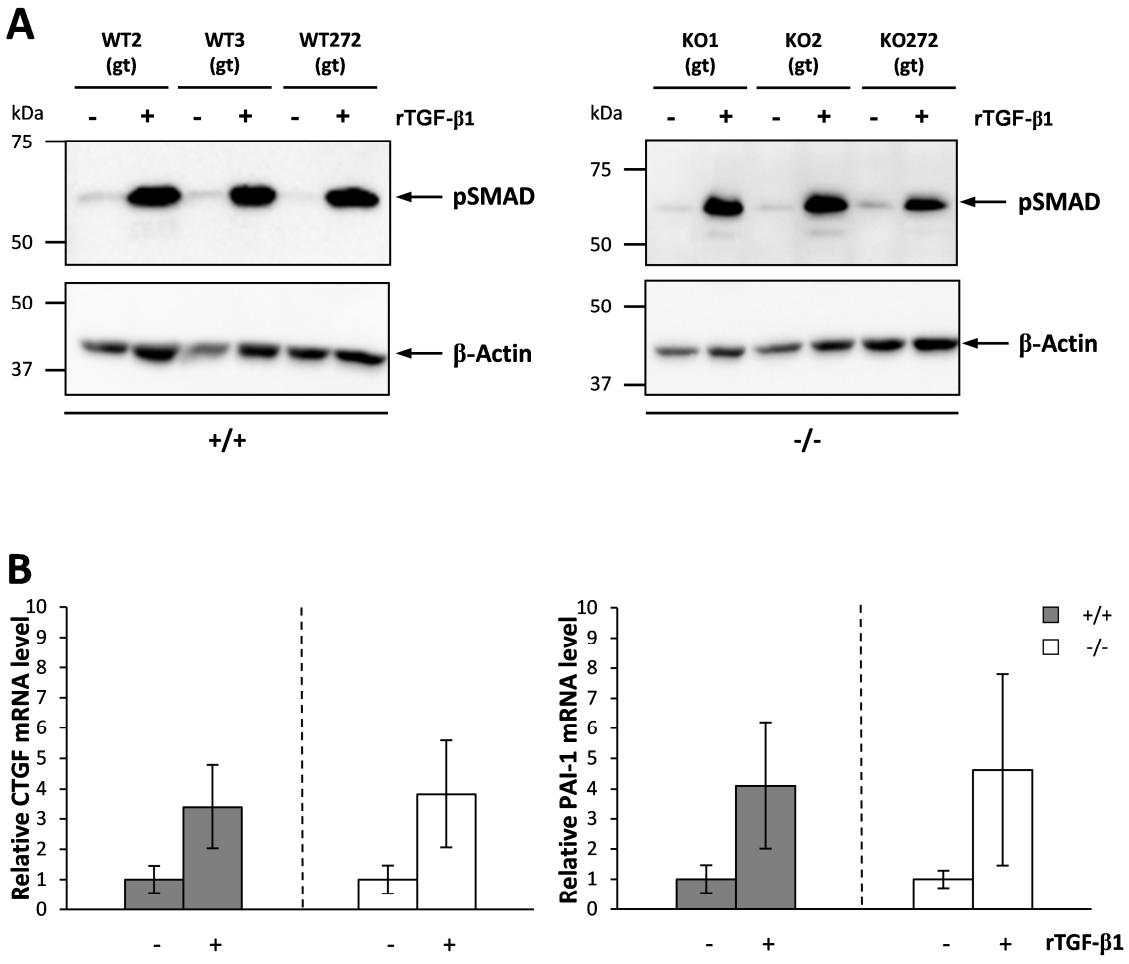

Figure 3.29: HtrA1$^{+/+}$ and HtrA1$^{-/-}$ MEF cells are induced upon TGF-β1 stimulation. (A) PhosphoSMAD2 levels were analyzed by immunoblotting of MEF cells isolated from HtrA1$^{+/+}$(gt) (left panel) and HtrA1$^{-/-}$(gt) (right panel) mice after stimulation for 12 h with rTGF-β1 using a phosphoSMAD2 antibody (upper panels). Equal expression of β-Actin (lower panels) in all samples guaranteed equivalent loadings. (B) MEF cells were stimulated for 12 h with rTGF-β1 and relative CTGF and PAI-1 mRNA levels were determined by real-time PCR (β-Actin was used for normalization). Not-stimulated cell values were set as 1. n=6-8; results are expressed as mean ±SEM.

These data suggest that HtrA1 deficiency leads to reduced TGF-β signaling in MEF cells.

3.4.3.3 Decreased TGF-β signaling in fibroblasts of CARASIL patients

The results of TGF-β signaling activity from HtrA1$^{-/-}$ brains and MEF cell cultures contradict previously published data on CARASIL patient brains and fibroblasts which indicated elevated TGF-β signaling (Hara et al., 2009, Shiga et al., 2011). We therefore used skin fibroblasts from two CARASIL patients and analyzed TGF-β target gene mRNA levels. One fibroblast line was derived from a 29-year-old Romanian female CARASIL patient carrying compound heterozygous *HTRA1*

mutations: c.961G>A in exon 4 (aa substitution p.A321T) and a G deletion c.126delG in exon 1 (frameshift p.E42fs; introduction of a stop codon at position 214) (Bianchi et al., 2014). The other cell line originated from a 34-year-old Pakistani female CARASIL patient carrying the homozygous *HTRA1* mutation c.517G>A in exon 2 (aa substitution p.A173T; D. Werring, unpublished). Control cells originated from a 45-year-old healthy subject. CTGF mRNA levels were reduced in both CARASIL cell lines (Figure 3.30 A). A similar effect was observed for PAI-1 mRNA levels (Figure 3.30 B). The homozygous and the compound heterozygous CARASIL cell line varied among each other, an effect that was also detected among mouse cell lines derived from animals of the same genotype. Thus, level variations do not necessarily have to be attributed to the different mutations. However, a clear reduction was observed in both patients compared to the control.

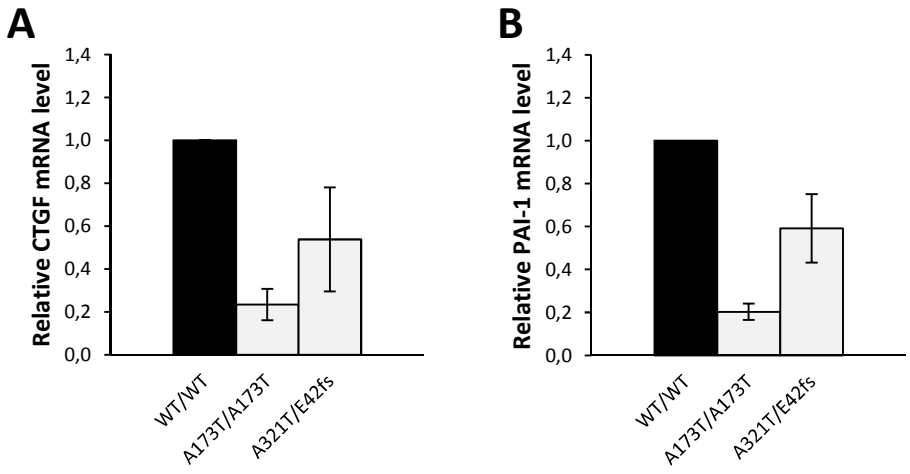

Figure 3.30: TGF-β target gene expression is reduced in fibroblasts derived from CARASIL patients. Relative CTGF (A) and PAI-1 (B) mRNA levels from human skin fibroblasts (cell passage numbers: WT/WT p22, p28; A173T/A173T: p15, p20; A321T/E42fs: p8, p9) were determined by real-time PCR (β-Actin was used for normalization). WT/WT: control fibroblasts; A173T/A173T, A321T/E42fs: CARASIL patient fibroblasts. n=2; results are expressed as mean ±SEM.

3.4.4 The HtrA1 substrate LTBP-1 might mediate the effects on TGF-β signaling

Our results showing a reduction of TGF-β activity in mouse tissue and cells as well as CARASIL patient cells cannot be explained by processing of previously identified HtrA1 substrates such as mature TGF-β, latency-associated peptide (LAP) or TGF-β receptors (Graham et al., 2013, Launay et al., 2008, Oka et al., 2004, Shiga et al., 2011), since their cleavage inevitably results in an attenuation of TGF-β signaling activity. Work in our group by N. Beaufort had provided evidence for an efficient processing of latent TGF-β-binding protein 1 (LTBP-1), an ECM-associated protein involved in TGF-β secretion, storage and activation, by purified HtrA1 *in vitro*. To follow up on this finding, we examined the proteolytic activity of wild-type HtrA1 and several mutants expressed in the human HEK293T embryonic kidney cell line.

Initially, we cloned the wild-type HtrA1 into the pcDNA4_TO vector resulting in the in-frame attachment of a C-terminal myc/HIS tag. The active site mutation S328A, the two CARASIL mutations A252T and V297M and the novel, biochemically uncharacterized G295R variant (Hara et al., 2009, Mendioroz et al., 2010) were introduced by site-directed mutagenesis. All HtrA1 constructs were expressed as ~55 kDa peptides and efficiently secreted upon transient transfection into HEK293T cells (Figure 3.31 A). In cells expressing the wild-type protease immunoreactive bands of lower molecular weight were detected likely representing autoproteolysis products (Hu et al., 1998). They could not be observed in any of the mutant-expressing cells indicating reduced proteolytic activity. When conditioned cell supernatants of transfected cells were used in a proteolysis assay with denatured bovine serum albumin (BSA) as substrate, degradation was only observed with wild-type HtrA1 (Figure 3.31 B; see chapter 2.6.7).

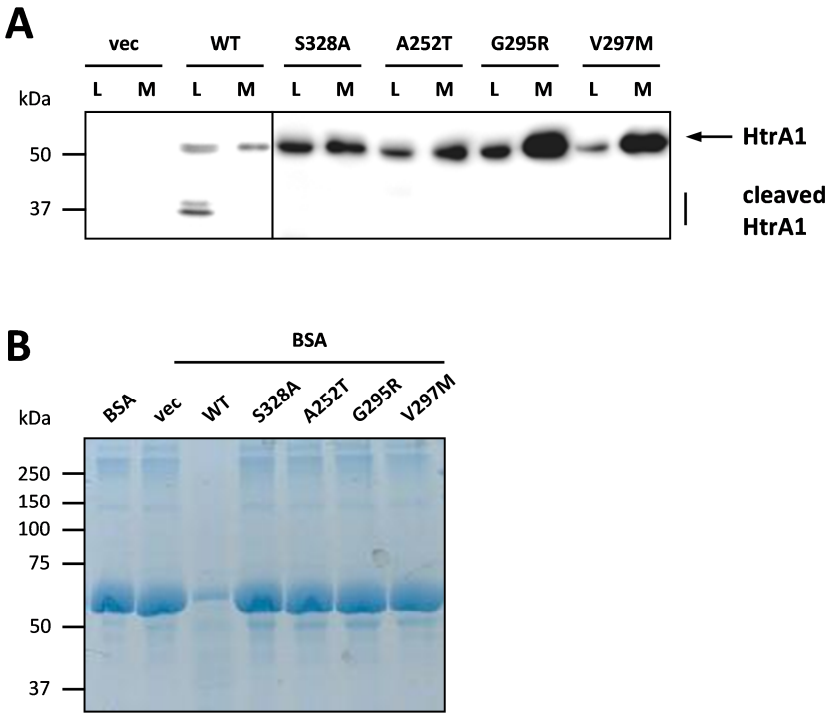

Figure 3.31: Only wild-type HtrA1 processes its analytical substrate denatured BSA while all HtrA1 constructs are expressed and secreted. (A) HEK293T cells were transiently transfected with pcDNA4_TOA plasmid (vec) or plasmids containing wild-type (WT), active site mutant (S328A) or CARASIL-mutant (A252T, G295R, V297M) HtrA1 fused to a C-terminal myc tag. HtrA1 expression was analyzed by immunoblotting of equal amounts of cell lysates (L) and conditioned medium (M) using a myc antibody. (B) Conditioned media from HEK293T cells transiently expressing HtrA1 variants were incubated with denatured bovine serum albumin (BSA) for 24 h. Samples were analyzed by SDS-PAGE followed by staining with CBB solution. Loading BSA without incubation served as a control.

Next, these supernatants were incubated with conditioned HEK293T cell medium containing full-length (~260 kDa) LTBP-1 and analyzed by immunoblotting: while active-site mutant (S328A) or CARASIL-mutant HtrA1 left LTBP-1 mainly unaffected, wild-type HtrA1 completely converted it to a stable ~220 kDa cleavage product (Figure 3.32 A). This demonstrated limited proteolysis rather than global degradation and suggested site-specific cleavage. Parallel *in vitro* studies had located the cleavage site to the amino-terminal LTBP-1 region and therefore the following experiments were performed with a shorter, more stable ~130 kDa C-terminal LTBP-1 deletion variant (ΔC-LTBP-1). Processing of ΔC-LTBP-1 was blocked in the presence of the HtrA1-specific inhibitor NVP-LBG976 (Grau et al., 2005) from Novartis Pharmaceuticals (HtrA1-I), but not by the metalloprotease inhibitor EDTA confirming the specificity of the cleavage (Figure 3.32 B). In order to evaluate the effects of HtrA family members HtrA3 and HtrA4, they were likewise overexpressed and conditioned supernatants co-incubated with ΔC-LTBP-1-containing medium. Although conversion of ΔC-LTBP-1 to a ~90 kDa fragment was also observed with HtrA3 and HtrA4 conditioned medium, it occurred with less efficiency than with HtrA1 (Figure 3.32 C, upper panel).

These results corroborated the data obtained with purified protease and confirmed LTBP-1 as promising HtrA1 substrate.

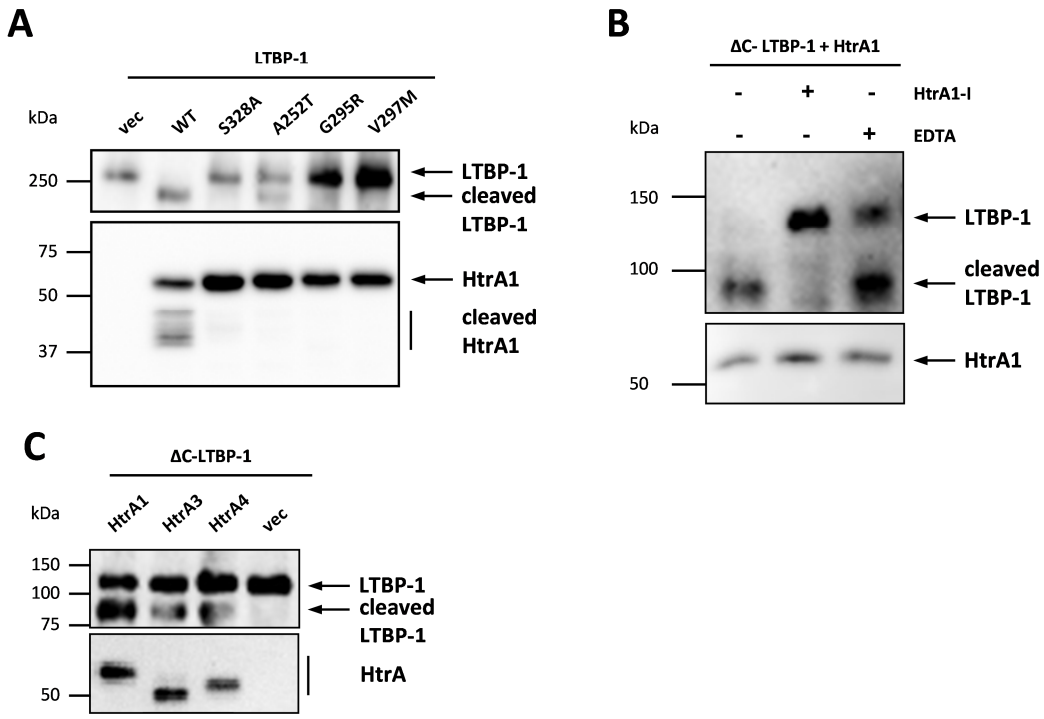

Figure 3.32: LTBP-1 is processed by active HtrA proteases. (A) V5 tagged full-length latent TGF-β-binding protein 1 (LTBP-1)-containing medium was exposed to supernatants from pcDNA4_TOA transfected cells (vec) or from cells expressing either wild-type human HtrA1 (WT), active site mutant (S328A) or CARASIL-mutant (A252T, G295R, V297M) hHtrA1 fused to a C-terminal myc tag for 24 h. Immunoblotting for LTBP-1 was performed using a V5 antibody (upper panel) and for HtrA1 using a myc antibody (lower panel). (B) ΔC-LTBP-1 was exposed to medium from HtrA1 transfected cells for 24 h in the absence or presence of an HtrA1 inhibitor (HtrA1-I) or EDTA and immunodetected by anti-V5 (upper panel) and anti-HtrA1(ΔMac) (lower panel). (C) Conditioned medium from HEK293T cells transiently expressing mHtrA1-myc, mHtrA3-myc or mHtrA4-myc was incubated with conditioned medium of V5 tagged ΔC-LTBP-1 for 24 h. Samples were analyzed by Western blot using a V5 antibody to detect LTBP-1 (upper panel) or using a myc antibody (lower panel) for the HtrA variants. Note, that all HtrA members have slightly different molecular weights due to diverse amino acid lengths: calculated molecular weight mHtrA1myc/HIS 54.45 kDa; mHtrA3myc/HIS 52.25 kDa, mHtrA4myc/HIS 55.09 kDa.

In order to examine cleavage by endogenous HtrA1 we used supernatants of our immortalized embryonic fibroblasts lines derived from $HtrA1^{+/+}$ and $HtrA1^{-/-}$ mice. To estimate the molar HtrA1 concentration present in conditioned MEF media, immunoblotting signals were compared to purified HtrA1 as standard. HtrA1 concentrations varying by roughly one order of magnitude were detected (5-50 nM; Figure 3.33 and data not shown; supernatants of HtrA1-overexpressing HEK293T cells contained concentrations of 50-300 nM, data not shown). Analysis of several medium batches taken from different passages indicated a relatively constant expression level within one cell line over time (Figure 3.35 A, B and data not shown). As expected, no HtrA1 protein

could be detected in lines from HtrA1-deficient embryos. The lower HtrA1 band in WT3(gt), the wild-type line with the highest HtrA1 levels, indicated autoproteolysis of endogenous HtrA1.

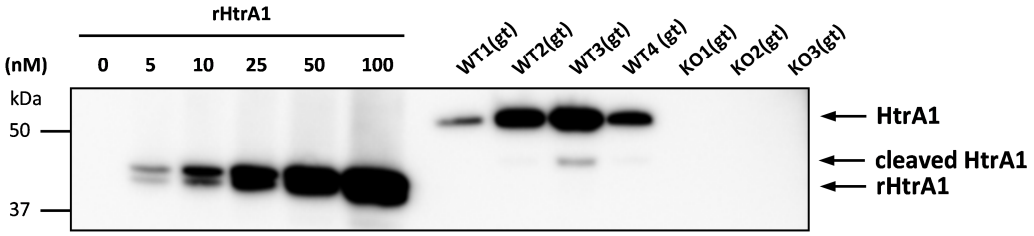

Figure 3.33: Analysis of HtrA1 expression levels in concentrated HtrA1$^{+/+}$ MEF cell medium. HtrA1 expression was evaluated by Western blotting of 10-fold concentrated MEF cell medium using the HtrA1(ΔMac) antibody. Purified, recombinant amino-terminally deleted human rHtrA1 (HtrA1-ΔMac; aa 158-480; ~40 kDa; a kind gift from M. Ehrmann, University Duisburg-Essen, Germany) served as a standard.

Using supernatants from the WT2(gt), WT3(gt), KO1(gt) and KO2(gt) lines, processing of the previously reported substrate TGF-β under endogenous conditions was investigated. Figure 3.34 shows a representative Western blot of HtrA1$^{+/+}$ and HtrA1$^{-/-}$ MEF media co-incubated with conditioned medium of TGF-β1 transfected cells. In addition to full-length TGF-β1 (pro TGF-β1) the processed forms LAP and mature TGF-β were detected. But none of the three peptides showed visible degradation upon wild-type medium exposure arguing against their relevance as physiological substrates.

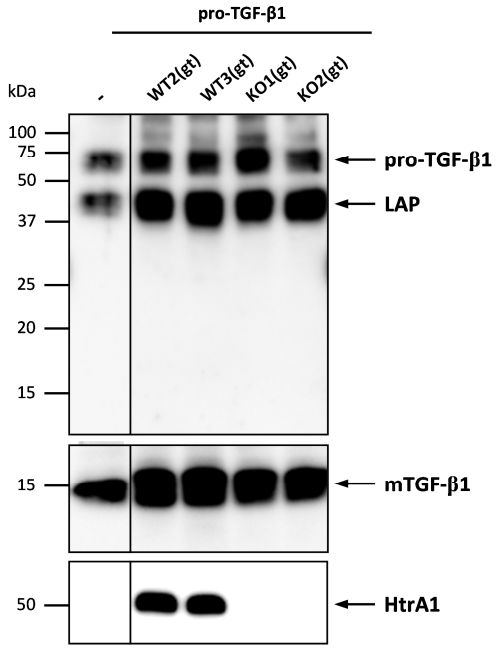

Figure 3.34: TGF-β1 is not processed by MEF cell-derived HtrA1. Conditioned medium of TGF-β1 transfected cells was exposed to concentrated medium derived from HTRA1$^{+/+}$ and HtrA1$^{-/-}$ MEF cell line or DMEM (-) as a control for 72 h and immunodetected by anti-TGF-β1 (upper panel), anti-V5 to better visualize mature TGF-β1 (middle panel) and anti-HtrA1(ΔMac) (lower panel).

In contrast, efficient processing of LTBP-1 was observed using HTRA1$^{+/+}$ MEF cell medium indicated by the appearance of a cleavage product of LTBP-1 with a molecular weight similar to that observed with transfected HtrA1 (Figure 3.35 A). Moreover, a dose-dependent effect between the low-expressing line WT1(gt) and the other three lines with higher HtrA1 levels could be detected (Figure 3.35 B). No processing was observed with conditioned medium from HTRA1$^{-/-}$ cells. In HtrA1$^{+/+}$ cell medium, processing of LTBP-1 was blocked in the presence of an HtrA1-specific inhibitor (HtrA1-I), but not by the metalloprotease inhibitor EDTA (Figure 3.35 C). Similar results were obtained with all other MEF cell lines analyzed (data not shown). This indicated that at least in MEF cells HtrA1 represents the major LTBP-1-processing protease and overexpressed LTBP-1 is cleaved by an endogenous HtrA1 concentration as low as 2.5 nM.

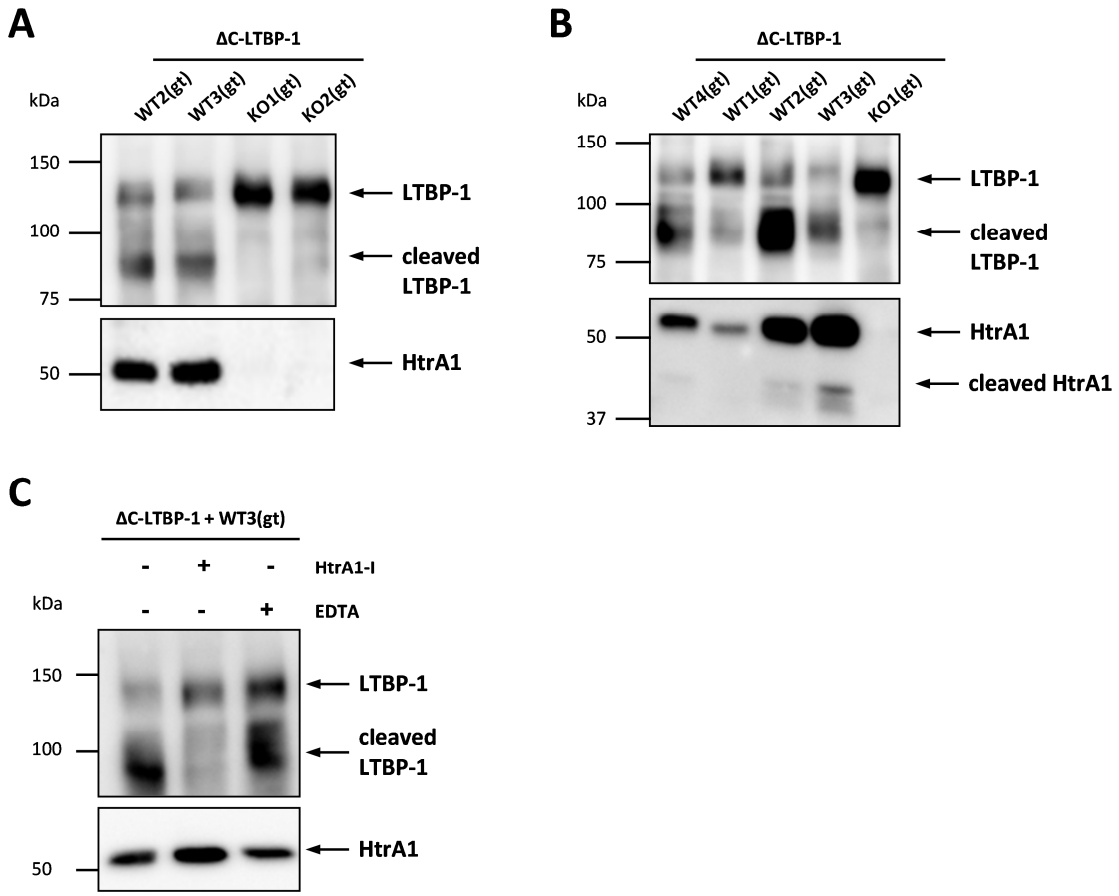

Figure 3.35: HtrA1 derived from HtrA1$^{+/+}$ MEF cells processes LTBP-1. (A) Concentrated supernatants from HTRA1$^{+/+}$ and HTRA1$^{-/-}$ MEF cell lines were incubated for 72 h with ΔC-LTBP-1 containing medium followed by LTBP-1 (upper panel) and HtrA1 (lower panel) immunodetection (used antibody: anti-V5 and anti-HtrA1(16C8)). (B) Media from four different HTRA1$^{+/+}$ cell lines and one HTRA1$^{-/-}$ cell line were incubated for 72 h with ΔC-LTBP-1 containing medium followed by LTBP-1 (upper panel) and HtrA1 (lower panel) immunodetection (used antibody: anti-V5 and anti-HtrA1(ΔMac)). (C) ΔC-LTBP-1 was exposed to concentrated medium derived from the HTRA1$^{+/+}$ MEF cell line WT3(gt) for 48 h at 37 °C in the absence or presence of an HtrA1 inhibitor (HtrA1-I) or EDTA and immunodetected by anti-V5 (upper panel) and anti-HtrA1(ΔMac) (lower panel).

In summary, it could be shown that, in contrast to CARASIL-mutant HtrA1, the wild-type protease processed LTBP-1 even under endogenous conditions, an observation that was not detected with the formerly proposed substrate TGF-β.

4 Discussion

Small vessel disease (SVD) accounts for ~20 % of all strokes and is a leading cause of cognitive decline and disability in adults worldwide (Pantoni, 2010). However, therapeutic options are limited compared to other common causes of stroke mainly due to a poor understanding of the disease pathogenesis. Monogenic inherited SVDs such as CARASIL resemble non-Mendelian forms on neuropathological and clinical level suggesting shared pathomechanisms. They are thus considered valuable model diseases to identify factors suitable for the development of novel treatment strategies. CARASIL is caused by homozygous mutations in the *HTRA1* gene, coding for the secreted serine protease high temperature requirement A1 (HtrA1) (Hara et al., 2009). Mutations either locate within the catalytic domain leading to a strong reduction in protease activity or result in nonsense-mediated mRNA decay. Thus, CARASIL likely develops as a consequence of a loss of HtrA1 function. In the present study we provide further support for this hypothesis by demonstrating strongly decreased proteolytic activity of the biochemically previously uncharacterized HtrA1 mutation G295R (Mendioroz et al., 2010). Similarly, the A173T mutation present in the patient skin fibroblasts used in this work was also shown to be proteolytically inactive (N. Beaufort, personal communication). While G295R like the majority of CARASIL mutations resides within the catalytic domain and possibly alters its three-dimensional structure, A173T locates within the preceding linker region. The underlying basis for its loss-of-function effect is yet unknown.

4.1 Characterization of HtrA1$^{-/-}$ mice

Gene ablation in mice was chosen as an approach to mimic loss of HtrA1 *in vivo*. At the beginning of this thesis, a novel HtrA1-deficient mouse strain was generated from embryonic stem cells harboring an *HTRA1* allele interrupted by gene trapping (gt). This strain was used for the majority of experiments, but contained a mixed genetic background of 129/SvEvBrd and C57BL/6J. At a later time point a second HtrA1 knockout strain generated by conventional targeted mutagenesis (tm) (Jones et al., 2011, Zhang et al., 2012) and containing a 98-99 % homogenous C57BL/6J background became available. Variations in the genetic background may influence the penetrance or severity of phenotypic features including alopecia (Sundberg et al., 1994), a major symptom of CARASIL patients. Thus, analysis of the extraneurological manifestations alopecia and spondylosis was performed in the HtrA1(tm) strain. The lack of HtrA1 expression was initially verified on mRNA level in both strains. During the course of this work we succeeded in generating a monoclonal anti-HtrA1 antibody and got access to a polyclonal antiserum (Vierkotten et al., 2011). Using these antibodies the absence of HtrA1 in both mouse strains could be verified on protein level.

HtrA1 knockout mice are viable and fertile, which is in agreement with the lack of lethality in humans. However, in contrast to patients, HtrA1$^{-/-}$ mice have a normal life expectancy and display no obvious disease symptoms. This includes the lack of alopecia and spondylosis. However, their relevance for the disease is unclear as for example not all CARASIL patients display signs of alopecia (Nozaki et al., 2014). It is possible that in humans these symptoms develop due to HtrA1 substrates different from those mediating neurological deficits. These substrates might well be part of cellular pathways whose impairment cannot be adequately recapitulated in mice. To rule out that compensatory mechanisms involving other HtrA1 family members might be responsible for the lack of these CARASIL symptoms in mice, we analyzed HtrA3 and HtrA4 mRNA expression levels, but no significant increase was observed.

In contrast, analysis of neurological features indeed revealed differences in HtrA1 knockout and wild-type mice. Within white matter diffuse demyelination was observed, a symptom also present in CARASIL patients. The histological analysis of brain vessels revealed a reduction of α-smooth muscle actin (α-SMA) in HtrA1-deficient mice reminiscent of the smooth muscle cell (SMC) loss observed in CARASIL patients (Fukutake, 2011, Oide et al., 2008). Interestingly, this loss was detected only in aged animals possibly reflecting the progressive nature of the disease. Moreover, decreased type IV collagen expression as reported in patients (Oide et al., 2008) was also detected in HtrA1$^{-/-}$ mouse brains.

In a mouse model for CADASIL, another monogenic SVD showing considerable phenotypic overlap with CARASIL, Joutel et al. (2010) reported increased cerebral glial fibrillary acidic protein (GFAP) expression as a marker for neurodegeneration. Upon investigation of HtrA1$^{-/-}$ mouse brains, we did not detect such an effect (data not shown). In addition, we were unable to demonstrate a higher number of white matter lesions as described for the CADASIL mouse model (Joutel et al., 2010). This might be explained by a lower severity of pathology in HtrA1-deficient compared to CADASIL mice. Moreover, the strain background which can be decisive for the development of a phenotype (Gould et al., 2006) might play a role. It has been shown, that 129/SvEvBrd mice are less susceptible to ischemic injury than C57BL/6 mice (Hara et al., 1996). Thus, the partial 129/SvEvBrd background of the HtrA1(gt)$^{-/-}$ strain might ameliorate the neurological damage.

Nevertheless, the observed alterations in white matter structure and cerebral vessel morphology indicated that HtrA1-deficient mice at least partially recapitulate CARASIL pathology. We therefore proceeded by analyzing the consequences of HtrA1 deficiency on transforming growth factor beta (TGF-β) signaling.

4.2 HtrA1 and TGF-β signaling

4.2.1 HtrA1 deficiency reduces TGF-β signaling

Previous studies had suggested a link between *HTRA1* mutations and impaired TGF-β signaling mediated by reduced cleavage of mature TGF-β, proTGF-β or TGF-β receptors TGFBRII and TGFBRIII (Graham et al., 2013, Hara et al., 2009, Launay et al., 2008, Oka et al., 2004, Shiga et al., 2011). To better define the mechanistic relationship between HtrA1 and TGF-β, we investigated HtrA1-deficient mice with respect to TGF-β at various levels including SMAD2 phosphorylation and expression of the target genes CTGF and PAI-1. Initially, we analyzed whole brain tissue and surprisingly observed a down-regulation of TGF-β activity, a finding being in contrast to previously reported data from CARASIL patients (Hara et al., 2009, Shiga et al., 2011).

Therefore, we set out to verify our findings using additional approaches. First, we established a method to isolate microvessels from mouse brain resulting in the removal of parenchymal tissue. Again, we observed reduced TGF-β signaling on phosphoSMAD2 and TGF-β target gene level demonstrating TGF-β dysregulation in the vasculature of HtrA1-deficient mice. This finding is in agreement with the severe vascular phenotype in CARASIL patients and supported our results obtained in whole-brain tissue. The availability of purified microvessels opens new possibilities for future biochemical studies of HtrA1 deficiency. For example transcriptome and proteome analyses of this material might help to elucidate details of the molecular mechanisms underlying CARASIL development.

To confirm the effects on TGF-β activity at cellular level mouse embryonic fibroblast (MEF) cell lines were generated. In HtrA1-deficient lines the reduction of SMAD2 phosphorylation as well as CTGF and PAI-1 expression was confirmed. In addition, levels of total and bioactive TGF-β could be evaluated in conditioned fibroblast media and again a significant decrease in $HtrA1^{-/-}$ MEF cells was measured. TGF-β concentrations could not be determined in tissue lysates as they were below the detection limit likely due to the short half-life of TGF-β in tissues (Kaminska et al., 2005). However, TGF-β levels were detectable in blood serum, but no significant differences between HtrA1-deficient and control mice were observed. Also CTGF and PAI-1 mRNA levels in lung and aorta tissue did not differ significantly excluding a systemic TGF-β dysregulation. The extraneurological symptoms observed in CARASIL patients might be caused by an impairment of TGF-β family members other than TGF-β itself (e.g. bone morphogenetic proteins) or by the lack of processing of alternative HtrA1 substrates. In summary, our results from mouse tissues and cells clearly suggested a reduction of TGF-β signaling under HtrA1-deficient conditions.

To investigate whether the discrepancy between our data and published findings in CARASIL patients might be due to species-specific differences, we used primary skin fibroblasts from two CARASIL subjects, a 29-year-old Romanian female being compound heterozygous for the *HTRA1*

mutations A321T and E42fs (Bianchi et al., 2014) and a 34-year-old Pakistani female homozygous for the A173T mutation (D. Werring, unpublished). Applying the various assays described before (TGF-β concentration and bioactivity, SMAD2 phosphorylation, CTGF and PAI-1 expression), we demonstrated a decrease in activity in both cell lines (Beaufort et al., 2014). The presence of this observation in two unrelated patient cell lines carrying different *HTRA1* mutations argued for the specificity of this finding. Moreover, skin fibroblasts derived from the heterozygous parents of the CARASIL patient with the compound heterozygous A321T/E42fs mutation displayed PAI-1 and CTGF mRNA levels in between those derived from patient and control fibroblasts (data not shown) arguing for the reliability of our measurements.

Even though HtrA1$^{-/-}$ mice and CARASIL patient fibroblasts do not cover all clinical and molecular aspects of CARASIL, we nevertheless consider the consistency of the results obtained from two different species as convincing evidence for their disease relevance.

4.2.2 Controversial findings concerning deregulated TGF-β signaling and loss of HtrA1

Our findings contrast with previous studies, which reported an up-regulation of TGF-β signaling in CARASIL brains as demonstrated by an increase in TGF-β, phosphoSMAD2, hyaluronan, fibronectin (extra domain-A) and versican (Hara et al., 2009, Shiga et al., 2011). TGF-β promotes the expression of extracellular matrix (ECM) components and represents a key mediator of fibrosis. Thus, it cannot be excluded that increased TGF-β activity reflects fibrotic changes of blood vessels in advanced CARASIL disease stages. In addition, the reported data were restricted to two autopsy cases with limited information on histopathological samples and individual differences with respect to TGF-β signaling cannot be ruled out. Moreover, increased TGF-β in the cerebrovasculature of CARASIL patients might be explained by the observation that TGF-β signaling is up-regulated after stroke (Doyle et al., 2010). Our mouse model allows the investigation of early disease stages and decreased TGF-β signaling was detected already in young knockout animals. With respect to published data in patient fibroblasts, mRNA levels of the TGF-β target gene Noggin were found to be elevated only in cells from a single patient (Hara et al., 2009). However, the presented data might be difficult to interpret since the Noggin gene contains only one exon and real-time PCR signals might thus also originate from residual genomic DNA present in the RNA sample.

Very recently, Graham et al. (2013) demonstrated an increase of TGF-β target gene expression in MEF cells derived from a third HtrA1 knockout mouse model with a targeted gene deletion of *HTRA1*. However, results were obtained with cells stimulated by recombinant TGF-β and furthermore, it was not clear whether they used only technical or also individual replicates. Performing this experiment under identical conditions, we did not observe a change in CTGF and

PAI-1 expression levels using 6-8 different embryonic cell lines per genotype derived from our mouse models (see Figure 3.29). Even though we detected differences among individual cell lines of the same genotype (see high error bars in Figure 3.29), we did not find significant differences between wild-type and knockout MEF cells. Though, in line with their data, Graham et al. (2013) demonstrated a slight but significant increase of bone volume and trabecular thickness in the distal femurs and the vertebrae by using microcomputed tomography (μCT), an effect possibly mediated by elevated TGF-β activity. This contrasts with our X-ray or μCT analysis which did not reveal abnormalities in HtrA1 knockout mice. Differences in the genetic background of the used mouse strains might be responsible for these discrepancies.

In order to address the different effects of a loss of HtrA1 function on TGF-β signaling on a molecular level, we started to investigate the relationship between HtrA1 and TGF-β *in vitro*. Under overexpression conditions and upon co-transfection, we detected an extracellular as well as intracellular degradation of TGF-β1 by wild-type HtrA1 (data not shown). However, mature and pro TGF-β were not processed by endogenous HtrA1 suggesting that they do not represent biologically relevant substrates. Previous studies claiming the identification of TGF-β as a substrate had primarily used purified or overexpressed HtrA1 (Launay et al., 2008, Shiga et al., 2011) raising doubts about the specificity of the observed effects. In addition, latency associated peptide (LAP) degradation (Shiga et al., 2011) was observed in the endoplasmic reticulum where proteases accumulate upon strong overexpression. We therefore had started to search for alternative HtrA1 substrates and during the course of this thesis latent TGF-β-binding protein (LTBP-1) had emerged as a promising candidate (Beaufort et al., 2014). LTBP-1 represents an ECM protein that mediates the sequestration of latent TGF-β. At physiological concentrations as low as 1 nM (An et al., 2010) HtrA1 had been shown to process LTBP-1 into a stable truncated fragment which no longer incorporates into the ECM (Beaufort et al., 2014). Within this thesis the lack of LTBP-1 cleavage in the presence of CARASIL mutant HtrA1 could be shown. To demonstrate LTBP-1 processing by endogenous HtrA1, conditioned supernatants of the various MEF cell lines generated in this study were used. Treatment of purified LTBP-1 with supernatants from wild-type lines indeed resulted in an HtrA1 dose-dependent cleavage and in a fragment similar to that observed with purified or overexpressed HtrA1. Moreover, processing was not seen when supernatants from HtrA1-deficient cell lines or from wild-type cell lines in the presence of a specific HtrA1 inhibitor were used. This suggested that, at least in MEF cells, HtrA1 is the predominant LTBP-1 cleaving protease strongly supporting the physiological relevance of LTBP-1 processing by HtrA1.

To examine whether other LTBP family members might also be subject to HtrA1-mediated processing we performed *in vitro* cleavage assays with LTBP-4- and HtrA1-containing supernatants and observed also a reduction of full-length LTBP-4 (data not shown). Hence, HtrA1 might regulate the function of LTBP proteins in general.

Site-specific LTBP-1 proteolysis followed by its dissociation from the ECM resulting in TGF-β release and activation has been described before (Dallas et al., 1994, Ge and Greenspan, 2006, Taipale et al., 1994, Tatti et al., 2008). Moreover, bone morphogenetic protein 1 (BMP-1)-mediated cleavage of LTBP-1 was reported to result in reduced TGF-β activity in BMP-1 knockout MEF cells (Ge and Greenspan, 2006). Upon HtrA1-mediated cleavage we observed decreased LTBP-1 incorporation into the ECM, and in HtrA1-deficient fibroblasts as well as cerebral tissues we detected reduced TGF-β signaling. Thus, we propose that HtrA1-mediated LTBP-1 processing results in a release of mature TGF-β from the ECM and, as a consequence, in excessive TGF-β signaling (Figure 4.1). In the absence of HtrA1, LTBP-1 cleavage is abolished leading to decreased TGF-β activity. Molecular details of the process how HtrA1-mediated LTBP-1 degradation facilitates TGF-β signaling remain to be elucidated.

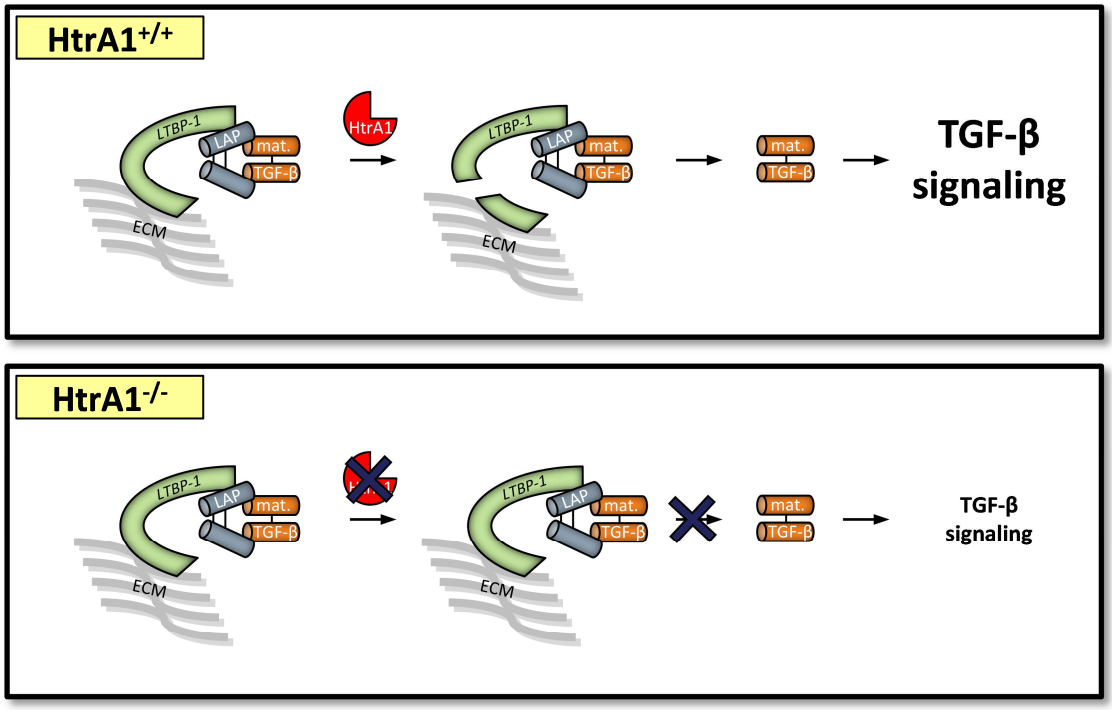

Figure 4.1: Lack of HtrA1 in mouse brain leads to reduced LTBP-1 processing and subsequently to decreased TGF-β signaling. Schematic representation of the consequences of HtrA1 deficiency on transforming growth factor beta (TGF-β) pathway in mouse brain. See text for details. ECM: extracellular matrix; LAP: latency associated peptide; mat. TGF-β: mature form of TGF-β; LTBP-1: latent TGF-β binding protein.

4.2.3 Deregulated TGF-β as a key mechanism involved in vascular diseases

Our findings add to current evidence suggesting a role of the TGF-β signaling pathway for normal vascular function. It is known, that mutations in components of the TGF-β pathway as well as its interacting partners mediating TGF-β sequestration into the ECM result in severe vascular defects. For instance, TGF-β signaling was demonstrated to be enhanced in Marfan syndrome (MFS), which is characterized by aortic root aneurysms and dissections. MFS is caused by mutations in *FBN1* encoding the ECM component fibrillin-1 (Dietz et al., 1991). Furthermore, Loeys-Dietz syndrome (LDS), a hereditary condition with considerable phenotypic overlap with MFS also results in severe vascular defects. LDS is caused by loss-of-function mutations in *TGFBRI* and *II* (Loeys et al., 2005), *SMAD3* (van de Laar et al., 2011) or *TGFB2* (Lindsay et al., 2012). Whereas all mutations are predicted to result in a down-regulation of TGF-β activation, surprisingly an up-regulation was detected in the aortic wall of patients as well as LDS mouse models. Several mechanisms have been proposed for this paradox phenomenon: due to mutations in the canonical components *TGFBR1/2*, *SMAD3* or *TGFB2* of the TGF-β signaling pathway, the non-canonical pathway (ERK/mitogen-activated protein kinase) might overcompensate for the missing canonical pathway (Holm et al., 2011, Li et al., 2014). Moreover, it has been suggested, that a shift from *TGFB2*-driven to *TGFB1*-driven signaling occurs in *TGFB2*-deficient patients and mice (Lindsay et al., 2012). An additional disease involving deregulated TGF-β signaling as a pathogenic mechanism is hereditary hemorrhagic telangiectasia (HHT), an autosomal dominant vascular disorder characterized by fragile blood vessels leading to telangiectasia and arteriovenous malformations (McAllister et al., 1994). HHT is caused by heterozygous mutations in the genes encoding the TGF-β pathway members *ENG* (endoglin), *ACVRL1* (activin receptor-like kinase 1) or *SMAD4* (ten Dijke and Arthur, 2007). In contrast to LDS- and MFS-mutations, HHT-mutations result in down-regulated TGF-β signaling (Letarte et al., 2005). Even though pathomechanisms involving down-regulation of TGF-β pathway are very rare, it is known, that a complete *TGFB1* knockout in mice leads to embryonic lethality with severe vascular defects or postnatal lethality from autoimmune disease (Dickson et al., 1995, Shull et al., 1992). Similar effects were reported for TGF-β2 and TGF-β3 knockout mice (Goumans and Mummery, 2000). Thus, loss of TGF-β or even reduction of TGF-β signaling has serious consequences for the vasculature in mice as well as humans.

Transforming growth factor beta (TGF-β) is known to induce expression of components of the ECM and other genes regulating the composition of the ECM (ten Dijke and Arthur, 2007) including type IV collagen (Grande et al., 1993). Thus, decreased type IV collagen expression found in the cerebral vasculature of CARASIL patients as well as HtrA1 knockout mice might be mediated by reduced TGF-β expression. Very likely, expression levels of other ECM proteins are also reduced leading to an abnormal composition of the ECM. Furthermore, it has been shown, that TGF-$\beta1^{-/-}$ mice show uncompact myelin (Day et al., 2003). Thus, diffuse white matter changes might result from deregulated TGF-β signaling in HtrA1-deficient mice and patients.

Interestingly, recent studies indicate that dysregulation of the TGF-β pathway is also involved in CADASIL development, another monogenic form of SVD. It is caused by mutations in the cell surface receptor Notch3 and characterized by aggregates containing the extracellular domain (ECD) of Notch3 in brain vessels walls. These aggregates might promote pathological processes leading to vessel dysfunction by recruiting extracellular proteins including ECM components (Monet-Lepretre et al., 2013). A study from our group investigated the details of this process and observed an accumulation of LTBP-1 protein in CADASIL-affected vessel walls (Kast et al., 2014). Moreover, an almost perfect co-localization with Notch3 suggested LTPB-1 as a constituent of Notch3 aggregates. Also a direct interaction of LTBP-1 with Notch3-ECD and a co-aggregation with mutant Notch3 *in vitro* could be demonstrated. Finally, evidence for increased levels of the TGF-β pro-domain in CADASIL patient vessels was provided. Since CADASIL shares the main clinical features with CARASIL, it seems likely that a dysregulation of TGF-β signaling represents a common feature in both diseases.

In conclusion, our findings provide a new and unexpected link between TGF-β pathway and CARASIL which might also be of relevance for other hereditary and even the more common forms of cerebral SVD.

5 Citations

ADAMS, H. P., JR., BENDIXEN, B. H., KAPPELLE, L. J., BILLER, J., LOVE, B. B., GORDON, D. L. & MARSH, E. E., 3RD 1993. Classification of subtype of acute ischemic stroke. Definitions for use in a multicenter clinical trial. TOAST. Trial of Org 10172 in Acute Stroke Treatment. *Stroke,* 24**,** 35-41.

AGUERO-TORRES, H., KIVIPELTO, M. & VON STRAUSS, E. 2006. Rethinking the dementia diagnoses in a population-based study: what is Alzheimer's disease and what is vascular dementia?. A study from the kungsholmen project. *Dement Geriatr Cogn Disord,* 22**,** 244-9.

AN, E., SEN, S., PARK, S. K., GORDISH-DRESSMAN, H. & HATHOUT, Y. 2010. Identification of novel substrates for the serine protease HTRA1 in the human RPE secretome. *Invest Ophthalmol Vis Sci,* 51**,** 3379-86.

ANNES, J. P., MUNGER, J. S. & RIFKIN, D. B. 2003. Making sense of latent TGFbeta activation. *J Cell Sci,* 116**,** 217-24.

ARIMA, K., YANAGAWA, S., ITO, N. & IKEDA, S. 2003. Cerebral arterial pathology of CADASIL and CARASIL (Maeda syndrome). *Neuropathology,* 23**,** 327-34.

BALDI, A., DE LUCA, A., MORINI, M., BATTISTA, T., FELSANI, A., BALDI, F., CATRICALA, C., AMANTEA, A., NOONAN, D. M., ALBINI, A., NATALI, P. G., LOMBARDI, D. & PAGGI, M. G. 2002. The HtrA1 serine protease is down-regulated during human melanoma progression and represses growth of metastatic melanoma cells. *Oncogene,* 21**,** 6684-8.

BAYRAKLI, F., BALABAN, H., GURELIK, M., HIZMETLI, S. & TOPAKTAS, S. 2014. Mutation in the HTRA1 gene in a patient with degenerated spine as a component of CARASIL syndrome. *Turk Neurosurg,* 24**,** 67-9.

BEAUFORT, N., SCHARRER, E., KREMMER, E., LUX, V., EHRMANN, M., HUBER, R., HOULDEN, H., WERRING, D., HAFFNER, C. & DICHGANS, M. 2014. Cerebral small vessel disease-related protease HtrA1 processes latent TGF-β binding protein 1 and facilitates TGF-β signaling. *Proceedings of the National Academy of Sciences*.

BIANCHI, S., DI PALMA, C., GALLUS, G. N., TAGLIA, I., POGGIANI, A., ROSINI, F., RUFA, A., MURESANU, D. F., CERASE, A., DOTTI, M. T. & FEDERICO, A. 2014. Two novel HTRA1 mutations in a European CARASIL patient. *Neurology,* 82**,** 898-900.

BOTCHKAREV, V. A. 2003. Bone morphogenetic proteins and their antagonists in skin and hair follicle biology. *J Invest Dermatol,* 120**,** 36-47.

BOWLER, J. V. & HACHINSKI, V. 1994. Progress in the genetics of cerebrovascular disease: inherited subcortical arteriopathies. *Stroke,* 25**,** 1696-8.

CAMPIONI, M., SEVERINO, A., MANENTE, L., TUDUCE, I. L., TOLDO, S., CARAGLIA, M., CRISPI, S., EHRMANN, M., HE, X., MAGUIRE, J., DE FALCO, M., DE LUCA, A., SHRIDHAR, V. & BALDI, A. 2010. The serine protease HtrA1 specifically interacts and degrades the tuberous sclerosis complex 2 protein. *Mol Cancer Res,* 8**,** 1248-60.

CAVAGLIA, M., DOMBROWSKI, S. M., DRAZBA, J., VASANJI, A., BOKESCH, P. M. & JANIGRO, D. 2001. Regional variation in brain capillary density and vascular response to ischemia. *Brain Res,* 910**,** 81-93.

CHABRIAT, H., JOUTEL, A., DICHGANS, M., TOURNIER-LASSERVE, E. & BOUSSER, M. G. 2009. Cadasil. *Lancet Neurol,* 8**,** 643-53.

CHEN, M. M., LAM, A., ABRAHAM, J. A., SCHREINER, G. F. & JOLY, A. H. 2000. CTGF expression is induced by TGF- beta in cardiac fibroblasts and cardiac myocytes: a potential role in heart fibrosis. *J Mol Cell Cardiol,* 32**,** 1805-19.

CHEN, Y., HE, Z., MENG, S., LI, L., YANG, H. & ZHANG, X. 2013. A novel mutation of the high-temperature requirement A serine peptidase 1 (HTRA1) gene in a Chinese family with cerebral autosomal recessive arteriopathy with subcortical infarcts and leukoencephalopathy (CARASIL). *J Int Med Res,* 41**,** 1445-55.

CHIEN, J., CAMPIONI, M., SHRIDHAR, V. & BALDI, A. 2009a. HtrA serine proteases as potential therapeutic targets in cancer. *Curr Cancer Drug Targets,* 9**,** 451-68.

CHIEN, J., OTA, T., ALETTI, G., SHRIDHAR, R., BOCCELLINO, M., QUAGLIUOLO, L., BALDI, A. & SHRIDHAR, V. 2009b. Serine protease HtrA1 associates with microtubules and inhibits cell migration. *Mol Cell Biol,* 29**,** 4177-87.

CLAUSEN, T., KAISER, M., HUBER, R. & EHRMANN, M. 2011. HTRA proteases: regulated proteolysis in protein quality control. *Nat Rev Mol Cell Biol,* 12**,** 152-62.

CLAUSEN, T., SOUTHAN, C. & EHRMANN, M. 2002. The HtrA family of proteases: implications for protein composition and cell fate. *Mol Cell,* 10**,** 443-55.

DALLAS, S. L., PARK-SNYDER, S., MIYAZONO, K., TWARDZIK, D., MUNDY, G. R. & BONEWALD, L. F. 1994. Characterization and autoregulation of latent transforming growth factor beta (TGF beta) complexes in osteoblast-like cell lines. Production of a latent complex lacking the latent TGF beta-binding protein. *J Biol Chem,* 269**,** 6815-21.

DAY, W. A., KOISHI, K. & MCLENNAN, I. S. 2003. Transforming growth factor beta 1 may regulate the stability of mature myelin sheaths. *Exp Neurol,* 184**,** 857-64.

DICHGANS, M. 2007. Genetics of ischaemic stroke. *Lancet Neurol,* 6**,** 149-61.

DICKSON, M. C., MARTIN, J. S., COUSINS, F. M., KULKARNI, A. B., KARLSSON, S. & AKHURST, R. J. 1995. Defective haematopoiesis and vasculogenesis in transforming growth factor-beta 1 knock out mice. *Development,* 121**,** 1845-54.

DIETZ, H. C., CUTTING, G. R., PYERITZ, R. E., MASLEN, C. L., SAKAI, L. Y., CORSON, G. M., PUFFENBERGER, E. G., HAMOSH, A., NANTHAKUMAR, E. J., CURRISTIN, S. M. & ET AL. 1991. Marfan syndrome caused by a recurrent de novo missense mutation in the fibrillin gene. *Nature,* 352**,** 337-9.

DIRNAGL, U., IADECOLA, C. & MOSKOWITZ, M. A. 1999. Pathobiology of ischaemic stroke: an integrated view. *Trends Neurosci,* 22**,** 391-7.

DIWAN, A. G., BHOSLE, D. G., VIKRAM, A., BINIWALE, A., CHAUDHARY, S. & PATODIYA, B. 2012. CARASIL. *J Assoc Physicians India,* 60**,** 59-61.

DONNAN, G. A., FISHER, M., MACLEOD, M. & DAVIS, S. M. 2008. Stroke. *Lancet,* 371**,** 1612-23.

DOYLE, K. P., CEKANAVICIUTE, E., MAMER, L. E. & BUCKWALTER, M. S. 2010. TGFbeta signaling in the brain increases with aging and signals to astrocytes and innate immune cells in the weeks after stroke. *J Neuroinflammation,* 7**,** 62.

DUBOIS, C. M., LAPRISE, M. H., BLANCHETTE, F., GENTRY, L. E. & LEDUC, R. 1995. Processing of transforming growth factor beta 1 precursor by human furin convertase. *J Biol Chem,* 270**,** 10618-24.

DUERING, M., CSANADI, E., GESIERICH, B., JOUVENT, E., HERVE, D., SEILER, S., BELAROUSSI, B., ROPELE, S., SCHMIDT, R., CHABRIAT, H. & DICHGANS, M. 2013. Incident lacunes preferentially localize to the edge of white matter hyperintensities: insights into the pathophysiology of cerebral small vessel disease. *Brain,* 136**,** 2717-26.

ESPOSITO, V., CAMPIONI, M., DE LUCA, A., SPUGNINI, E. P., BALDI, F., CASSANDRO, R., MANCINI, A., VINCENZI, B., GROEGER, A., CAPUTI, M. & BALDI, A. 2006. Analysis of HtrA1 serine protease expression in human lung cancer. *Anticancer Res,* 26**,** 3455-9.

FACCIO, L., FUSCO, C., CHEN, A., MARTINOTTI, S., BONVENTRE, J. V. & ZERVOS, A. S. 2000. Characterization of a novel human serine protease that has extensive homology to bacterial heat shock endoprotease HtrA and is regulated by kidney ischemia. *J Biol Chem,* 275**,** 2581-8.

FEDERICO, A., DI DONATO, I., BIANCHI, S., DI PALMA, C., TAGLIA, I. & DOTTI, M. T. 2012. Hereditary cerebral small vessel diseases: a review. *J Neurol Sci,* 322**,** 25-30.

FISHER, S. A., ABECASIS, G. R., YASHAR, B. M., ZAREPARSI, S., SWAROOP, A., IYENGAR, S. K., KLEIN, B. E., KLEIN, R., LEE, K. E., MAJEWSKI, J., SCHULTZ, D. W., KLEIN, M. L., SEDDON, J. M., SANTANGELO, S. L., WEEKS, D. E., CONLEY, Y. P., MAH, T. S., SCHMIDT, S., HAINES, J. L., PERICAK-VANCE, M. A., GORIN, M. B., SCHULZ, H. L., PARDI, F., LEWIS, C. M. & WEBER, B. H. 2005. Meta-analysis of genome scans of age-related macular degeneration. *Hum Mol Genet,* 14**,** 2257-64.

FRANK, K. M., SHARPLESS, N. E., GAO, Y., SEKIGUCHI, J. M., FERGUSON, D. O., ZHU, C., MANIS, J. P., HORNER, J., DEPINHO, R. A. & ALT, F. W. 2000. DNA ligase IV deficiency in mice leads to defective neurogenesis and embryonic lethality via the p53 pathway. *Mol Cell,* 5**,** 993-1002.

FUGATE, J. E. & RABINSTEIN, A. A. 2014. Update on intravenous recombinant tissue plasminogen activator for acute ischemic stroke. *Mayo Clin Proc,* 89**,** 960-72.

FUKUTAKE, T. 2011. Cerebral autosomal recessive arteriopathy with subcortical infarcts and leukoencephalopathy (CARASIL): from discovery to gene identification. *J Stroke Cerebrovasc Dis,* 20**,** 85-93.

FUKUTAKE, T. & HIRAYAMA, K. 1995. Familial young-adult-onset arteriosclerotic leukoencephalopathy with alopecia and lumbago without arterial hypertension. *Eur Neurol,* 35**,** 69-79.

GE, G. & GREENSPAN, D. S. 2006. BMP1 controls TGFbeta1 activation via cleavage of latent TGFbeta-binding protein. *J Cell Biol,* 175**,** 111-20.

GOULD, D. B., PHALAN, F. C., VAN MIL, S. E., SUNDBERG, J. P., VAHEDI, K., MASSIN, P., BOUSSER, M. G., HEUTINK, P., MINER, J. H., TOURNIER-LASSERVE, E. & JOHN, S. W. 2006. Role of COL4A1 in small-vessel disease and hemorrhagic stroke. *N Engl J Med,* 354**,** 1489-96.

GOUMANS, M. J. & MUMMERY, C. 2000. Functional analysis of the TGFbeta receptor/Smad pathway through gene ablation in mice. *Int J Dev Biol,* 44**,** 253-65.

GRAHAM, J. R., CHAMBERLAND, A., LIN, Q., LI, X. J., DAI, D., ZENG, W., RYAN, M. S., RIVERA-BERMUDEZ, M. A., FLANNERY, C. R. & YANG, Z. 2013. Serine protease HTRA1 antagonizes transforming growth factor-beta signaling by cleaving its receptors and loss of HTRA1 in vivo enhances bone formation. *PLoS One,* 8**,** e74094.

GRANDE, J., MELDER, D., ZINSMEISTER, A. & KILLEN, P. 1993. Transforming growth factor-beta 1 induces collagen IV gene expression in NIH-3T3 cells. *Lab Invest,* 69**,** 387-95.

GRAU, S., BALDI, A., BUSSANI, R., TIAN, X., STEFANESCU, R., PRZYBYLSKI, M., RICHARDS, P., JONES, S. A., SHRIDHAR, V., CLAUSEN, T. & EHRMANN, M. 2005. Implications of the serine protease HtrA1 in amyloid precursor protein processing. *Proc Natl Acad Sci U S A,* 102**,** 6021-6.

GRAU, S., RICHARDS, P. J., KERR, B., HUGHES, C., CATERSON, B., WILLIAMS, A. S., JUNKER, U., JONES, S. A., CLAUSEN, T. & EHRMANN, M. 2006. The role of human HtrA1 in arthritic disease. *J Biol Chem,* 281**,** 6124-9.

GRAY, C. W., WARD, R. V., KARRAN, E., TURCONI, S., ROWLES, A., VIGLIENGHI, D., SOUTHAN, C., BARTON, A., FANTOM, K. G., WEST, A., SAVOPOULOS, J., HASSAN, N. J., CLINKENBEARD, H., HANNING, C., AMEGADZIE, B., DAVIS, J. B., DINGWALL, C., LIVI, G. P. & CREASY, C. L. 2000. Characterization of human HtrA2, a novel serine protease involved in the mammalian cellular stress response. *Eur J Biochem,* 267**,** 5699-710.

HABASHI, J. P., JUDGE, D. P., HOLM, T. M., COHN, R. D., LOEYS, B. L., COOPER, T. K., MYERS, L., KLEIN, E. C., LIU, G., CALVI, C., PODOWSKI, M., NEPTUNE, E. R., HALUSHKA, M. K., BEDJA, D., GABRIELSON, K., RIFKIN, D. B., CARTA, L., RAMIREZ, F., HUSO, D. L. & DIETZ, H. C. 2006. Losartan, an AT1 antagonist, prevents aortic aneurysm in a mouse model of Marfan syndrome. *Science,* 312**,** 117-21.

HANSEN, G. & HILGENFELD, R. 2013. Architecture and regulation of HtrA-family proteins involved in protein quality control and stress response. *Cell Mol Life Sci,* 70**,** 761-75.

HARA, H., HUANG, P. L., PANAHIAN, N., FISHMAN, M. C. & MOSKOWITZ, M. A. 1996. Reduced brain edema and infarction volume in mice lacking the neuronal isoform of nitric oxide synthase after transient MCA occlusion. *J Cereb Blood Flow Metab,* 16**,** 605-11.

HARA, K., SHIGA, A., FUKUTAKE, T., NOZAKI, H., MIYASHITA, A., YOKOSEKI, A., KAWATA, H., KOYAMA, A., ARIMA, K., TAKAHASHI, T., IKEDA, M., SHIOTA, H., TAMURA, M., SHIMOE, Y., HIRAYAMA, M., ARISATO, T., YANAGAWA, S., TANAKA, A., NAKANO, I., IKEDA, S., YOSHIDA, Y., YAMAMOTO, T., IKEUCHI, T., KUWANO, R., NISHIZAWA, M., TSUJI, S. & ONODERA, O. 2009. Association of HTRA1 mutations and familial ischemic cerebral small-vessel disease. *N Engl J Med,* 360**,** 1729-39.

HOLM, T. M., HABASHI, J. P., DOYLE, J. J., BEDJA, D., CHEN, Y., VAN ERP, C., LINDSAY, M. E., KIM, D., SCHOENHOFF, F., COHN, R. D., LOEYS, B. L., THOMAS, C. J., PATNAIK, S., MARUGAN, J. J., JUDGE, D. P. & DIETZ, H. C. 2011. Noncanonical TGFbeta signaling contributes to aortic aneurysm progression in Marfan syndrome mice. *Science,* 332**,** 358-61.

HOU, J., CLEMMONS, D. R. & SMEEKENS, S. 2005. Expression and characterization of a serine protease that preferentially cleaves insulin-like growth factor binding protein-5. *J Cell Biochem,* 94**,** 470-84.

HU, S. I., CAROZZA, M., KLEIN, M., NANTERMET, P., LUK, D. & CROWL, R. M. 1998. Human HtrA, an evolutionarily conserved serine protease identified as a differentially expressed gene product in osteoarthritic cartilage. *J Biol Chem,* 273**,** 34406-12.

IHN, H. 2002. Pathogenesis of fibrosis: role of TGF-beta and CTGF. *Curr Opin Rheumatol,* 14**,** 681-5.

ISOGAI, Z., ONO, R. N., USHIRO, S., KEENE, D. R., CHEN, Y., MAZZIERI, R., CHARBONNEAU, N. L., REINHARDT, D. P., RIFKIN, D. B. & SAKAI, L. Y. 2003. Latent transforming growth factor beta-binding protein 1 interacts with fibrillin and is a microfibril-associated protein. *J Biol Chem,* 278**,** 2750-7.

JACOBS, J. J., KIEBOOM, K., MARINO, S., DEPINHO, R. A. & VAN LOHUIZEN, M. 1999. The oncogene and Polycomb-group gene bmi-1 regulates cell proliferation and senescence through the ink4a locus. *Nature,* 397**,** 164-8.

JONES, A., KUMAR, S., ZHANG, N., TONG, Z., YANG, J. H., WATT, C., ANDERSON, J., AMRITA, FILLERUP, H., MCCLOSKEY, M., LUO, L., YANG, Z., AMBATI, B., MARC, R., OKA, C., ZHANG, K. & FU, Y. 2011. Increased expression of multifunctional serine protease, HTRA1, in retinal pigment epithelium induces polypoidal choroidal vasculopathy in mice. *Proc Natl Acad Sci U S A,* 108**,** 14578-83.

JOUTEL, A., CORPECHOT, C., DUCROS, A., VAHEDI, K., CHABRIAT, H., MOUTON, P., ALAMOWITCH, S., DOMENGA, V., CECILLION, M., MARECHAL, E., MACIAZEK, J., VAYSSIERE, C., CRUAUD, C., CABANIS, E. A., RUCHOUX, M. M., WEISSENBACH, J., BACH, J. F., BOUSSER, M. G. & TOURNIER-LASSERVE, E. 1996. Notch3 mutations in CADASIL, a hereditary adult-onset condition causing stroke and dementia. *Nature,* 383**,** 707-10.

JOUTEL, A., MONET-LEPRETRE, M., GOSELE, C., BARON-MENGUY, C., HAMMES, A., SCHMIDT, S., LEMAIRE-CARRETTE, B., DOMENGA, V., SCHEDL, A., LACOMBE, P. & HUBNER, N. 2010. Cerebrovascular dysfunction and microcirculation rarefaction precede white matter lesions in a mouse genetic model of cerebral ischemic small vessel disease. *J Clin Invest,* 120**,** 433-45.

JUDGE, D. P., BIERY, N. J., KEENE, D. R., GEUBTNER, J., MYERS, L., HUSO, D. L., SAKAI, L. Y. & DIETZ, H. C. 2004. Evidence for a critical contribution of haploinsufficiency in the complex pathogenesis of Marfan syndrome. *J Clin Invest,* 114**,** 172-81.

KAMIJO, T., VAN DE KAMP, E., CHONG, M. J., ZINDY, F., DIEHL, J. A., SHERR, C. J. & MCKINNON, P. J. 1999. Loss of the ARF tumor suppressor reverses premature replicative arrest but not radiation hypersensitivity arising from disabled atm function. *Cancer Res,* 59**,** 2464-9.

KAMIJO, T., ZINDY, F., ROUSSEL, M. F., QUELLE, D. E., DOWNING, J. R., ASHMUN, R. A., GROSVELD, G. & SHERR, C. J. 1997. Tumor suppression at the mouse INK4a locus mediated by the alternative reading frame product p19ARF. *Cell,* 91**,** 649-59.

KAMINSKA, B., WESOLOWSKA, A. & DANILKIEWICZ, M. 2005. TGF beta signalling and its role in tumour pathogenesis. *Acta Biochim Pol,* 52**,** 329-37.

KAST, J., HANECKER, P., BEAUFORT, N., GIESE, A., JOUTEL, A., DICHGANS, M., OPHERK, C. & HAFFNER, C. 2014. Sequestration of latent TGF-beta binding protein 1 into CADASIL-related Notch3-ECD deposits. *Acta Neuropathol Commun,* 2**,** 96.

KATZMAN, W. B., WANEK, L., SHEPHERD, J. A. & SELLMEYER, D. E. 2010. Age-related hyperkyphosis: its causes, consequences, and management. *J Orthop Sports Phys Ther,* 40**,** 352-60.

KLEMPT, N. D., SIRIMANNE, E., GUNN, A. J., KLEMPT, M., SINGH, K., WILLIAMS, C. & GLUCKMAN, P. D. 1992. Hypoxia-ischemia induces transforming growth factor beta 1 mRNA in the infant rat brain. *Brain Res Mol Brain Res,* 13**,** 93-101.

LAIHO, M., SAKSELA, O., ANDREASEN, P. A. & KESKI-OJA, J. 1986. Enhanced production and extracellular deposition of the endothelial-type plasminogen activator inhibitor in cultured human lung fibroblasts by transforming growth factor-beta. *J Cell Biol,* 103**,** 2403-10.

LANE, D. P. 1992. Cancer. p53, guardian of the genome. *Nature,* 358**,** 15-6.

LAUNAY, S., MAUBERT, E., LEBEURRIER, N., TENNSTAEDT, A., CAMPIONI, M., DOCAGNE, F., GABRIEL, C., DAUPHINOT, L., POTIER, M. C., EHRMANN, M., BALDI, A. & VIVIEN, D. 2008. HtrA1-dependent proteolysis of TGF-beta controls both neuronal maturation and developmental survival. *Cell Death Differ,* 15**,** 1408-16.

LETARTE, M., MCDONALD, M. L., LI, C., KATHIRKAMATHAMBY, K., VERA, S., PECE-BARBARA, N. & KUMAR, S. 2005. Reduced endothelial secretion and plasma levels of transforming growth factor-beta1 in patients with hereditary hemorrhagic telangiectasia type 1. *Cardiovasc Res,* 68**,** 155-64.

LI, W., LI, Q., JIAO, Y., QIN, L., ALI, R., ZHOU, J., FERRUZZI, J., KIM, R. W., GEIRSSON, A., DIETZ, H. C., OFFERMANNS, S., HUMPHREY, J. D. & TELLIDES, G. 2014. Tgfbr2 disruption in postnatal smooth muscle impairs aortic wall homeostasis. *J Clin Invest,* 124**,** 755-67.

LI, W., SRINIVASULA, S. M., CHAI, J., LI, P., WU, J. W., ZHANG, Z., ALNEMRI, E. S. & SHI, Y. 2002. Structural insights into the pro-apoptotic function of mitochondrial serine protease HtrA2/Omi. *Nat Struct Biol,* 9**,** 436-41.

LINDSAY, M. E., SCHEPERS, D., BOLAR, N. A., DOYLE, J. J., GALLO, E., FERT-BOBER, J., KEMPERS, M. J., FISHMAN, E. K., CHEN, Y., MYERS, L., BJEDA, D., OSWALD, G., ELIAS, A. F., LEVY, H. P., ANDERLID,

B. M., YANG, M. H., BONGERS, E. M., TIMMERMANS, J., BRAVERMAN, A. C., CANHAM, N., MORTIER, G. R., BRUNNER, H. G., BYERS, P. H., VAN EYK, J., VAN LAER, L., DIETZ, H. C. & LOEYS, B. L. 2012. Loss-of-function mutations in TGFB2 cause a syndromic presentation of thoracic aortic aneurysm. *Nat Genet,* 44**,** 922-7.

LIPINSKA, B., SHARMA, S. & GEORGOPOULOS, C. 1988. Sequence analysis and regulation of the htrA gene of Escherichia coli: a sigma 32-independent mechanism of heat-inducible transcription. *Nucleic Acids Res,* 16**,** 10053-67.

LIVAK, K. J. & SCHMITTGEN, T. D. 2001. Analysis of relative gene expression data using real-time quantitative PCR and the 2(-Delta Delta C(T)) Method. *Methods,* 25**,** 402-8.

LOEYS, B. L., CHEN, J., NEPTUNE, E. R., JUDGE, D. P., PODOWSKI, M., HOLM, T., MEYERS, J., LEITCH, C. C., KATSANIS, N., SHARIFI, N., XU, F. L., MYERS, L. A., SPEVAK, P. J., CAMERON, D. E., DE BACKER, J., HELLEMANS, J., CHEN, Y., DAVIS, E. C., WEBB, C. L., KRESS, W., COUCKE, P., RIFKIN, D. B., DE PAEPE, A. M. & DIETZ, H. C. 2005. A syndrome of altered cardiovascular, craniofacial, neurocognitive and skeletal development caused by mutations in TGFBR1 or TGFBR2. *Nat Genet,* 37**,** 275-81.

LONG, S. Y. 1972. Hair-nibbling and whisker-trimming as indicators of social hierarchy in mice. *Anim Behav,* 20**,** 10-2.

MAEDA, S., NAKAYAMA, H., ISAKA, K., AIHARA, Y. & NEMOTO, S. 1976. Familial unusual encephalopathy of Binswanger's type without hypertension. *Folia Psychiatr Neurol Jpn,* 30**,** 165-77.

MARKEL, P., SHU, P., EBELING, C., CARLSON, G. A., NAGLE, D. L., SMUTKO, J. S. & MOORE, K. J. 1997. Theoretical and empirical issues for marker-assisted breeding of congenic mouse strains. *Nat Genet,* 17**,** 280-4.

MATT, P., SCHOENHOFF, F., HABASHI, J., HOLM, T., VAN ERP, C., LOCH, D., CARLSON, O. D., GRISWOLD, B. F., FU, Q., DE BACKER, J., LOEYS, B., HUSO, D. L., MCDONNELL, N. B., VAN EYK, J. E. & DIETZ, H. C. 2009. Circulating transforming growth factor-beta in Marfan syndrome. *Circulation,* 120**,** 526-32.

MCALLISTER, K. A., GROGG, K. M., JOHNSON, D. W., GALLIONE, C. J., BALDWIN, M. A., JACKSON, C. E., HELMBOLD, E. A., MARKEL, D. S., MCKINNON, W. C., MURRELL, J. & ET AL. 1994. Endoglin, a TGF-beta binding protein of endothelial cells, is the gene for hereditary haemorrhagic telangiectasia type 1. *Nat Genet,* 8**,** 345-51.

MENDIOROZ, M., FERNANDEZ-CADENAS, I., DEL RIO-ESPINOLA, A., ROVIRA, A., SOLE, E., FERNANDEZ-FIGUERAS, M. T., GARCIA-PATOS, V., SASTRE-GARRIGA, J., DOMINGUES-MONTANARI,

S., ALVAREZ-SABIN, J. & MONTANER, J. 2010. A missense HTRA1 mutation expands CARASIL syndrome to the Caucasian population. *Neurology,* 75**,** 2033-5.

MILNER, J. M., PATEL, A. & ROWAN, A. D. 2008. Emerging roles of serine proteinases in tissue turnover in arthritis. *Arthritis Rheum,* 58**,** 3644-56.

MONET-LEPRETRE, M., HADDAD, I., BARON-MENGUY, C., FOUILLOT-PANCHAL, M., RIANI, M., DOMENGA-DENIER, V., DUSSAULE, C., COGNAT, E., VINH, J. & JOUTEL, A. 2013. Abnormal recruitment of extracellular matrix proteins by excess Notch3 ECD: a new pathomechanism in CADASIL. *Brain,* 136**,** 1830-45.

MOUSTAKAS, A. & HELDIN, C. H. 2009. The regulation of TGFbeta signal transduction. *Development,* 136**,** 3699-714.

MURWANTOKO, YANO, M., UETA, Y., MURASAKI, A., KANDA, H., OKA, C. & KAWAICHI, M. 2004. Binding of proteins to the PDZ domain regulates proteolytic activity of HtrA1 serine protease. *Biochem J,* 381**,** 895-904.

NEPTUNE, E. R., FRISCHMEYER, P. A., ARKING, D. E., MYERS, L., BUNTON, T. E., GAYRAUD, B., RAMIREZ, F., SAKAI, L. Y. & DIETZ, H. C. 2003. Dysregulation of TGF-beta activation contributes to pathogenesis in Marfan syndrome. *Nat Genet,* 33**,** 407-11.

NG, C. M., CHENG, A., MYERS, L. A., MARTINEZ-MURILLO, F., JIE, C., BEDJA, D., GABRIELSON, K. L., HAUSLADEN, J. M., MECHAM, R. P., JUDGE, D. P. & DIETZ, H. C. 2004. TGF-beta-dependent pathogenesis of mitral valve prolapse in a mouse model of Marfan syndrome. *J Clin Invest,* 114**,** 1586-92.

NIE, G. Y., HAMPTON, A., LI, Y., FINDLAY, J. K. & SALAMONSEN, L. A. 2003a. Identification and cloning of two isoforms of human high-temperature requirement factor A3 (HtrA3), characterization of its genomic structure and comparison of its tissue distribution with HtrA1 and HtrA2. *Biochem J,* 371**,** 39-48.

NIE, G. Y., LI, Y., MINOURA, H., BATTEN, L., OOI, G. T., FINDLAY, J. K. & SALAMONSEN, L. A. 2003b. A novel serine protease of the mammalian HtrA family is up-regulated in mouse uterus coinciding with placentation. *Mol Hum Reprod,* 9**,** 279-90.

NISHIMOTO, Y., SHIBATA, M., NIHONMATSU, M., NOZAKI, H., SHIGA, A., SHIRATA, A., YAMANE, K., KOSAKAI, A., TAKAHASHI, K., NISHIZAWA, M., ONODERA, O. & SUZUKI, N. 2011. A novel mutation in the HTRA1 gene causes CARASIL without alopecia. *Neurology,* 76**,** 1353-5.

NOVAK, M. A. & MEYER, J. S. 2009. Alopecia: possible causes and treatments, particularly in captive nonhuman primates. *Comp Med,* 59**,** 18-26.

NOZAKI, H., NISHIZAWA, M. & ONODERA, O. 2014. Features of Cerebral Autosomal Recessive Arteriopathy With Subcortical Infarcts and Leukoencephalopathy. *Stroke*.

OIDE, T., NAKAYAMA, H., YANAGAWA, S., ITO, N., IKEDA, S. & ARIMA, K. 2008. Extensive loss of arterial medial smooth muscle cells and mural extracellular matrix in cerebral autosomal recessive arteriopathy with subcortical infarcts and leukoencephalopathy (CARASIL). *Neuropathology,* 28**,** 132-42.

OKA, C., TSUJIMOTO, R., KAJIKAWA, M., KOSHIBA-TAKEUCHI, K., INA, J., YANO, M., TSUCHIYA, A., UETA, Y., SOMA, A., KANDA, H., MATSUMOTO, M. & KAWAICHI, M. 2004. HtrA1 serine protease inhibits signaling mediated by Tgfbeta family proteins. *Development,* 131**,** 1041-53.

OZARK, S. D. & JAUCH, E. C. 2014. Putting it all together for best stroke practice, all the time. *Stroke,* 45**,** 1243-4.

PANTONI, L. 2010. Cerebral small vessel disease: from pathogenesis and clinical characteristics to therapeutic challenges. *Lancet Neurol,* 9**,** 689-701.

PAXINOS, G. & FRANKLIN, K. B. J. 2001. *The Mouse Brain in Stereotaxic Coordinates,* San Diego, CA, Elsevier Academic Press.

PETTY, G. W., BROWN, R. D., JR., WHISNANT, J. P., SICKS, J. D., O'FALLON, W. M. & WIEBERS, D. O. 2000. Ischemic stroke subtypes : a population-based study of functional outcome, survival, and recurrence. *Stroke,* 31**,** 1062-8.

PINKSTON, J. B., ALEKSEEVA, N. & GONZALEZ TOLEDO, E. 2009. Stroke and dementia. *Neurol Res,* 31**,** 824-31.

RUIZ-ORTEGA, M., RODRIGUEZ-VITA, J., SANCHEZ-LOPEZ, E., CARVAJAL, G. & EGIDO, J. 2007. TGF-beta signaling in vascular fibrosis. *Cardiovasc Res,* 74**,** 196-206.

SAHARINEN, J. & KESKI-OJA, J. 2000. Specific sequence motif of 8-Cys repeats of TGF-beta binding proteins, LTBPs, creates a hydrophobic interaction surface for binding of small latent TGF-beta. *Mol Biol Cell,* 11**,** 2691-704.

SAHARINEN, J., TAIPALE, J. & KESKI-OJA, J. 1996. Association of the small latent transforming growth factor-beta with an eight cysteine repeat of its binding protein LTBP-1. *Embo j,* 15**,** 245-53.

SARNA, J. R., DYCK, R. H. & WHISHAW, I. Q. 2000. The Dalila effect: C57BL6 mice barber whiskers by plucking. *Behav Brain Res,* 108**,** 39-45.

SATO, Y. & RIFKIN, D. B. 1989. Inhibition of endothelial cell movement by pericytes and smooth muscle cells: activation of a latent transforming growth factor-beta 1-like molecule by plasmin during co-culture. *J Cell Biol,* 109**,** 309-15.

SHARPLESS, N. E., BARDEESY, N., LEE, K. H., CARRASCO, D., CASTRILLON, D. H., AGUIRRE, A. J., WU, E. A., HORNER, J. W. & DEPINHO, R. A. 2001. Loss of p16Ink4a with retention of p19Arf predisposes mice to tumorigenesis. *Nature,* 413**,** 86-91.

SHI, Y. & MASSAGUE, J. 2003. Mechanisms of TGF-beta signaling from cell membrane to the nucleus. *Cell,* 113**,** 685-700.

SHIGA, A., NOZAKI, H., YOKOSEKI, A., NIHONMATSU, M., KAWATA, H., KATO, T., KOYAMA, A., ARIMA, K., IKEDA, M., KATADA, S., TOYOSHIMA, Y., TAKAHASHI, H., TANAKA, A., NAKANO, I., IKEUCHI, T., NISHIZAWA, M. & ONODERA, O. 2011. Cerebral small-vessel disease protein HTRA1 controls the amount of TGF-beta1 via cleavage of proTGF-beta1. *Hum Mol Genet,* 20**,** 1800-10.

SHRIDHAR, V., SEN, A., CHIEN, J., STAUB, J., AVULA, R., KOVATS, S., LEE, J., LILLIE, J. & SMITH, D. I. 2002. Identification of underexpressed genes in early- and late-stage primary ovarian tumors by suppression subtraction hybridization. *Cancer Res,* 62**,** 262-70.

SHULL, M. M., ORMSBY, I., KIER, A. B., PAWLOWSKI, S., DIEBOLD, R. J., YIN, M., ALLEN, R., SIDMAN, C., PROETZEL, G., CALVIN, D. & ET AL. 1992. Targeted disruption of the mouse transforming growth factor-beta 1 gene results in multifocal inflammatory disease. *Nature,* 359**,** 693-9.

SINGH, N., KUPPILI, R. R. & BOSE, K. 2011. The structural basis of mode of activation and functional diversity: a case study with HtrA family of serine proteases. *Arch Biochem Biophys,* 516**,** 85-96.

SKORKO-GLONEK, J., KRZEWSKI, K., LIPINSKA, B., BERTOLI, E. & TANFANI, F. 1995. Comparison of the structure of wild-type HtrA heat shock protease and mutant HtrA proteins. A Fourier transform infrared spectroscopic study. *J Biol Chem,* 270**,** 11140-6.

SPIESS, C., BEIL, A. & EHRMANN, M. 1999. A temperature-dependent switch from chaperone to protease in a widely conserved heat shock protein. *Cell,* 97**,** 339-47.

STROZIK, E. & FESTING, M. F. 1981. Whisker trimming in mice. *Lab Anim,* 15**,** 309-12.

SUNDBERG, J. P., CORDY, W. R. & KING, L. E., JR. 1994. Alopecia areata in aging C3H/HeJ mice. *J Invest Dermatol,* 102**,** 847-56.

TAIPALE, J., MIYAZONO, K., HELDIN, C. H. & KESKI-OJA, J. 1994. Latent transforming growth factor-beta 1 associates to fibroblast extracellular matrix via latent TGF-beta binding protein. *J Cell Biol,* 124**,** 171-81.

TATTI, O., VEHVILAINEN, P., LEHTI, K. & KESKI-OJA, J. 2008. MT1-MMP releases latent TGF-beta1 from endothelial cell extracellular matrix via proteolytic processing of LTBP-1. *Exp Cell Res,* 314**,** 2501-14.

TEN DIJKE, P. & ARTHUR, H. M. 2007. Extracellular control of TGFbeta signalling in vascular development and disease. *Nat Rev Mol Cell Biol,* 8**,** 857-69.

TESSEUR, I., ZOU, K., BERBER, E., ZHANG, H. & WYSS-CORAY, T. 2006. Highly sensitive and specific bioassay for measuring bioactive TGF-beta. *BMC Cell Biol,* 7**,** 15.

THOMPSON, C. S. & HAKIM, A. M. 2009. Living beyond our physiological means: small vessel disease of the brain is an expression of a systemic failure in arteriolar function: a unifying hypothesis. *Stroke,* 40**,** e322-30.

TOCHARUS, J., TSUCHIYA, A., KAJIKAWA, M., UETA, Y., OKA, C. & KAWAICHI, M. 2004. Developmentally regulated expression of mouse HtrA3 and its role as an inhibitor of TGF-beta signaling. *Dev Growth Differ,* 46**,** 257-74.

TRIFUNOVIC, A., WREDENBERG, A., FALKENBERG, M., SPELBRINK, J. N., ROVIO, A. T., BRUDER, C. E., BOHLOOLY, Y. M., GIDLOF, S., OLDFORS, A., WIBOM, R., TORNELL, J., JACOBS, H. T. & LARSSON, N. G. 2004. Premature ageing in mice expressing defective mitochondrial DNA polymerase. *Nature,* 429**,** 417-23.

TRUEBESTEIN, L., TENNSTAEDT, A., MONIG, T., KROJER, T., CANELLAS, F., KAISER, M., CLAUSEN, T. & EHRMANN, M. 2011. Substrate-induced remodeling of the active site regulates human HTRA1 activity. *Nat Struct Mol Biol,* 18**,** 386-8.

TSUCHIYA, A., YANO, M., TOCHARUS, J., KOJIMA, H., FUKUMOTO, M., KAWAICHI, M. & OKA, C. 2005. Expression of mouse HtrA1 serine protease in normal bone and cartilage and its upregulation in joint cartilage damaged by experimental arthritis. *Bone,* 37**,** 323-36.

URANO, T., NARUSAWA, K., KOBAYASHI, S., SHIRAKI, M., HORIE-INOUE, K., SASAKI, N., HOSOI, T., OUCHI, Y., NAKAMURA, T. & INOUE, S. 2010. Association of HTRA1 promoter polymorphism with spinal disc degeneration in Japanese women. *J Bone Miner Metab,* 28**,** 220-6.

VAN DE LAAR, I. M., OLDENBURG, R. A., PALS, G., ROOS-HESSELINK, J. W., DE GRAAF, B. M., VERHAGEN, J. M., HOEDEMAEKERS, Y. M., WILLEMSEN, R., SEVERIJNEN, L. A., VENSELAAR, H., VRIEND, G., PATTYNAMA, P. M., COLLEE, M., MAJOOR-KRAKAUER, D., POLDERMANS, D., FROHN-MULDER, I. M., MICHA, D., TIMMERMANS, J., HILHORST-HOFSTEE, Y., BIERMA-ZEINSTRA, S. M., WILLEMS, P. J., KROS, J. M., OEI, E. H., OOSTRA, B. A., WESSELS, M. W. & BERTOLI-AVELLA, A. M. 2011. Mutations in SMAD3 cause a syndromic form of aortic aneurysms and dissections with early-onset osteoarthritis. *Nat Genet,* 43**,** 121-6.

VIERKOTTEN, S., MUETHER, P. S. & FAUSER, S. 2011. Overexpression of HTRA1 leads to ultrastructural changes in the elastic layer of Bruch's membrane via cleavage of extracellular matrix components. *PLoS One,* 6**,** e22959.

WANG, X. L., LI, C. F., GUO, H. W. & CAO, B. Z. 2012. A novel mutation in the HTRA1 gene identified in Chinese CARASIL pedigree. *CNS Neurosci Ther,* 18**,** 867-9.

WARDLAW, J. M., ALLERHAND, M., DOUBAL, F. N., VALDES HERNANDEZ, M., MORRIS, Z., GOW, A. J., BASTIN, M., STARR, J. M., DENNIS, M. S. & DEARY, I. J. 2014. Vascular risk factors, large-artery atheroma, and brain white matter hyperintensities. *Neurology,* 82**,** 1331-8.

WARDLAW, J. M., SMITH, E. E., BIESSELS, G. J., CORDONNIER, C., FAZEKAS, F., FRAYNE, R., LINDLEY, R. I., O'BRIEN, J. T., BARKHOF, F., BENAVENTE, O. R., BLACK, S. E., BRAYNE, C., BRETELER, M., CHABRIAT, H., DECARLI, C., DE LEEUW, F. E., DOUBAL, F., DUERING, M., FOX, N. C., GREENBERG, S., HACHINSKI, V., KILIMANN, I., MOK, V., OOSTENBRUGGE, R., PANTONI, L., SPECK, O., STEPHAN, B. C., TEIPEL, S., VISWANATHAN, A., WERRING, D., CHEN, C., SMITH, C., VAN BUCHEM, M., NORRVING, B., GORELICK, P. B. & DICHGANS, M. 2013. Neuroimaging standards for research into small vessel disease and its contribution to ageing and neurodegeneration. *Lancet Neurol,* 12**,** 822-38.

WARLOW, C., SUDLOW, C., DENNIS, M., WARDLAW, J. & SANDERCOCK, P. 2003. Stroke. *Lancet,* 362**,** 1211-24.

WRANA, J. L., ATTISANO, L., CARCAMO, J., ZENTELLA, A., DOODY, J., LAIHO, M., WANG, X. F. & MASSAGUE, J. 1992. TGF beta signals through a heteromeric protein kinase receptor complex. *Cell,* 71**,** 1003-14.

WYSS-CORAY, T., LIN, C., SANAN, D. A., MUCKE, L. & MASLIAH, E. 2000. Chronic overproduction of transforming growth factor-beta1 by astrocytes promotes Alzheimer's disease-like microvascular degeneration in transgenic mice. *Am J Pathol,* 156**,** 139-50.

YAMAMOTO, Y., CRAGGS, L., BAUMANN, M., KALIMO, H. & KALARIA, R. N. 2011. Review: molecular genetics and pathology of hereditary small vessel diseases of the brain. *Neuropathol Appl Neurobiol,* 37**,** 94-113.

YAMAMURA, T., NISHIMURA, M., SHIRABE, T. & FUJITA, M. 1987. Subcortical vascular encephalopathy in a normotensive, young adult with premature baldness and spondylitis deformans. A clinicopathological study and review of the literature. *J Neurol Sci,* 78**,** 175-87.

YANAGAWA, S., ITO, N., ARIMA, K. & IKEDA, S. 2002. Cerebral autosomal recessive arteriopathy with subcortical infarcts and leukoencephalopathy. *Neurology,* 58**,** 817-20.

YOON, B. S. & LYONS, K. M. 2004. Multiple functions of BMPs in chondrogenesis. *J Cell Biochem,* 93**,** 93-103.

YU, Q. & STAMENKOVIC, I. 2000. Cell surface-localized matrix metalloproteinase-9 proteolytically activates TGF-beta and promotes tumor invasion and angiogenesis. *Genes Dev,* 14**,** 163-76.

ZAMBROWICZ, B. P., ABUIN, A., RAMIREZ-SOLIS, R., RICHTER, L. J., PIGGOTT, J., BELTRANDELRIO, H., BUXTON, E. C., EDWARDS, J., FINCH, R. A., FRIDDLE, C. J., GUPTA, A., HANSEN, G., HU, Y., HUANG, W., JAING, C., KEY, B. W., JR., KIPP, P., KOHLHAUFF, B., MA, Z. Q., MARKESICH, D., PAYNE, R., POTTER, D. G., QIAN, N., SHAW, J., SCHRICK, J., SHI, Z. Z., SPARKS, M. J., VAN SLIGTENHORST, I., VOGEL, P., WALKE, W., XU, N., ZHU, Q., PERSON, C. & SANDS, A. T. 2003. Wnk1 kinase deficiency lowers blood pressure in mice: a gene-trap screen to identify potential targets for therapeutic intervention. *Proc Natl Acad Sci U S A,* 100**,** 14109-14.

ZHANG, L., LIM, S. L., DU, H., ZHANG, M., KOZAK, I., HANNUM, G., WANG, X., OUYANG, H., HUGHES, G., ZHAO, L., ZHU, X., LEE, C., SU, Z., ZHOU, X., SHAW, R., GEUM, D., WEI, X., ZHU, J., IDEKER, T., OKA, C., WANG, N., YANG, Z., SHAW, P. X. & ZHANG, K. 2012. High temperature requirement factor A1 (HTRA1) gene regulates angiogenesis through transforming growth factor-beta family member growth differentiation factor 6. *J Biol Chem,* 287**,** 1520-6.

ZHENG, D. M., XU, F. F., GAO, Y., ZHANG, H., HAN, S. C. & BI, G. R. 2009. A Chinese pedigree of cerebral autosomal recessive arteriopathy with subcortical infarcts and leukoencephalopathy (CARASIL): clinical and radiological features. *J Clin Neurosci,* 16**,** 847-9.

ZUMBRUNN, J. & TRUEB, B. 1996. Primary structure of a putative serine protease specific for IGF-binding proteins. *FEBS Lett,* 398**,** 187-92.

6 List of figures

7 List of tables

8 Abbreviations

°C	centigrade
α-SMA	α-smooth muscle actin
aa	amino acid
BMP	bone morphogenetic protein
bp	base pairs
BSA	bovine serum albumin
CARASIL	cerebral autosomal recessive arteriopathy with subcortical infarcts and leukoencephalopathy
CBB	coomassie brilliant blue
cDNA	complementary deoxyribonucleic acid
Ct	cycle threshold
C-terminal	carboxy-terminal
CTGF	connective tissue growth factor
ΔC	carboxy-terminal deletion
DAPI	4',6-diamidino-2-phenylindole
DMEM	Dulbecco's Modified Eagle Medium
DMSO	dimethyl sulfoxide
DNA	deoxyribonucleic acid
dNTP	deoxynucleoside triphosphate
DTT	dithiothreitol
E. coli	*Escherichia coli*
ECM	extracellular matrix
ELISA	enzyme-linked immunosorbent assay
et al.	et alii (and others)
FBS	fetal bovine serum
fs	frameshift
g	gram or earth´s gravity
GOM	granular osmiophilic material
gt	gene trap
h	hour(s)
H_2O_{DI}	deionized water
HEK	human embryonic kidney
HRP	horseradish peroxidase
HtrA	high temperature requirement A
HtrA1-I	HtrA1 inhibitor
kDa	kilodalton
KO	knockout
l	liter
LB	Luria-Bertani
LTBP	latent TGF-β-binding protein
µ	micro

m	milli
M	molar
MEF	mouse embryonic fibroblasts
MFS	Marfan syndrome
min	minute(s)
MRI	magnetic resonance imaging
mRNA	messenger ribonucleic acid
n	nano
NEO	neomycin
N-terminal	amino-terminal (of a protein)
PAGE	polyacrylamide gel electrophoresis
PAI-1	plasminogen activator inhibitor-1
PBS	phosphate-buffered saline
PCR	polymerase chain reaction
PI	protease inhibitor(s)
r	recombinant
RNA	ribonucleic acid
s	second(s)
SBE	SMAD binding element
SDS	sodiumdodecylsulfate
SEAP	secreted alkaline phosphatase
SMAD	from Sma and Mad (Mothers against decapentaplegic)
SMCs	smooth muscle cells
SVD	small vessel disease
TGFBR	TGF-β receptor
TGF-β	transforming growth factor beta
tm	targeted mutation
vec	vector
vSMCs	vascular smooth muscle cells
w/v	mass/volume
WM	white matter
WT	wild-type

9 Acknowledgements

Mein besonderer Dank gilt **Prof. Dr. Christian Wahl-Schott** für die freundliche Übernahme der Fachvertretung, seine investierte Zeit und seinem Interesse an meiner Arbeit.

Bei **PD Dr. Christof Haffner** bedanke ich mich für die kompetente Betreuung meiner Arbeit, sowie seinem Vertrauen, seiner Wissensfülle, seinen Ratschlägen zu Problemen jeder Art und dass er immer ein offenes Ohr für mich hatte. Richtig gut, hat wirklich Spaß gemacht!

Herrn **Prof. Dr. Martin Dichgans** danke ich für die Überlassung eines sehr spannenden Themas, die Möglichkeit meine Doktorarbeit an seinem sehr gut ausgestatteten Institut durchführen zu dürfen und seinem Interesse an meinem Thema.

Prof. Dr. Nikolaus Plesnila, **Prof. Dr. Martin Biel**, **Prof. Dr. Stefan Zahler** und **Prof. Dr. Angelika Vollmar** danke ich für die Bewertung dieser Arbeit und deren Bereitschaft an der Prüfungskommission teilzunehmen.

Des Weiteren möchte ich mich ganz herzlich bei **Dr. Rebekka Fischer**, **Dr. Manuela Schneider**, **Dr. Elisabeth Kremmer**, **Dr. Marco Düring**, **Dr. Anne Joutel**, **Prof. Dr. Nikolaus Plesnila**, **Prof. Dr. Michael Ehrmann** und **Dr. Mitrajit Gosh** für deren Hilfe und Beitrag an meiner Arbeit bedanken.

Außerdem danke ich **Daniel Loose** und **Barbara Lindner** für die tatkräftige technische und nicht-technische Unterstützung jeglicher Art, ihre Hilfsbereitschaft egal wann und für diverse private Schunkeleien. Danke an **Natalie Leistner** und **Melanie Schneider** für ihre technische Hilfe. Melanie danke ich besonders für die Unterstützung während meiner ersten Zeit am ISD, ohne die ich aufgeschmissen gewesen wäre. En plus je veux remercier **Nathalie Beaufort** pour sa contribution scientifique et pour m´avoir aider tout au long de ma thèse.

Da ich in diesem Rahmen leider nicht jedem einzeln danken kann, möchte ich mich gesammelt bei allen derzeitigen und ehemaligen **Kollegen** und Doktoranden am ISD für eine wirklich schöne Zeit und die Unterstützung im Laboralltag bedanken.

Den einzigartigen Labor-W. danke ich für eine wunderschöne, hervorragende, grandiose, teereiche, lustige, schlechte witzlastige, einzigartige Zeit und für ihre Freundschaft. **Jessica Kast** für ihre herzliche Art und die vielen hilfreichen (auch) wissenschaftliche Diskussionen, **Patrizia Hanecker** für ihre lustige, unkomplizierte und beruhigende Art und **Caroline Prell**, mit der ich mit Hilfe von viel Ironie und Witz vor allem unsere schwierige Startphase bewältigt habe, dafür dass sie immer für mich da ist.

Danke an **Xandra**, **Sabrina**, **Leonie**, **Pia**, **Metti**, **Jana** und **Dani** für ihre Unterstützung jeglicher Art, dass ihr immer für mich da seid und Verständnis dafür hattet, dass ich immer so wenig Zeit hatte. Ihr seid die besten Freunde, die man sich vorstellen kann.

Besonders möchte ich mich bei meiner **Familie** bedanken, die dieses Werk in allen Phasen mit jeder möglichen Unterstützung bedacht haben und mich immer wieder auf einen guten Weg gebracht haben, wenn ich nicht mehr weiter wusste. Derjenige, der wohl am meisten unter dieser Arbeit zu leiden hatte, war **Martin**. Danke für Deine Liebe, tatkräftige Unterstützung, willkommene Ablenkung, vielen Ideen und Tipps, unendliche Geduld – einfach FÜR ALLES!

10 Publications and meetings

Article

BEAUFORT, N.*, **SCHARRER, E.***, KREMMER, E., LUX, V., EHRMANN, M., HUBER, R., HOULDEN, H., WERRING, D., HAFFNER, C. & DICHGANS, M. 2014. Cerebral small vessel disease-related protease HtrA1 processes latent TGF-β binding protein 1 and facilitates TGF-β signaling. *Proceedings of the National Academy of Sciences U.S.A.* doi:10.1073/pnas.1418087111. (* equal contribution)

Talks at international meetings

Research Meeting 2 of the Transatlantic Network of Excellence on the Pathogenesis of Small Vessel Disease of the Brain, Sept. 2013, Paris, France:
Scharrer, E., Beaufort, N., Haffner, C., Dichgans, M.: HtrA1 deficiency and TGF-β signalling

30th Winter School on Proteinases and Inhibitors, March 2013, Tiers, Italy:
Scharrer, E., Beaufort, N., Kast, J., Lindner, B., Dichgans, M., Haffner, C.: Latent TGF-β-binding protein 1 (LTBP-1) is a novel substrate for the CARASIL-relevant serine protease HtrA1

Research Meeting 1 of the Transatlantic Network of Excellence on the Pathogenesis of Small Vessel Disease of the Brain, March 2013, Munich, Germany:
Scharrer, E., Beaufort, N., Haffner, C., Dichgans, M.: HtrA1-deficient mice: A model for CARASIL?

28th Winter School on Proteinases and Inhibitors, Feb. 2011, Tiers, Italy:
Scharrer, E., Beaufort, N., Dichgans, M., Haffner, C.: The role of the serine protease HtrA1 in inherited cerebral small-vessel disease